UNIVERSITAT POLITÈCNICA
DE CATALUNYA
BARCELONATECH

Suppression and Control of Modulation Instability

A thesis submitted for the degree of
Doctor of Philosophy in Physical Science of

Shubham Kumar

Directors:

Prof. Kestutis Staliunas

Prof. Muriel Botey i Cumella

Prof. Ramon Herrero Simon

Departament de Física

Terrassa, Spain, 2017

Contents

Chapter 1

Modulation Instability and Pattern Formation

Contents

1.1 The Study of Pattern Formation

Dynamical instabilities of spatially continuous systems have long been a subject of intense scientific research. Stationary and oscillatory waves in such systems with intrinsic instabilities lead to many interesting phenomena and fascinating spatiotemporal structures. The dynamical properties of propagating waves, in linear systems, can be easier understood by the superposition principle, where the different Fourier components of the wave (wavevectors) do not interact and remain unaffected by each other, leading to relatively simple dynamics. Purely linear systems in nature, however, are rare or exist in limited parameter ranges. In reality, most systems generally display nonlinear behavior, where the properties of the medium and the system parameters are nonlinearly dependent on the amplitude of the wave. In such systems, the superposition principle is not valid, that is, the different Fourier components of the system are not completely independent from each other but interact and exert mutual influence. This interaction may be of many different types, but can be broadly classified as attractive or repulsive in single variable systems (generally represented by the sign of the nonlinearity coefficient in the wave equation), and forms the basis of most of the observed nonlinear phenomenon.

This basic nonlinear interaction also lies at the root of spontaneous pattern formation, which may be of many different types, occurring in a wide variety of systems in nature and in technology [Stal03, Tli14, Cros93]. A few examples of common patterns are shown in Fig. 1.1.1, which help illustrate the wide variety and diversity of the phenomena.

Although the term ‘pattern formation’ is very generic, in this thesis it is used to specifically refer to patterns which break out spontaneously from homogenous states. It is not to be confused with other types of patterns which arise, for instance, from *self-organization* processes, emergent behaviors and *fractals* etc., which are also widely prevalent in the natural world and equally fascinating

[Ball99, Whit02]. A few examples of such self-organized patterns are also shown in Fig. 1.1.1(h-i).

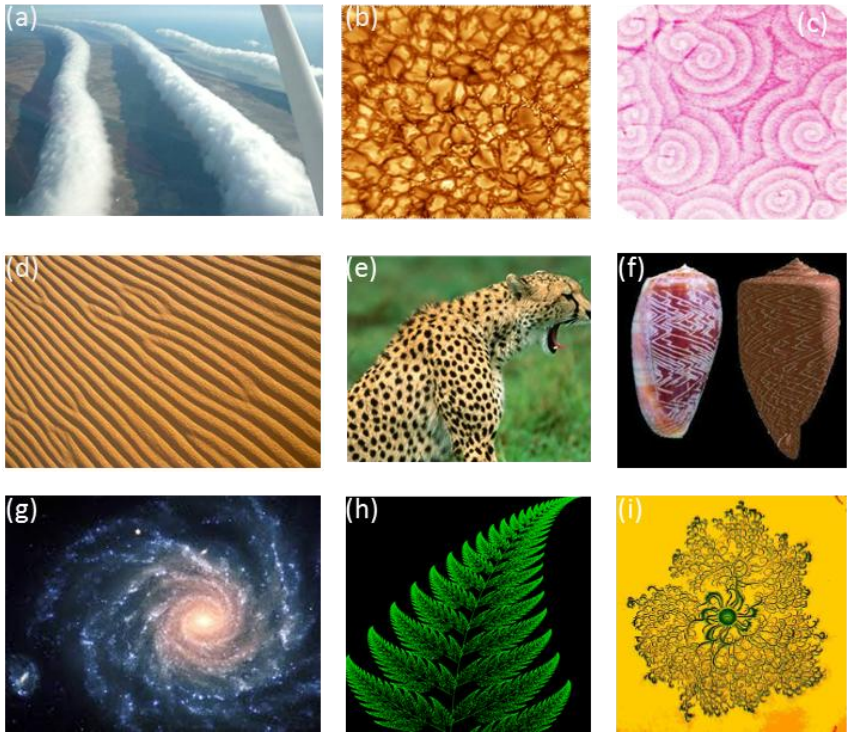

Figure 1.1.1: Some examples of pattern formation in nature. (a) The so-called 'morning glory' clouds, (Credit: [Petr09]) display spectacular roll-patterns. (b) Granular patterns and a sunspot observed in the sun's photosphere (Image: [Gora03]). (c) The spiral patterns of the famous Belousov–Zhabotinsky chemical reaction (Credit: [Epst06]). (d) Regular patterns on sand dunes. Regular Turing-patterns on the skin of many animals (e) and on the shells of many marine creatures (e). (g) A spiral galaxy is an example of pattern formation at astronomical scales. (h) Self-similar fractal patterns of a common fern. (i) Self-organization in a colony of the P. vortex (Ben-Jacob's) bacteria displaying emergent patterns (credit: [Jaco97]).

The phenomenon of pattern formation in the natural world has fascinated humans from the earliest of times. Patterns which appear seemingly from nowhere, with intensely varying structures, and displaying such an intricate combination of logical structure and atheistic beauty- surely must have been a potent stimulation for the ancient mind [Abas01]! It is plausible that such

patterns were the major inspiration behind the development of much of art and mathematics. One of the most concrete examples of such development can be traced far back to the 10th century when complex geometric tessellation patterns were elaborately incorporated into architecture (see Fig. 1.1.2) [Kapl00, Kapl04]. It is interesting, and a rather curious fact, that research into such geometric patterns was at the forefront of mathematics then and remains a hot research topic that still attracts interest even today [Lu07, Dell05]!

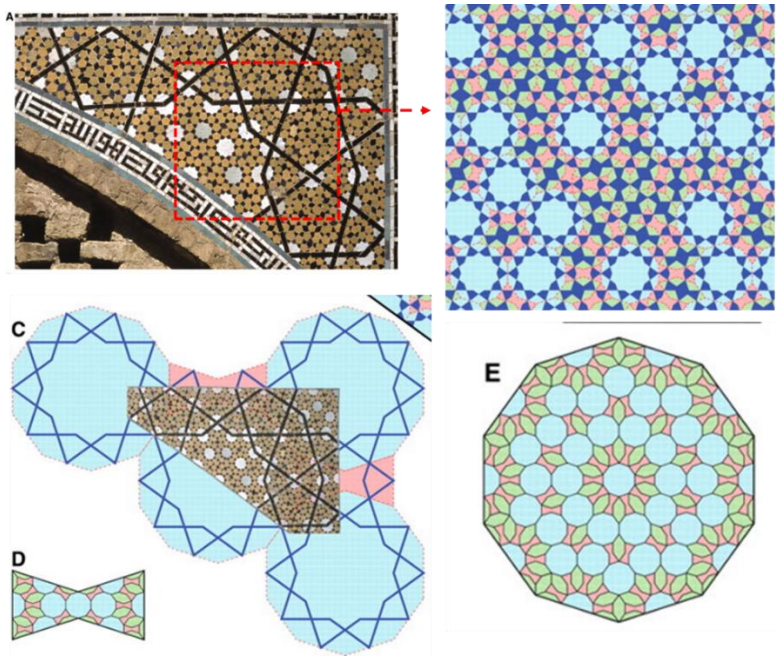

Figure 1.1.2: Complex star-patterns were a common theme in medieval architecture starting from around the 10th century. These tessellations often have complex quasi-crystal-like geometries. Image: [Lu07].

In the modern context, the study of spontaneous pattern formation got a major impetus from the seminal paper of Alan Turing [Turi52] in the year 1952, where he exposed the underlying 'simplicity' of seemingly complex biological patterns in nature for the first time. He showed that in the presence of just two ingredients

of ‘reacting and diffusing’ chemical pigments, a myriad variety of complicated shapes and patterns could emerge (see Fig. 1.1.3), through a phenomenon which is known as the Turing instability [Kond10].

Pattern formation was also deeply explored in the context of self-organisation and appearance of order from an underlying disorder and a rich literature exists on this subject [Nico77, Prig84].

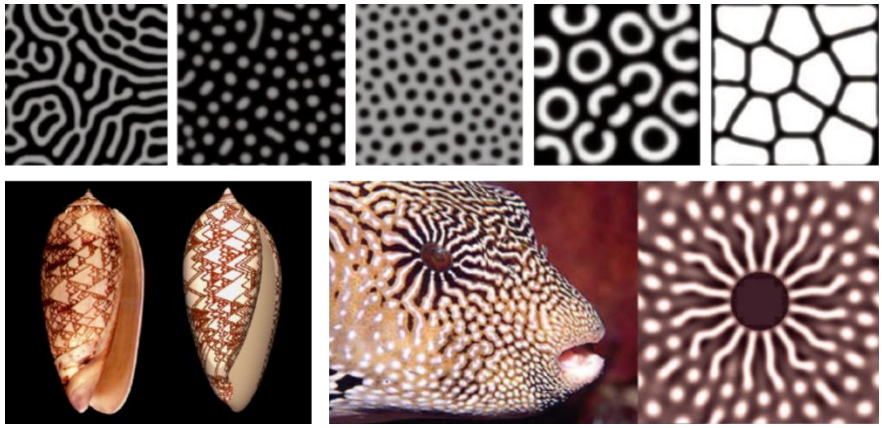

Figure 1.1.3 (Top panel) The various, most common types of Turing patterns found in biological systems. (Bottom panel) Turing patterns on the surface of a sea shell and similar patterns generated by numerical simulation, Turing patterns found on the skin of a fish (Images: [Kond10]).

Dynamical systems can be classified into two general categories from a thermodynamic point of view, the first of which are the conservative or Hamiltonian systems: These can be described as ‘closed’ systems where no exchange of energy between the system and the environment takes place. While on the other hand are the so-called dissipative systems, which are ‘open’, that is, there is a constant exchange of energy with the environment. In the phase space representation, Hamiltonian systems have the property of preserving the volume, whereas dissipative systems can grow or shrink arbitrarily in volume. Spontaneous pattern formation is observed only in dissipative systems and all examples in nature belong to this class. In contrast, in Hamiltonian systems, such

spontaneous pattern formation are limited by the entropic principles of thermodynamics: a system in thermal equilibrium does not create order but moves spontaneously towards disorder [Kond14]. Since dissipative systems are not near equilibrium, the thermodynamic principle of stability- that the system moves towards higher stability, which in this case will be the pattern state, by minimizing it's Gibbs free energy functional does not necessarily hold. However, there have been attempts to provide such a rationale behind such pattern formation, backed not by proofs *per se*, but by empirical evidence [Stal00].

In the context of dissipative patterns, many well-known theoretical and experimental models have been established over last few decades. Widely popular and ground-breaking (in their time) models of such pattern formation include Rayleigh-Benard convection [Bena01], Taylor–Couette flow [Tayl23] and Benjamin-Feir instability [Benj67a] in hydrodynamical systems, the Turing instability in the so-called reaction-diffusion type and the Faraday patterns [Fara31] in parametrically driven systems.

The **Rayleigh-Benard** convection describes stationary convective patterns which appear spontaneously in a fluid held between two surfaces with a temperature gradient. For low temperature gradients, the fluid remains in a conductive-flux state which is characterized by a homogenous surface. The patterns spontaneously arise as the temperature gradient is raised beyond some threshold when the fluid spontaneously switches to a convective state. Thus, in this case, the pattern formation phenomena can be viewed as a more efficient means of energy transport for the fluid. The commonly observed patterns are rolls and hexagons, as shown in Fig. 1.1.4(a).

The **Taylor-Couette** flow describes the process when a fluid, held between two counter-rotating cylinders, spontaneously shifts from a state of laminar flow (pattern forming state), at low angular speeds, as shown in Fig. 1.1.4(b), to a state of turbulent flow, when the angular speed increases beyond a certain threshold.

The **Benjamin-Feir** instability is another well-known pattern-forming hydrodynamic instability, usually described in the context of deep water waves. Here, a periodic train of traveling waves becomes unstable with respect to the carrier wavelength, leading to the generation of exponentially growing sidebands and consequently, to modulated patterns, see Fig. 1.1.4(c). In a general context, this is known as Modulation Instability (MI) and is widely observed in many different physical systems, which will be described in subsequent sections.

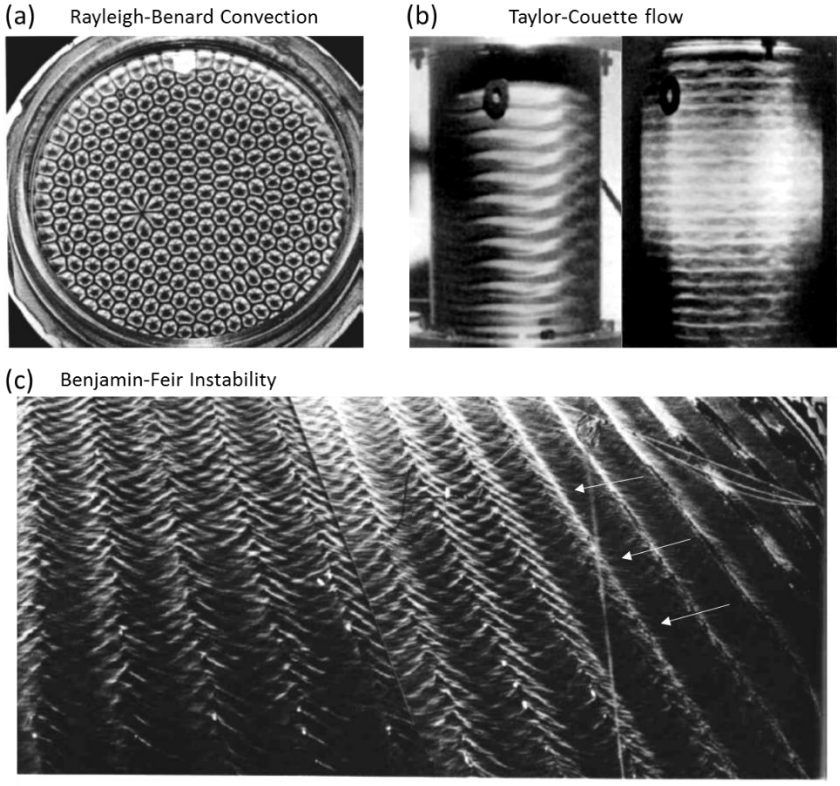

Figure 1.1.4: (a) Roll patterns in the Rayleigh-Benard convection [Kosc74] (b) Horizontal stripe patterns in counter-rotating Taylor-Couette cells in the laminar regime [Trit88] (c) Benjamin-Feir instability leading to the breakdown of a train of plane waves originating from the right side [Dyke82]

Yet another type of pattern formation phenomenon occurs through the process of **parametric instability** or Faraday instability, named after Michael Faraday who first observed it in a layer of vertically oscillating fluid [Fara31]. In this case, a spatially uniform *time*-dependent parametric oscillation, at frequency ω_0, triggers an instability which leads to *spatial* patterns, with wavenumber q, related, via the dispersion relation, $k(\omega)$, to half the driving frequency: $q = k(\omega_0/2)$. For example, in the original experiment, the periodic vertical oscillation of a fluid surface essentially modulates the gravitation acceleration term, g, in the system equations. This triggers the instability which leads to the spatial surface patterns, as shown in Fig. 1.1.5(a). Faraday instability has also been reported in various physical systems such as Bose-Einstein Condensates [Stal02], see Fig. 1.1.5(b), among others [Doua90, Mile90] and has also led to the discovery of interesting new physics and fundamental, new instabilities [Pere16].

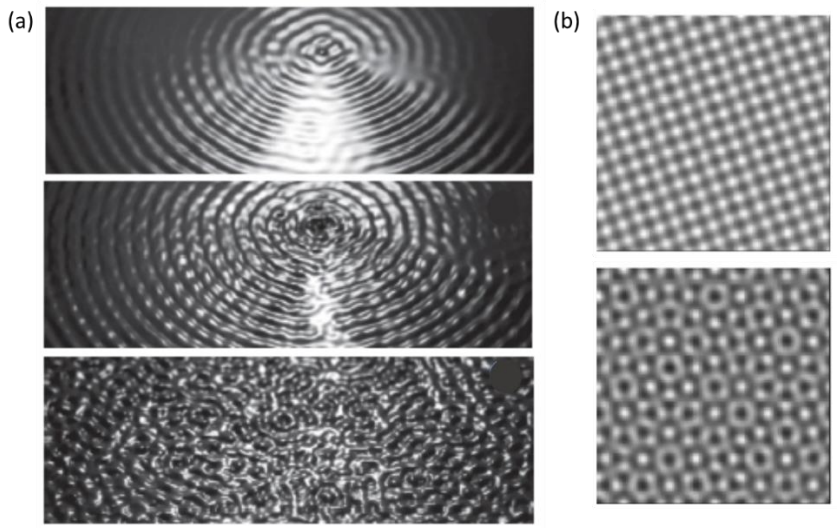

Figure 1.1.5: (a) Parametric exciting of Faraday patterns in water, at different modulation frequencies leading from the regular pattern (top) to turbulent regimes (bottom) [Xia10]. (b) Faraday patterns in Bose-Einstein condensate [Stal02].

Due to the wide interest in pattern formation phenomena over many decades, this field has become perhaps one of the most diverse, encompassing the disciplines of nonlinear dynamics, chaos, complex systems etc… [Stro14]. A huge amount of theoretical and experimental studies which have been conducted, with some becoming ideal models for the description of entire classes of systems showing similar properties.

All spontaneously occurring patterns bifurcate from the breaking of spatial or temporal symmetry of a previously homogenous state. The various mechanisms leading to these patterns develop via different types of instabilities. Most patterns encountered in such spatially-extended systems can be classified into three broad categories based on their spatiotemporal dynamics: patterns which are stationary in time and periodic in space, patterns which are periodic in time and uniform in space (these are not patterns in the colloquial sense of the word, but formally can also be included), and lastly patterns which are periodic in both space and time (spatiotemporal patterns).

Despite the apparent complexity and variety in the physical mechanisms of the different classes of patterns and pattern forming instabilities, there are underlying, common characteristics shared by these systems. One would also intuitively expect so, given the remarkable similarities of patterns appearing in completely unrelated physical systems: biological patterns in animal skins appear strikingly similar to convective patterns in fluids, patterns arising in cloud formations remind us of patterns in optical resonators and so on... This 'qualitative universality' of the characteristics of pattern formation has been perhaps one of the main motivations for the search of simpler, universal models for the description of the pattern formation processes [Pass94].

Spontaneous pattern formation processes always arise out of some underlying instability which may be modeled using a 'control parameter' of the system. When the value of such a parameter is increased (or decreased) beyond a particular threshold, the instability spontaneously arises and the system switches from one pattern (or homogenous) state to another, and vice-versa. For such

types of continuous (supercritical) instabilities, near the instability threshold, the dynamics may be generally described by certain so-called 'amplitude equations' [Cros93].

Amplitude equations describe the large-scale dynamics in space and time near the threshold for an instability and their form is universal for each type of the instability. They describe critical aspects of pattern formation such as the type of instability and the nature of pattern dynamics etc. and are, most often, not concerned with the microscopic variable of the different systems, which are often much too complicated to be described fully by these relatively simple equations.

Some examples of popular amplitude equations include the Swift-Hohenberg Equation, the Complex Ginzburg-Landau Equation, the Nonlinear Schrodinger Equation, the class of Reaction-Diffusion Equations, etc., which will be briefly described later in Section 1.3. Sometimes *order-parameter* models are derived by systematically using the distance from threshold as a convenient parameter for mathematical manipulations, such that they lead to the correct amplitude equations near the instability threshold [Newe93].

In the following section, a brief overview of the pattern-forming systems, various linear instabilities, and their characteristic nonlinear pattern states is presented. Further on, in Section 1.3, a brief discussion on different types of instabilities and various model equations are described. Finally, in section 1.4, an overview of Modulation Instability (MI) in different systems is provided. The implications of this type of instability on the stability properties of the systems are discussed, and finally, in Section 1.5, up to date methods for the control of MI is presented. Concluding this introductory chapter in Section 1.6, the motivation for the development of a new type of stabilization mechanism is given and the outline of this thesis is presented.

1.2 Characterization of Linear Instabilities and Patterns

Dynamical systems can either be discrete (for example a system of coupled pendulums) or continuous (for example an oscillating liquid surface), being described respectively by ordinary differential equations (ODEs) or partial differential equations (PDEs). Although the properties of discrete dynamical systems are, in general, simpler to analyze than that of continuous systems, primarily due to a finite, often much smaller, dimensionality of the *phase space*, they both share many common characteristics which form part of nonlinear analysis.

In this thesis, however, we are concerned only with continuous systems, or more specifically, spatially-extended systems. Although, it should be kept in mind that all numerical studies are essentially, in a strict sense, a study of discrete systems, due to the discretization of space and time required in computation. The full analysis of spatially-extended systems in all their complexity is generally very challenging and usually many simplifications need to be compromised upon. For instance, the presence of boundaries and defects are sometimes ignored in the pursuit of ideal patterns, and often an infinite region of space is considered to maintain translational invariance.

Patterns in such spatially-extended systems arise when a particular state spontaneously loses stability with respect to certain Fourier modes of the system. Although the exact physical mechanisms of the onset and growth of the instability are specific to the microscopic description of the different systems, there exist general macroscopic mechanisms which provide universal descriptions of the instabilities close to the threshold. The general form such models can be expressed as the PDE:

$$\partial_t \boldsymbol{A}(x,t) = F(\boldsymbol{A}, \varepsilon) \tag{1.2.1}$$

where, $\boldsymbol{A}$ represets the dynamical variable in the spatial, x, and temporal, t, domains, ε represents the control parameter and F is an arbitrary nonlinear function.

As the control parameter, ε, is increased across the instability threshold, the stability of the system's solutions undergo a qualitative change. This critical change is referred to as a bifurcation in the context of spatially-extended dynamical systems [Stro14] and in the simplest forms may be of the following four types: Saddle-node, Transcritical, Pitchfork (supercritical and subcritical) and Hopf bifurcations. Each of these bifurcations can be ideally described by very simple PDEs, described below in Eqs.(1.2.2), which differ from each other essentially in their characterization of the spatial and temporal symmetries. For instance, the saddle node bifurcation maintains reflection symmetry around the y-axis: $f(-U) = f(U)$, whereas, in the case of the pitchfork bifurcation, there is symmetry across the origin: $f(-U) = -f(U)$. A point to note is that the first three bifurcations only involves a single variable a, that is, a single physical quantity changing in time, and therefore can only describe instabilities leading to stationary, homogenous or pattern states. Whereas the Hopf bifurcation, defined by a coupled equation of two variables, $a_{1,2}$, describes more complex phenomenon such as oscillatory waves, which have amplitude and phase components coupled to each other.

Saddle-node bifurcation: $\partial_t a = R - a^2$ (1.2.2a)

Transcritical bifurcation: $\partial_t a = Ra - a^2$ (1.2.2b)

Pitchfork bifurcation: $\partial_t a = Ra - fa^3$ (1.2.2c)

Hopf bifurcation:
$$\begin{cases} \partial_t a_1 = -a_2 + Ra_1 - (a_1^2 + a_2^2)^2 a_1 \\ \partial_t a_2 = a_1 + Ra_2 - (a_1^2 + a_2^2)^2 a_2 \end{cases} \quad (1.2.2d)$$

The stability characteristics of the solutions for these different bifurcations are illustrated in Fig.1.2.1.

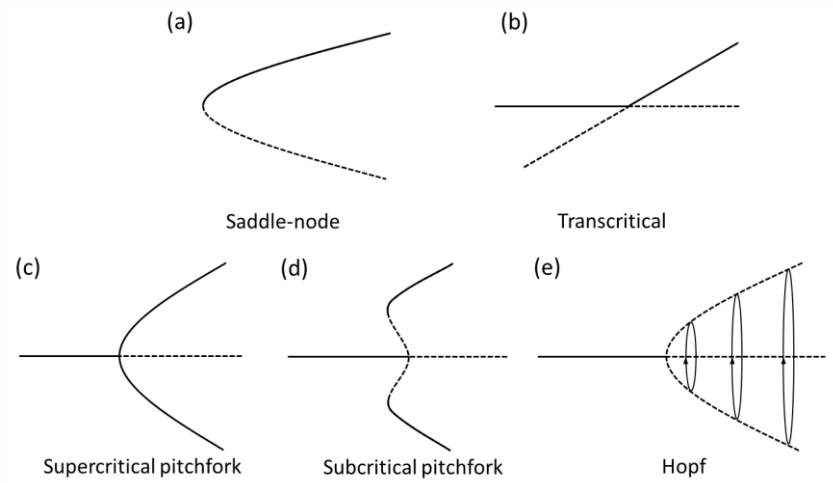

Figure 1.2.1: The simplest four types of Bifurcations for dynamical systems. The control parameter, ε, increases from left to right. The solid and dashed lines represent, respectively, stable and unstable solutions of the system.

1.2.1 Instabilities of Linearized Systems

The first step in the analysis of any dynamical system is to characterize its stability in a linear sense, that is, the stability of the solution with respect to small random perturbations. Consider the system described by Eq. (1.2.1), with the solution $A(x,t) = A_0$. To analyse the linear stability of the solution, a small perturbation is applied:

$$A(x,t) = A_0 + a(x,t) \tag{1.2.3}$$

with,
$$a(x,t) = a_0 exp(ikx + \lambda t) \tag{1.2.4}$$

and where a_0 represents small amplitude of the perturbation, $a_0 \ll A_0$. Solving these two equations simultaneously and linearizing around A_0 leads to:

$$\partial_t a = \boldsymbol{J}.a \tag{1.2.5}$$

where, $\boldsymbol{J_{ij}} = \partial F_i/\partial a_j$ is the Jacobian of the function *F*, evaluated at A_0. The solution of Eq. (1.2.5) leads to a set of eigenvalues $\lambda_i(k)$, the real part of the which represent the growth rates of the possibly many eigenvectors: $\lambda_{Re}(k) = Re[\lambda_i(k)]$. The largest growth exponent, $\lambda_0(k) = Max[\lambda_{Re}(k)]$ represents the value of the eigenvector which grows the fastest and generally dictates the spatiotemporal scales of the growth and forms the 'characteristic wavelength' of the emerging pattern.

As one nears the threshold of the control parameter, ε, i.e. to the threshold of the instability, distinct types of patterns that can occur depending on the character of the eigenvalue λ_0 and the spatial wavevector k.

For $\varepsilon > \varepsilon_{TH}$, a band of wavenumbers $(k_0 \pm \Delta k)$ becomes unstable, either with purely real eigenvalues $Im[\lambda_i] = 0$, leading to (short-wavelength) stationary patterns, or with complex eigenvalues $Im[\lambda_i] \neq 0$, leading to (short-wavelength) oscillatory patterns. An example of this type of instability is Turing instability, found in reaction-diffusion systems, or pattern formation in biological tissues.

The patterns formed here are generally called short-wavelength patterns because the characteristic wavelengths of the pattern in these cases are far away from zero-mode in the Fourier space. The growth spectrum of this type of instability is represented in Fig. 1.2.2(a).

Another class of instability, as shown in Fig. 1.2.2(b), occurs when the zero mode $(k = 0)$ remains always equal to zero, i.e.: $\lambda|_{k=0} = 0$ in all situations. In this case, modulating patterns appear spontaneously on an otherwise stable constant background. This kind of instability may be found in optical systems with Kerr nonlinearity, for example, leading to spatial patterns with a constant average intensity.

The third class of instability is defined when the zero mode is the most unstable. Patterns in these systems may not be visible, as the size of the patterns would be limited by the size of the system itself; one would rather observe the growth dynamics of the homogenous background state itself. The instability spectrum, in this case, is shown in Fig. 1.2.2(c).

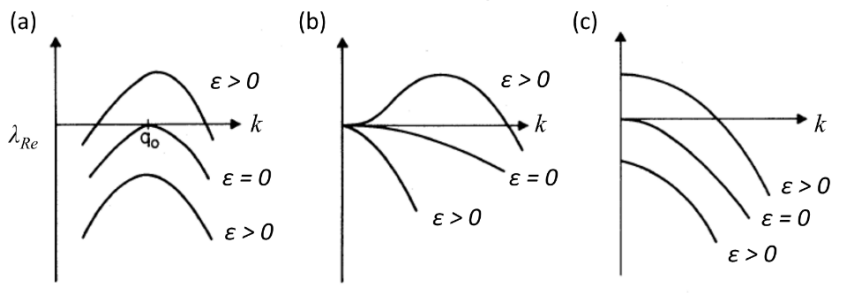

Figure 1.2.2: The spectrum of the growth exponents for the three different kinds of spatiotemporal instabilities in spatially-extended systems (adapted from [Cros93]). Examples of these instabilities are Turing patterns of biological tissues (a), patterns in optical systems with Kerr nonlinearity (b) and scale-free patterns (c).

1.2.2 Nonlinear States and Pattern Formation

The nonlinearity sometimes (usually) plays the role of saturating the growth of the linearly unstable modes. In such cases, the linear instabilities lead to nonlinear states characterized by a uniquely set pattern. In cases where there are more than one unstable growing modes, the nonlinearity can also have a role in selecting one or the either or a combination of them.

In many cases, the saturating nonlinearity could also have a positive feedback effect on the fastest growing mode, that is, the spatial mode, k_0 with the largest eigenvalue, λ_0 leading to its enhancement at the expense (suppression) of all other growing modes in a 'winner takes all' scheme. The resulting stationary pattern in this scenario is a sinusoidal shape with spatial frequency k_0, which is the well-known 'roll pattern' found in many nonlinear systems, such as in the Rayleigh-Benard convection. When two such perpendicular wavevectors are present, which is often the case in two dimensional systems, the resulting patterns are of square or rectangle geometry. Square patterns are generally unstable and often lead to the stable hexagonal patterns, which are characterized by the presence of three such equiangular wavevectors. These three basic types of most commonly observed 'primary' patterns in stationary

two dimensional systems are illustrated in Fig. 1.2.3. One may note that while the rolls and the square pattern maintains inversion symmetry, in the case of the hexagons this symmetry is lost. Finally, it must be kept in mind that these patterns are an ideal case; in real systems, one or more of them may coexist and small perturbations near threshold may shift the system from one to the other state.

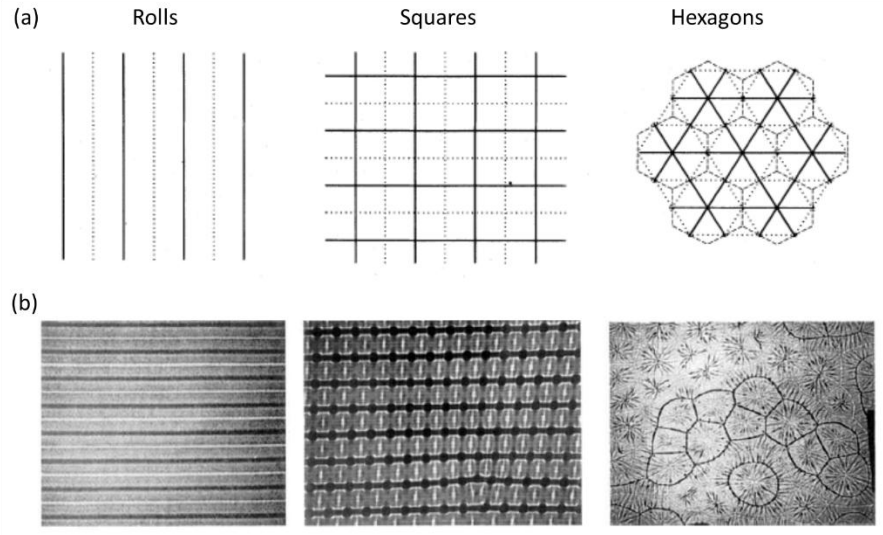

Figure 1.2.3: (a) The most commonly observed stationary patterns in systems with saturating nonlinearity (from [Cros93]). (b) An example of such 'primary' patterns in a convective pattern-forming system for increasing (left to right) Rayleigh number. At low values simple roll patterns are present (left). Increasing values cause rolls to develop in the perpendicular direction too, leading to square patterns (center). At even higher Rayleigh numbers, the pattern becomes hexagonal, before eventually leading to turbulent regimes (from [Trit88]).

In systems with saturating nonlinearity and oscillatory linear instability, that is, when the eigenvalue has a positive real and nonzero imaginary part, the simplest nonlinear state is an oscillating pattern with a spatial wavevector $\vec{k}$. If two unstable modes coexist with wavevectors $\vec{k}$ and $-\vec{k}$, then we have standing wave patterns which remains stationary in time. Although not considered as patterns in the traditional sense, a large number of complex structures are possible for

such instabilities, such as vortices, breathers and others. Detailed descriptions of these, however, can be found elsewhere [Pere83, Mann95].

These basic spatial patterns, or nonlinear state, arising from the saturation of the linear instabilities are not always stable and can sometimes lead via secondary instabilities to further differentiated nonlinear states. Two of the most well-known are the Eckhaus [Eckh65] and the zigzag [Buss71] instabilities, which lead, via transverse destabilization, to secondary patterns in many two-dimensional stationary patterns forming systems such as fluids, chemical systems etc. [Kram85, Pena03]. Very often, however, nonlinearities lead to spatiotemporal chaos, which is again a very broad branch of science [Stro14, Hilb94, Walg12].

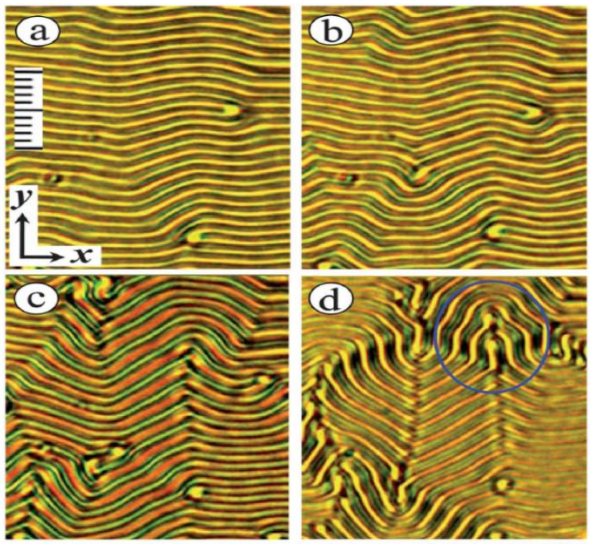

Figure 1.2.5: An example of secondary instability in liquid crystals. The images show the temporal evolution of an initial roll state evolving via transverse instabilities into more complex zigzag patterns (from [Tada12]).

1.3 Model Equations

As we have briefly reviewed, there are many different systems which show similar instabilities and pattern formation. While on the microscopic level every system is different from the other, it is evident that there are deep-lying similarities which manifest at the macroscopic scale. An attempt to generalize such features leads us to the formulation of simple enough model equations, which describe qualitatively similar pattern formation phenomenon in arbitrarily different systems. In other words, we aim to devise universal equations which are general enough to describe the dynamical behavior of a broad class of systems at a sufficiently basic level of detail. The trade-off, however, is that these models it themselves, cannot be expected to describe completely *all* the complexities of any of the given physical systems in full detail outside certain parameter regions.

One of the main motivations of this search for universality is this: by studying a certain behavior of the model, one can essentially understand the phenomenon occurring in *all* the various different systems belonging to that class. For instance, in the early decades of research in this field, many nonlinear phenomena which were well-known in hydrodynamics were being rediscovered in the context of lasers, so much so that this field was often referred to as the field of 'optical hydrodynamics' [Stal93, Long96]. Some of the most well-known model equations, describing common classes of instabilities in spatially-extended systems, are outlined in the following sections, with brief explanations.

1.3.1 Swift-Hohenberg Model

One such popular model is the Swift-Hohenberg equation, which in the most common form, is written as the real-valued order parameter equation:

$$\partial_t A = \varepsilon A - (\nabla^2 + 1)^2 A - A^3 \quad (1.3.1)$$

Originally defined in the context of hydrodynamics for describing the convective instability [Swif77], it has been widely used for the description of a large class of pattern-forming systems. The real-valued Swift-Hohenberg model describes a wealth of different pattern forming states and nonlinear structures [Lega94, Kozy07, Tlid94].

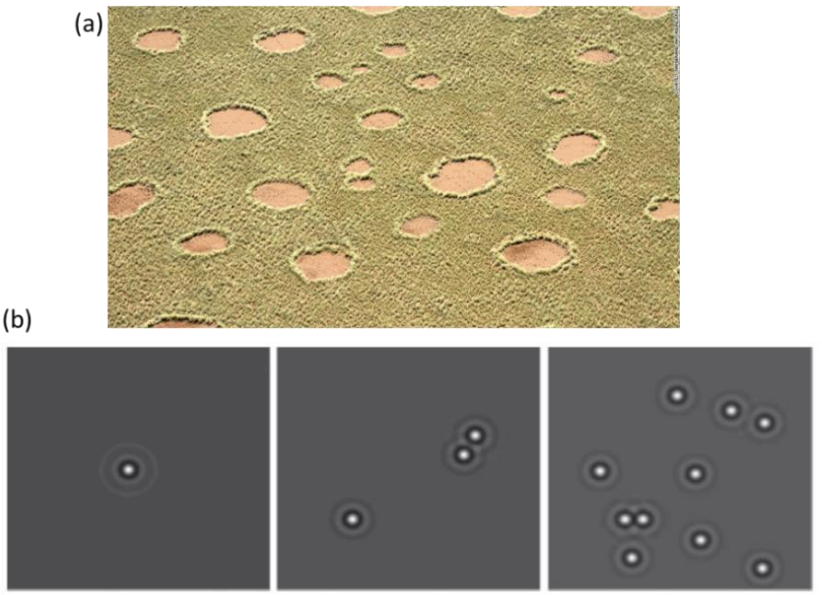

Figure 1.3.1: (a) An example of localized patterns in nature are these striking structures in vegetation, known as 'fairy-circles', found across the south-African continent in semi-arid climate regions. (b) The Swift-Hohenberg model is a good candidate for the modelling of these localized patterns, as shown in this study [Tlid08], where the spots represent bare-patches (white regions) on a background of homogeneous vegetation (gray region) (from [Tlid08]).

It has been especially successful in the description of spatially localized stable solutions [Burk06, Akhm05] across many different systems, from optics [Tara98] to semiconductor lasers [Tlid12] and vegetation patterns in ecology [Tlid08]. An extension of the real Swift-Hohenberg model to complex variables is sometimes used to describe many different types of pattern formation phenomena [Stal97,

Ques16]. A detailed description of the SH model is not the aim of this chapter, and much literature on it can found elsewhere, for instance in [Lega94, Kozy07] and references therein.

1.3.2 Reaction-Diffusion Models

Then there are the reaction-diffusion models, which as the name suggests, describe the dynamics of quantities reacting with each other, and diffusing in space at different rates [Miur04]. The model, in a simplified general form, for two-component systems may be written as:

$$\begin{aligned} \partial_t u &= f(u,v) + D\nabla^2 u \\ \epsilon\partial_t u &= g(u,v) + \nabla^2 v \end{aligned} \tag{1.3.2}$$

where f, g are arbitrary nonlinear functions, *D* is the ratio of the diffusion coefficients of *u* and *v*, and $\epsilon \ll 1$. This small ϵ parameter introduces different time scales for the reaction dynamics while *D* controls the ratio of the diffusion rates of the two quantities. The well-known Turing mechanism [Turi52] is based on the reaction-diffusion model and thus, it naturally finds application in the description of chemical systems [Winf72, Kapr12] such as the Belousov–Zhabotinsky reactions. It is also widely applied to various biological [Kond10, Brit86] and ecological models of pattern formation [Cant04].

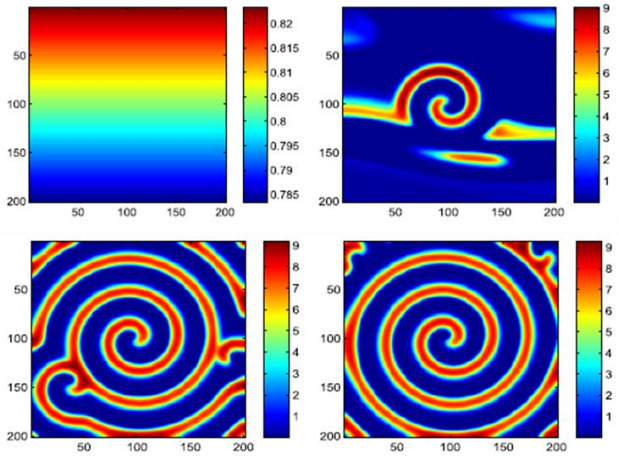

Figure 1.3.2: (Clockwise from top-left) Starting from the homogenous initial state, the formation and evolution of a rotating spiral wave in a reaction-diffusion model [Lian13].

1.3.3 Complex Ginzburg-Landau Model

While previous models represent the time evolution of real quantities, and thus describe non-oscillating pattern formation only, for the description of oscillatory systems a universal model is the Complex Ginzburg-Landau equation (CGLE). In a general from the CGLE can be written as:

$$\partial_t A = (d_1 + ib_1)\nabla^2 A + (p - ic_1)(1 - |A|^2)A \tag{1.3.3}$$

Where, d_1 and b_1 are the coefficients of diffusion and diffraction respectively, and c_1 is the coefficient of nonlinearity. In this form, the CGLE is known as the cubic CGLE. Other forms of the equations also exist, such as the cubic-quartic CGLE and the cubic-quintic CGLE, which include terms with higher order nonlinearities and have been described in various different contexts [Aran02].

The CGLE is a universally suitable model for homogeneous, spatially-extended systems close to the threshold of a finite (or long) wavelength oscillatory

instability, or in other words, at the threshold of a supercritical Hopf Bifurcation [Saar92, Moha05].

It has been derived systematically as the order parameter equation for many such pattern-forming systems. Some examples include the laser [Kart11, Vlad06, Coul89, Oppo91, Stal93], oscillatory chemical systems [Ipse97, Kura76], polariton condensates [Keel08, Caru13], hydrodynamic flows, electroconvection in liquid crystals [Kram95], among others [Hake75].

The CGLE exhibits the long-wavelength modulation instability, or the Benjamin Feir instability in hydrodynamics and supports a large number of fascinating nonlinear structures like solitons, spirals, two-dimensional vortices and three-dimensional vortex filaments etc. [Aran02], as well as demonstrating nonlinear phenomena such as turbulence and spatiotemporal chaos [Bart90, Shra92]. Some complex vortex structures supported by the CGLE are shown in Fig.1.3.3. All these properties make it an excellent candidate for a generic study of modulation instability in spatially-extended nonlinear systems.

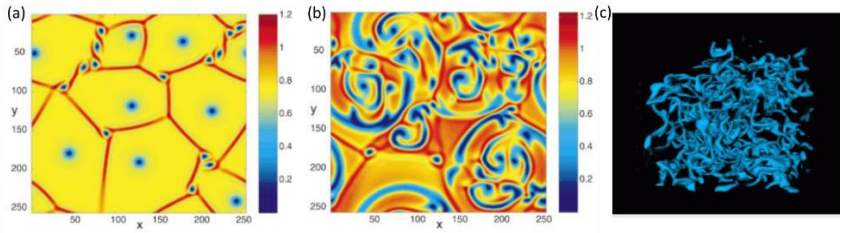

Figure 1.3.3: Examples of spatiotemporal pattern formation CGLE. A stable 'vortex glass' state (a), and turbulent vortices (b), in the 2D CGLE (see [Kevr02]). (c) An unstable 3D vortex filament (from [Aran02]).

1.3.4 Nonlinear Schrödinger Equation

In the conservative limit, the CGLE reduces to the very well-known Nonlinear Schrodinger equation (NLSE), which is one of the most important equations of

mathematical physics for describing conservative systems. It is a universal model for nonlinear dispersive waves in many physical systems including fluids [Ablo11, Osbo10], optical fibers [Agra07], plasmas [Zakh72], magnetic spin waves [Zved83], and Bose-Einstein condensates. In the latter system, the NLSE is known as the Gross-Pitaevskii equation [Pita03]. The NLSE, despite its apparent simplicity, supports a variety of fascinating nonlinear structures like solitons, breathers, recurrences, etc. [Trom01], and more recently, traveling 'bullet' solutions on finite backgrounds [Kuma17]. It is hence, undoubtedly one of the most fundamental, attractive and rich models for physicists and mathematicians.

1.4 Modulation Instability in Various Physical Systems

Linear instabilities lead to pattern formation or spatiotemporal chaos in many spatially-extended nonlinear systems. One of the most predominant of these is the Modulation Instability (MI), also known as the Benjamin-Feir instability in the context of hydrodynamics or the Bespalov-Talanov instability [Besp66]. MI has been a subject of a great deal of research in the past decades [Zakh09], and a brief overview of this phenomenon for different physical systems in various branches of science is provided in this section.

1.4.1 MI in Spatially-Extended Systems

In **optics,** this instability is ubiquitous and manifests at operating powers in the nonlinear regimes. In self-focusing (Kerr) materials, a spatially homogeneous wavefront breaks up due to the presence of MI, leading to *filamentation* (see Fig.

1.4.1(a)) and ultimately to wave collapse [Berg98, Camp73]. This phenomenon, both in isotropic and anisotropic optical media, is responsible for pattern formation in optical resonators [Stal03], in nonlinear optics [Stal98] and optical devices [Fang00, Male01].

MI is observed in various different optical systems including anisotropic media, incoherent light sources, nonlocal media, and other optical structures. [Mama96, Kip00, Pecc03, Tikh96]. In many devices, such as lasers, MI poses serious limitations on the operating power, as it leads to serious deterioration of the beam quality at higher operating powers [Prat07].

However, in some materials where the nonlinearity causes a strong saturation of the intensity, leading to a stabilizing effect such collapse may be prevented. In such cases, the MI provides a way for the generation of optical solitons and also optical bullets [Mcle95], which has opened up an exciting field of research and applications. MI has also been used for the generation of novel optical fields such as supercontinuum sources of light [Demi05], ultrashort pulse generation [Agra07] and more recently, optical rogue waves [Soll07, Gibs16] as shown in Fig. 1.4.1(b). All of these lie at the forefront of current research in photonics.

MI has also been widely studied in **plasma** physics, where it leads to many significant effects. For example, the modulation instability of plasma oscillations can lead to weak or strong turbulent states [Thor78, Gold84] and spatiotemporal structures such as filaments, solitons [Wong75, Anti81] and other nonlinear states [Ikez76]. Evidence for such phenomena has been found in numerous experiments in the laboratory [Saye15], and in the natural world [Stub92].

Bose-Einstein Condensates (BECs) provide another good playground for the observation of MI in spatially-extended systems [Kevr04, Carr04]. MI in BECs originates from the nonlinear atomic interactions in the system that may be attractive (modulationally unstable) or repulsive (modulationally stable) in simple single component BECs, while the interactions can be manipulated in two component systems. BECs support many fascinating nonlinear structures such as

bright and dark solitons, vortices (see Fig.1.4.1(c)), quantum filaments etc. as well as other complex dynamics [Sala03, Smer02, Wach16] where MI plays a critical role in their generation [Kono02, Li05].

MI was first studied in the field of **hydrodynamics**, by Benjamin and Feir [Benj67a, Benj67b], who demonstrated the existence of nonlinear surface waves on a deep body of water. Although these waves can exist, they are unstable, and the instability grows through small modulations of the carrier wave. The resulting sidebands grow exponentially, leading to the eventual breakup of the wave itself. This growth of the unstable sidebands, through small amplitude modulation of the stationary wave, came to be widely known as modulation instability.

As a result of the intense research on MI in fluids a few decades ago [Yuen82, Zakh68], many fascinating nonlinear phenomena have been discovered such as solitons, breathers, recurrence phenomenon etc. and more recently, perhaps also the generation of rogue waves [Zhou12, Lake77, Khar03, Chab11].

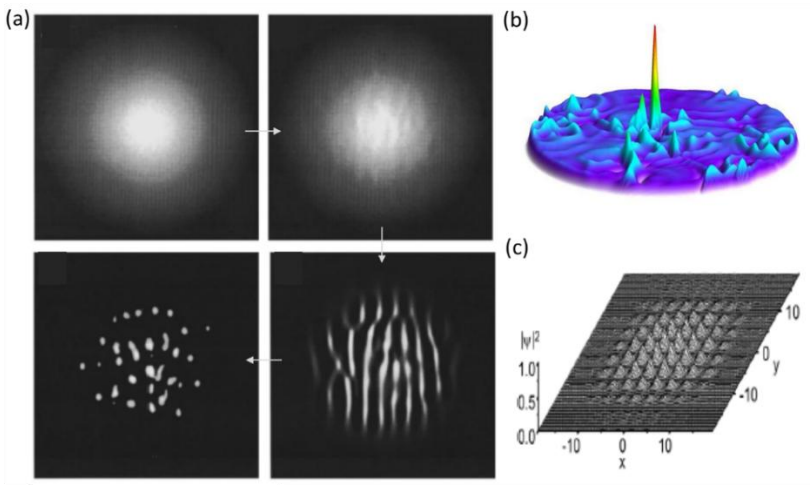

Figure 1.4.1: (a) Snapshots during the process of MI induced filamentation of a radially symmetric Gaussian beam at different propagation distances [Mama96] (b) Generation of an optical rogue wave [Gibs16]. (c) Formation of a vortex lattice in BECs, from an initially symmetric state [Baiz02].

Apart from the above more intensely studied systems, there are a lot of evidence of MI in various other spatially-extended systems. Such instabilities have been found in surface plasmon polaritons [Lin09, Kuma17], in electromagnetic waves [Ostr72], astrophysics [Haar81] and many others [Krol2001, He12].

1.4.2 MI in Discrete and Spatially-Confined Systems

The research on MI has a long history in discrete and spatially confined systems as well, where it finds huge applications. Although discrete systems are not a focus of this thesis, some very common examples of MI in these systems, such as waveguide arrays and optical fibers, are worth mentioning. In optical fibers, for instance, it has been one of the most extensively studied phenomena in the last decades [Agra07]. Solitons, soliton trains, ultrashort pulses and supercontinuum sources of light are a few of the applications resulting directly from the exploitation of the MI phenomenon which finds huge applications in modern technology. The rapid pace and growth of modern telecommunications drive an intense research and engineering effort into fiber optics where the presence of MI is universal. The vast literature, however, is beyond the scope of this introductory chapter on MI, and since it is not the aim of this thesis to study MI in such systems, a literature review on it is left untouched.

1.5 Existing Methods of Controlling Instability

It is evident from the vast array of examples, that there are two sides of the phenomenon of MI relevant to technology. On one hand, this phenomenon is useful and exploited in modern technology to generate a large number of useful spatiotemporal fields and structures such as solitons, ultrashort pulses, spectrally broad sources of light, etc. And on the other hand, its presence adversely affects the spatial field structures in many systems, leading to unwanted and often

limiting phenomenon such as filamentation of light in many laser systems. In this context, a mechanism for the suppression of MI is highly desirable.

The control of instabilities, spatiotemporal turbulence and in general the complex behavior of a dynamical system is broadly known in the literature as the control of chaos. Due to the presence of nonlinearities and feedback loops, the variables of such systems have a critical dependence on the initial conditions of the system with exponentially diverging different trajectories in the phase space that further add to the property of unpredictability.

In many applications these features are undesirable and a dynamical control of these instabilities is needed to stabilize the systems into simple phase-space trajectories such as periodic orbits or stationary states.

The control of chaos in low-dimensional systems (or discrete systems), which have a finite number of degrees of freedom, several methods have been proposed [Bocc00]. The main idea of the stabilization of such systems is the introduction of appropriate, small temporal perturbations to the system when its natural trajectory is close to the desired, stable trajectory. This is essentially exploiting the property of the extreme sensitivity of the system to small changes, in order to push the system back into the stable manifold through small temporal perturbations of a control parameter. The first example of such chaos control was given by Ott, Grebogi and Yorke [Ott90] and it has been demonstrated in different physical systems [Garf92, Munk97, Biel94]. Another major technique for such systems has been the use feedback and delayed feedback control to stabilize a periodic orbit of the system [Pyra92, Pyra93].

However, the stabilization of high-dimensional, spatially-extended systems turns out to be a significantly more ambitious goal. Such systems show pattern formations due to a continuum (an infinite number) of unstable spatial modes. Therefore the stabilization of spatially-extended systems means the suppression of an infinite number of unstable modes within the instability band, which is possible only in very limited extents by such feedback schemes.

One such attempt to stabilize spatiotemporal systems is the use of external driving (forcing) of the system with spatiotemporal functions. These methods too have only limited applicability, which is for systems presenting low-dimensional chaos [Gome15].

Another such mechanism relies on applying a tightly focused potential to the homogenous field, which has been observed to control long wavelength instabilities, for example in plasmas [Kevr04]. While yet another approach has been through the introduction of higher dissipation into the system with narrow unstable bands [Segu05]. However, these two approaches, while applicable to some extend in specific scenarios, are not generic mechanisms of suppression of MI. In the first case, of a tightly binding spatial modulation with sufficiently small periods, the mechanism simply acts as a filter for wavelengths larger than the size of the half-period of the modulation; in a manner similar to a resonator which supports wavelength only smaller than its 'cut-off wavelength'. In the second scenario, the decrease of MI with increasing dissipation in a system is a well-known property.

While these mechanisms have been applied in a very limited sense in some cases, a general mechanism for the suppression of MI still eludes us. In this thesis, a new mechanism for the suppression and manipulation of MI for spatially-extended oscillatory systems is presented. This new mechanism is based on a new understanding of a fundamental physical phenomenon, which is the link between the dispersion relations of oscillatory systems with the presence and character of the MI present in it. Using a spatiotemporal modulation of the potential, under a unique, 'resonant' geometric relation, the MI in a system can be suppressed and manipulated with unprecedented control. Moreover, this phenomenon has a general character, which is expected to be universally applicable to various different spatially-extended oscillatory systems across many fields of physics.

1.6 Conclusions

Patterns in nature have always been a fascination and inspiration for mankind. Beginning with the first scientific approach to simple, geometric patterns in art and mathematics many centuries ago, we have come to a much deeper understanding of the underlying universal laws and mechanisms that govern the formation of patterns across different fields of science.

In this brief introduction, an overview of different dynamical instabilities and the nonlinear route to pattern formation was presented. In the search for 'qualitative universal' models of pattern formation phenomena, certain order parameter equations like the Swift-Hohenberg and Complex Ginzburg-Landau Equations have provided a paradigm shift. An introduction to some of these mathematical equations used to describe and study the linear instabilities in such systems was provided. The MI, which is the main concern of this thesis work was presented in the case of various different systems, and a brief review of the methods for the control of instabilities was presented.

The main work of this thesis, presented in the following chapters, is the development of a new method for the control and stabilization of MI is developed. The thesis can be roughly divided into two main parts: proposal of the idea and application of the idea. The first part is covered in Chapters 2 and 3, where the main idea of the thesis is developed, and the suppression and manipulation of MI in spatially-extended oscillatory systems is demonstrated on a model of the CGLE. Using a spatiotemporal modulation of the potential with a 'resonant' geometry, the MI in a system can be suppressed. And generalizing this idea to more complex spatiotemporal modulation geometries, the MI in the system can be manipulated to an unprecedented degree of control. The analysis being based on the Complex Ginzburg-Landau equation, lends its universal applicability, as this is often used as the order parameter model in a huge range of different physical systems.

In the second part, presented in Chapter 4, the applicability of the proposed method is demonstrated in real physical systems. In this chapter, we demonstrate the stabilization of Broad Area Semiconductor amplifiers and Vertical Cavity Surface Emitting Semiconductor Lasers by these techniques. These results successfully establish the proof of principle of these new stabilization methods and open the door to potential applications in various different systems.

Chapter 2

Suppression of Modulation Instability via Spatiotemporal Modulation

Contents

2.1 Introduction

We have seen in the previous chapter that Modulation Instability (MI) is a persistent phenomenon in nonlinear spatially extended systems which leads to a spontaneous deformation of the homogenous, steady-state solution through exponentially growing sidebands. This instability, although heavily exploited for many useful applications in spatially *confined* systems such as optical fibers, is often a serious hindrance in many spatially extended systems (see Section 1.3 of the previous chapter). Often in such systems, the growth of unstable sidebands from MI leads to turbulence of the field, spatiotemporal chaos, and other nonlinear structures. [Shra92]. In fact, the origin of most complex structures in such nonlinear systems lies in the MI, which dominates in the linear stages of field propagation and eventually dictates the long term spatiotemporal dynamics of the system.

In this chapter, we will explore the phenomenon of MI, using the Complex Ginzburg-Landau Equation (CGLE) model, which provides a universal representation of this phenomenon in such spatially extended systems [Aran02]. The aim of this study is to provide a mechanism for the suppression of this instability- a stabilization technique- such that the steady-state solution remains stable in propagation in the presence of noise, for arbitrarily long times. Although being developed on a model of the CGLE, this stabilization mechanism entails a general character, meaning that it could be applied to a large class of systems which are described asymptotically by the CGLE.

The chapter is structured as follows: we begin by characterizing the mechanism of MI in the CGLE, in Section 2.2, by performing a standard linear stability analysis of its stationary, steady-state solution. The results reveal that an intricate link connects the dispersion profile of the system and the character of its MI. This connection is explored in Section 2.3, and a new idea is proposed for the control of MI in a system based on the manipulation of dispersion. A stabilization method

is then proposed, in Section 2.4, based on a spatiotemporal modulation of the potential of the system. Following that, in section 2.5, a numerical procedure for a modified Floquet linear stability analysis is developed for the analysis of MI in spatiotemporally modulated systems. The stabilization performance is analyzed and the results presented in Section 2.6, for one-dimensional CGLE. Finally, Section 2.7 shows how the entire analysis is extended to (2 spatial + 1 temporal) dimension CGLE, with positive results. Lastly, Section 2.8, summarizes the most relevant conclusions from this study.

The model of the CGLE used in this thesis can be written in a conveniently normalized form, for one spatial dimension as:

$$\partial_t A = (i + d)\partial_{xx}^2 A + (1 - ic)(1 - |A|^2)A \tag{2.1.1}$$

The notations ∂_t and ∂_{xx}^2 represent the partial derivative with respect to time and partial double derivative with respect to space respectively. The gain threshold and the dispersion coefficient in Eq. (2.1.1) are normalized to unity, without any loss of generality. In this form, the CGLE contains only two independent parameters: the coefficient of the cubic nonlinearity, c, and the diffusion coefficient d.

2.2 Linear Stability Analysis of the Complex Ginzburg-Landau Equation

To characterize the stability of the CGLE one must perform a standard linear stability analysis [Besp66]. In this procedure the stationary (steady-state), a non-zero homogenous solution of Eq. (2.1.1), is subjected to a small spatial perturbation of the form: $A(x,t) = A_0 + a(t)\cos(kx)$ where, $A_0 = 1,\ |a| \ll 1$.

Substituting $A(x,t)$ back into Eq. (2.1.1) and simplifying for the first order terms leads to:

$$\partial_t a = -k^2(i+d)a \; - \; (1-ic)(a+a^*) \tag{2.2.1}$$

By replacing the complex perturbation a into the form: $a = a_1 + ia_2$ and separating out the real and imaginary parts, we obtain a set of coupled equations:

$$\begin{pmatrix} \partial_t a_1 \\ \partial_t a_2 \end{pmatrix} = \begin{pmatrix} -dk^2 - 2 & k^2 \\ -k^2 + 2c & -dk^2 \end{pmatrix} \begin{pmatrix} a_1 \\ a_2 \end{pmatrix} \tag{2.2.2}$$

This is now an eigenvalue problem for the complex perturbation, of the form: $\partial_t a(t) = \lambda a(t)$, whose solution represents an exponential dependence of the complex perturbation in time $a(t) = a_0 exp(\lambda t)$. Thus the solution of Eq.(2.2.2) provides us with the spectrum of the eigenvalues, of the growing or decaying perturbation modes:

$$\lambda(k) = -(1+dk^2) \; \pm \; \sqrt{1+2ck^2-k^4} \tag{2.2.3}$$

The real part of the eigenvalues in Eq. (2.2.3) is called the growth exponent, which in the case of spatially confined systems is commonly known as the Lyapunov exponent $\lambda_{Re}(k) = Re\{\lambda(k)\}$ - a term which we shall use in this thesis as well, although we deal with spatially extended systems.

In the case when the Lyapunov exponents are positive, $\lambda_{Re}(k) > 0$ the perturbation modes grow exponentially with time, signifying an unstable system. While conversely, when $\lambda_{Re}(k) < 0$, the perturbation modes decay exponentially with time and the system is stable with respect to small complex perturbations. This is the meaning of linear stability analysis and it is an important tool for analysing the stability of the system in the initial stages of growth of the perturbation.

From Eq. (2.2.3) it becomes clear that MI can only occur when $c > 0$. Such is the situation, for example, in the so-called 'focusing' or Kerr nonlinearity in case of optics or 'attractive-condensates' in case of Bose-Einstein Condensates (BECs).

On the contrary, for $c < 0$, the system is modulationally stable, that is, all perturbations to the stationary solution decay exponentially, and the system remains in the original state.

Since this work is focused on the stabilization of modulationally unstable system, we shall be concerned with the cases of $c > 0$, for the entire thesis.

It is also true that for a given set of parameters, the value of $\lambda_{Re}(k)$ decreases with increasing coefficient of diffusion, d [Zakh09]. In simple terms, it means that the presence of diffusion in the system tends to stabilize it- the higher is the coefficient of diffusion, the smaller are the Lyapunov exponents.

In pursuit of simplicity, however, we will generally only consider the most symmetric case of $d = 0$, that is, without the presence of diffusion in the system. Nevertheless, without loss of any qualitative effects, all the results can be generally extended to positive or negative diffusion values: In those cases, the CGLE is simply more or less stable, respectively, than in the case of $d = 0$.

In the modulationally unstable case $(c > 0)$, the range of the unstable spatial wavevectors can be determined by solving Eq. (2.2.3) for $\lambda_{Re}(k) > 0$. This leads to the inequality: $0 < k_{unstable}^2 < 2(c - d)/(1 + d^2)$ which in the case of $d = 0$ is:

$$0 < k_{unstable}^2 < 2c \tag{2.2.4}$$

A typical Lyapunov spectrum for such a system is plotted using Eq. (2.2.3) in Fig. 2.2.1.

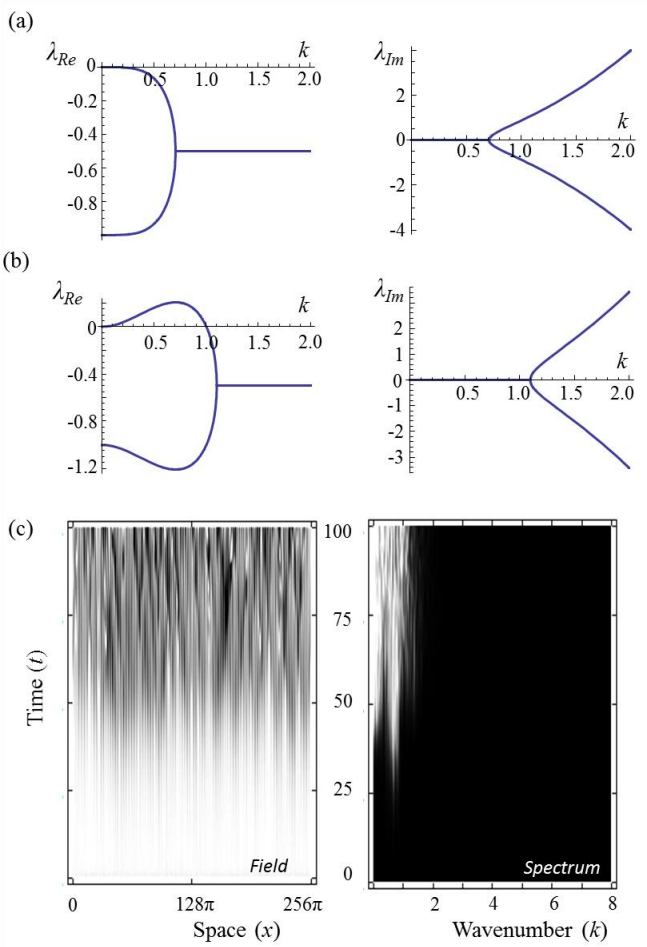

Figure 2.2.1: The typical shape of the Lyapunov spectra in modulationally stable (a) and unstable (b) systems, showing the real (left) and imaginary (right) parts of the Lyapunov growth exponents. (c) Temporal evolution in the unstable regime leads to spatiotemporal chaos as shown in the field (left) and spectral (right) dynamics.

2.3 Modulation Instability and Dispersion

A more detailed inspection of the linear stability analysis indicates that, for a fixed coefficient of nonlinearity, the character of the MI depends uniquely on the character of the dispersion relation of the system. The Laplace operator ∂_{xx}^2 in Eq.

(2.1.1) introduces, into the system, a parabolic dispersion profile: $\omega(k) = -k^2$ where $\omega(k)$ represents the frequency spectrum of the spatial modes.

It is evident, from Eq. (2.2.4), that for this parabolic dispersion profile there exists a range of unstable frequencies lying within the band: $-2c < \omega(k) < 0$. This is illustrated in Fig. 2.3.1(a). Assuming for a moment that the dispersion profile can be modified, a generalized CGLE can be written, for an arbitrary operator of the dispersion $\widehat{\omega}(\partial_x)$:

$$\partial_t A = i\widehat{\omega}(\partial_x)A + (1 - ic)(1 - |A|^2)A \tag{2.3.1}$$

Where the spatial differential operator of the dispersion, $\widehat{\omega}(\partial_x)$, has a corresponding dispersion profile $\widetilde{\omega}(k)$. The dispersion for the neutral mode may be normalized to zero, without any loss of generality. In such a scenario, the stability analysis of the CGLE with generalized dispersion, Eq. (2.3.1), results in:

$$\lambda(k) = -1 \pm \sqrt{1 - 2c\widetilde{\omega}(k) - \widetilde{\omega}^2(k)} \tag{2.3.2}$$

This implies that the instability of the spatial modes, k, is entirely determined by the profile of the dispersion, $\widetilde{\omega}(k)$, and the condition for the occurrence of MI, following directly from Eq. (2.2.4), becomes: $-2c < \widetilde{\omega}(k) < 0$. This means that the stability of the stationary solution of the CGLE with generalized dispersion depends solely upon the presence of spatial modes with frequencies within a particular unstable frequency band, as illustrated in Fig. 2.3.1.

Thus, the shape of the dispersion profile is the critical determining factor for the character of the MI in the system. This leads to the possibility of manipulating the MI in a system by reshaping its dispersion profile. This manipulation could, in general, be of different kinds- suppression or enhancement, partial or complete, depending on the scope of reshaping the dispersion. In this thesis, we will mainly focus on suppression or elimination of MI from the system in order to stabilize it.

In fact, it is known that the spatial dispersion profile of linear systems can be modified by introducing small-scale spatial or temporal modulations of the

potential [Yalb87, Stal06a]. The modification of dispersion by small-scale spatial modulations is, for instance, the basis of controlling light-matter interactions in many periodic systems.

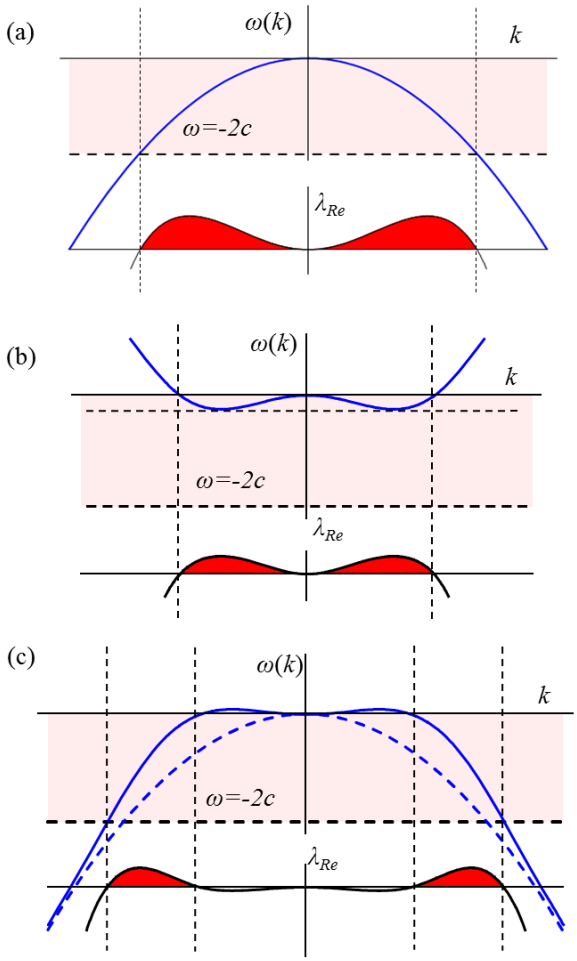

Figure 2.3.1: A schematic representation of the origin of MI arising from unstable bands in the dispersion profile of a system. (a) The parabolic dispersion profile of the CGLE, with the unstable band denoted by the pink region. All spatial wavevectors, k, falling in this region are unstable, with a corresponding instability spectrum shown directly under it. (b) The modification of the dispersion lifts larger wavevectors outside the instability spectrum leading to partial stabilization with a remaining long-wavelength instability. (c) Modifying dispersion for to remove smaller wavevectors from the instability band leads to partial stabilization with remaining short- wavelength instability.

In Photonic Crystals, for example, small-scale periodic modulations result in the formation of photonic bandgaps which lead to unprecedented control of light in novel ways in these materials [Yalb87]. In this context, a large variety of different phenomena from light collimation, to spatial filtering have been demonstrated [Maig14, Maig15, Joan11]. Such dispersion management, by purely spatial small-scale periodic modulations of the potential, also underlies the phenomenon of bandgap solitons in atomic condensates [Stee98, Ostr03, Eier03, Cont04, Stal06b, Stal06c], solitons in cavities [Egor07, Stal07], and can lead to filtering effects in BECs [Stal11]. On the other hand, the tailoring of diffraction by a spatiotemporal modulation, in the case of defocusing nonlinear media, can lead to sub-diffractive solitons [Stal08a, Stal08b]. Similar modulation schemes have also been reported in different gain/loss materials in photonics, leading to effects such as subdiffractive propagation [Stal09a, Kuma12] and beam shaping [Herr12, Radz13] which is related to the spatial filtering (in linear limits) in optics [Stal09b, Maig15] and photonic [Gail16].

Thus, we have seen two different ideas: (i) The MI depends essentially on the shape of the spatial dispersion and (ii) spatial and temporal periodic modulations of the potential can lead to a reshaping of the dispersion profile of the system. If one could effectively combine these two ideas, a new method for the control of MI would be created. That is, through an appropriate spatiotemporal modulation of the potential, a reshaping of the dispersion profile and ultimately of the Lyapunov spectrum would become possible. For appropriately designed modulations, a suppression of the MI- partially or even completely, would be made possible.

The rest of this chapter is devoted to exploring and substantiating this proposal on the basis of the CGLE model.

2.4 Manipulation of MI through Periodic Spatiotemporal Modulation of the Potential

In this section, the effect of a periodic spatiotemporal modulation on the dispersion of a *linear* system is analyzed. The analysis is presented for the simplest case of a periodic spatiotemporal modulation– sinusoidal modulation in both, the longitudinal (time) and transverse (space) coordinates. The modulation potential in such case can be described as $M(x,t) = imCos(qx)Cos(\Omega t)$, where m is the amplitude, q is the spatial wavenumber and Ω the temporal frequency of the modulation. The profile of such a modulation is shown in Fig. 2.4.1.

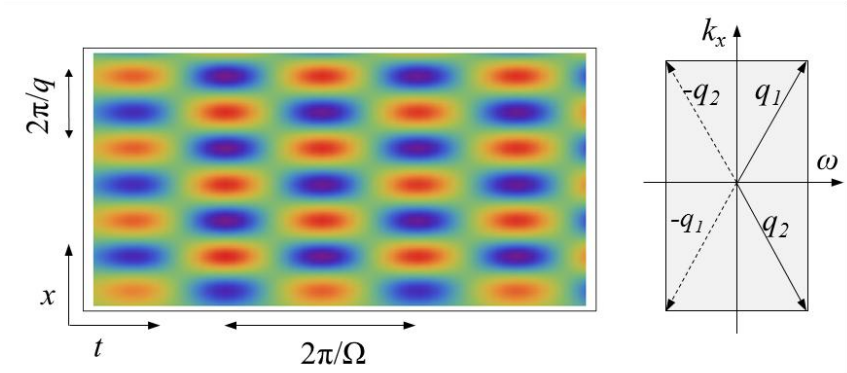

Figure 2.4.1: The profile of the spatiotemporal modulation in space-time (left) and its representation in the Fourier space (right).

This periodic spatiotemporal modulation is introduced phenomenologically into the *linear* CGLE, which now reads:

$$\partial_t A = (i+d)\partial_{xx}^2 A + (1-ic)A + imCos(qx)Cos(\Omega t)A \qquad (2.4.1)$$

The modulation is considered on small space and fast time scales, that is, $|q| \gg |k|$ and $|\Omega| \gg |\lambda|$, where k and λ are the typical wavenumber and growth exponent of the MI in unmodulated CGLE.

The solution of the modulated CGLE Eq. (2.4.1) can be represented as a series of harmonic Bloch modes of the form:

$$A(x,t) = \sum_{j,l} A_{j,l} exp[i(k+jq)x + i(\omega + l\Omega)t] \tag{2.4.2}$$

where, $(j,l) = \{\dots -2, -1, 0, 1, 2 \dots\}$. When this ansatz is substituted into Eq.(2.4.1) and subsequently expanded, it leads to an equation where, depending on the truncation order of the series, the different (j,l) harmonics are present. These harmonics are independently separated and result in a system of $(j \times l + 1)$ coupled equations.

In the simplest case, considering two spatial and one temporal mode, that is, $j = \{-1,1\}$ and $l = 1$ (the reason for choosing such will become apparent later) we have the following set of coupled equations:

$$\frac{\partial}{\partial t}\begin{pmatrix} A_{-1,1} \\ A_{0,0} \\ A_{1,1} \end{pmatrix} = \begin{pmatrix} \xi(-q) & im & 0 \\ im & \xi(0) & im \\ 0 & im & \xi(q) \end{pmatrix}\begin{pmatrix} A_{-1,1} \\ A_{0,0} \\ A_{1,1} \end{pmatrix} \tag{2.4.3}$$

where, $\xi(\theta) = 1 - ic + i\Omega - (i+d)(k+\theta)^2$.

The eigenvalues of these three coupled equations result in the dispersion relations for the Bloch modes, which is represented schematically in Fig. 2.4.2.

The dispersion relation of the zero modes $(j, l = 0)$ is the parabola $\omega = -k^2$, represented by the central parabola in Fig. 2.4.2(a). The presence of the spatiotemporal modulation results in the generation of additional parabolas centred around $(\pm q, \Omega)$, as shown by the dashed curves in Fig. 2.4.2. When the modulation amplitude is zero $(m = 0)$, the couplings between the different harmonics is also zero (given by the off-diagonal terms in Eq.(2.4.3)) and the parabolas do not interact. In this situation the system behaves identical to the unmodulated CGLE as shown in Fig. 2.4.2(a).

However, when the modulation strength is slowly increased, the degeneracy is lifted and the parabolas split up at the points of crossing, forming 'gaps'

(equivalent to the well-known bandgaps) in the dispersion relation as shown in Fig. 2.4.2(b).

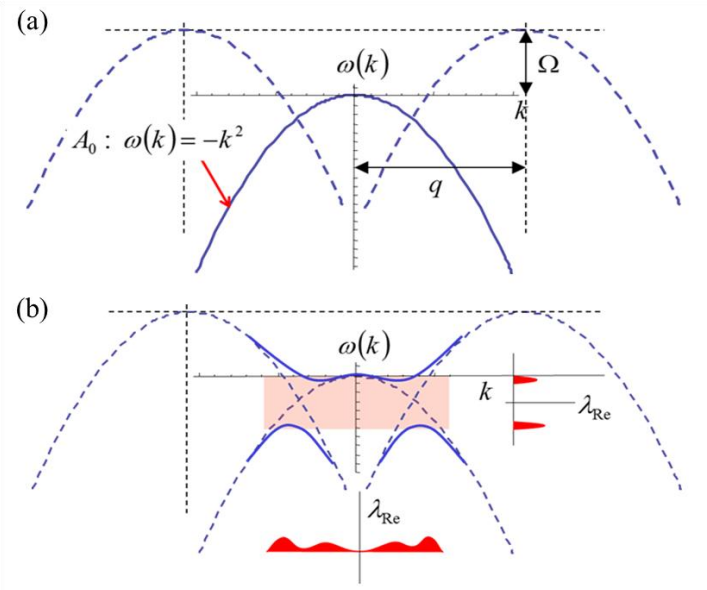

Figure 2.4.2: The dispersion profile of spatiotemporally modulated CGLE for zero-amplitude modulation ($m = 0$) (a), and nonzero-amplitude modulation ($m \neq 0$) (b). The introduction of the modulation with spatial frequency, q, and temporal frequency, Ω, leads to the generation of additional parabolas (dashed curves), shifted with respect to the central (solid curve) by $(\pm q, \pm\Omega)$ in the respective coordinates. Only the three most relevant parabolas are shown in the picture.

The above discussion is the case when we consider only two spatial harmonics and one temporal harmonic. The consideration of only two spatial harmonics has been deemed sufficient in various cases [Stal06a] and as this is more a proof of concept, than a rigorous calculation, this is a sufficient. Moreover, the higher spatial harmonics are far away from the smaller modes around $k = 0$, and thus have diminishingly small effect on the shape of dispersion around this point, which is in fact the region of primary importance for finite wavelength instabilities. In the temporal case, the above schematic represents only the positive harmonics; the presence of the negative harmonics would lead to two more identical parabolas

but shifted negatively by an equal amount. These two parabolas, however, are again not very relevant to the study of the bandgaps close to the smaller modes and can be similarly ignored.

The spatiotemporal modulation frequencies are now redefined in a more convenient form, the one which will be used throughout the rest of the thesis. An adimensional variable Q is defined as $Q = k_0\Omega/q_x^2$ where k_0 is the free space wavenumber of the propagating wave. This parameter Q is called the 'resonance parameter', as it represents a resonance between the spatial and the temporal harmonics when $Q \approx 1$. Around this point, the two lateral parabolas cross close to the origin in the (k, ω) plane, and most significantly affect the long-wavelength instabilities. This phenomenon is more clearly understood from Fig. 2.4.3. The plots demonstrate the effects of the modulation amplitude, m, and the resonance parameter, Q, in various different cases.

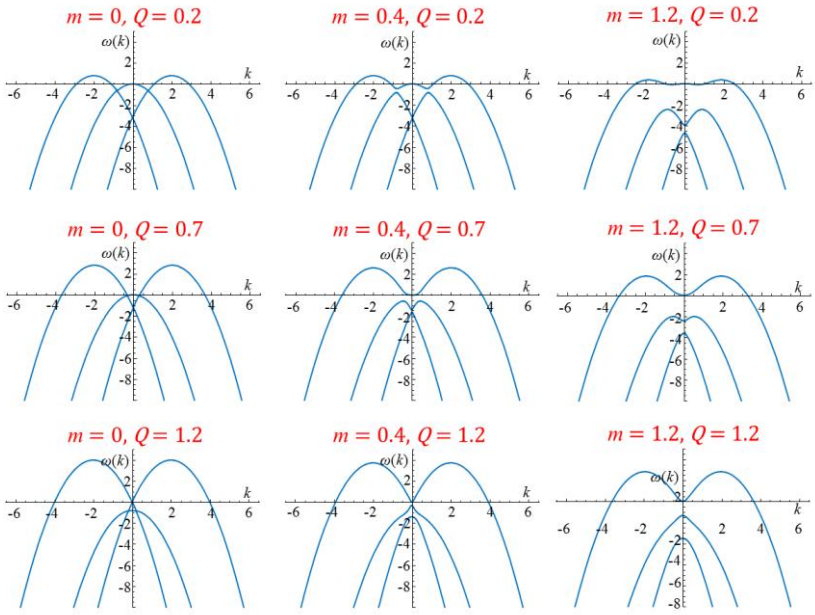

Figure 2.4.3: The plots show the dependence of the dispersion relation on the modulation strength, m, and resonance parameter, Q, for various different values. It is evident that the modulation strength dictates the size of the bandgap while the resonance parameter is responsible for the position and shape of the bandgap.

It is evident from Fig. 2.4.3 that the modulation amplitude, m, has a direct influence on the strength of the coupling between the parabolas, with larger bandgaps for larger amplitudes. On the other hand Q is closely related to the form of the bandgaps; for $Q < 1$, the two lateral parabolas intersect the central parabola before crossing the perpendicular axis, while for $Q > 1$, they cross the central parabola after crossing the perpendicular axis. At 'resonance', $Q = 1$, the parabolas cross the central parabola exactly on the perpendicular axis. These are qualitatively different regimes, which ultimately lead to different types of behaviour of the modulated steady-state solution. It is important to note, however, that the results are most interesting and of maximum significance only close to the resonance condition, $Q \approx 1$, on either sides.

It must also be kept in mind that this analysis of the dispersion relation in the presence of spatiotemporal modulations, is for a linear CGLE, that is, without the presence of nonlinearity. In the full nonlinear model, however, the dispersion relations will no doubt be slightly modified, depending on the strength of the nonlinearity. Yet, the general idea always holds; the manipulation of dispersion is possible through a spatiotemporal modulation of the potential of the system which leads to the appearance of bandgaps in the system. This phenomenon, when combined with the idea presented in Section 2.3, hints that the MI in the system can be directly affected, possibly even controlled, through an appropriate spatiotemporal modulation of the potential.

The following sections provide a detailed study of the properties of such spatiotemporally modulated CGLE and the suppression and control of the modulation instability in this system.

2.5 Spatiotemporal Modulation of the CGLE

Upon introducing the spatiotemporal modulation into the CGLE, the full model- the modulated CGLE becomes:

$$\partial_t A = (i+d)\partial_{xx}^2 A + (1-ic)(1-|A|^2)A + i4mCos(qx)Cos(\Omega t)A \quad (2.5.1)$$

In the presence of such spatiotemporal modulation, it is not feasible to perform the linear stability analysis analytically and one must resort to numerical techniques for the same. The numerical linear stability analysis technique described in this section is roughly based on the standard Floquet stability analysis procedure [Klau08]. The Floquet stability analysis, however, is for systems homogeneous in space but periodic in time. Therefore a modified procedure has been developed here, in order to incorporate the spatial periodicity. It is referred to as the modified Floquet linear stability analysis, or simply the modified Floquet analysis.

We begin by calculating the steady-state solution of Eq. (2.5.1), by truncating the expansion of the spatiotemporal harmonics to the fundamental and the two most significant harmonics, shifted by $(\pm q, +\Omega)$. This truncation has been proved useful for various linear [Stal06a] and nonlinear systems [Stal08a, Stal08b]. These three spatiotemporal harmonics, namely $(n,l) = (0,0), (-1,-1) \text{ and } (1,-1)$ are at, or close to, mutual resonance for $Q \approx 1$.

The steady-state solution in most cases, depending on the modulation parameters, is analogous to a Bloch mode, that is, a spatiotemporally periodic function with spatial period q and temporal period Ω, and with average amplitude equal to unity, as shown in Fig. 2.5.1.

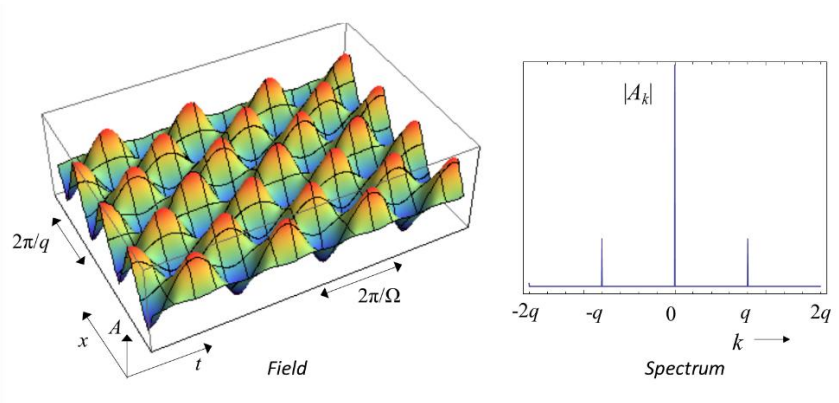

Figure 2.5.1: A representative plot of the steady-state Bloch mode of the spatiotemporally modulated CGLE showing the field (left) and the spatial spectrum (right) of the solution. The periodicities in the spatial and temporal domains of the field are related to the spatial frequency, q, and temporal frequency, Ω, of the modulation.

The numerical stability analysis proceeds by introducing a set of random perturbations to the steady-state Bloch modes in the form of separate, independent real and imaginary perturbations at each wavenumbers $+k$ and $-k$. For each case, the evolution of this set of perturbations is calculated by numerically integrating the perturbed steady solution over one temporal period Ω, illustrated as a Poincaré diagram in Fig. 2.5.2.

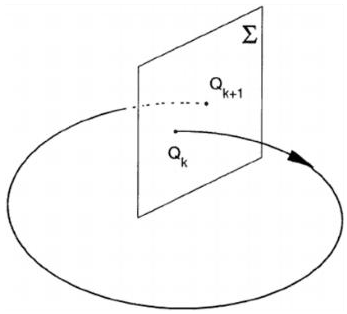

Figure 2.5.2: The Floquet linear stability analysis calculates the distance between the initial and final points for a given Poincaré section, as shown in this representation. The Floquet stability analysis calculates the distance between the points Q_{k+1} and Q_k, located infinitesimally small distance away from each other, after one temporal period Ω.

2.5.1 Modified Floquet Linear Stability Analysis

In the standard Floquet analysis, that is, in the absence of spatial modulation, the harmonics of small complex perturbations at wavenumbers $+k$ and $-k$ (in the Fourier space) are coupled. In such case, the evolution of four independent perturbations (real and imaginary perturbations for $\pm k$) must be numerically calculated for each pair of perturbation modes $a_1(k)$ and $a_2(-k)$. This leads to an evolution matrix of size (4×4). Diagonalizing the evolution matrix, we obtain the eigenvalues, $\lambda(k)$, for the perturbation modes, and the real part of these eigenvalues are the Lyapunov growth exponents, $\lambda_{Re}(k)$. This standard Floquet procedure must be modified in view of the spatial modulation of the potential, which causes a linear coupling between the spatial harmonics of the perturbation k, $k \pm q, k \pm 2q$ … In this case, a perturbation at any wavenumber k, is coupled to all these harmonics, which is represented in Fig.2.5.3.

By considering n spatial harmonics, the linear evolution matrix dimension is $(4n \times 4n)$. The diagonalization of this evolution matrix results in a set of eigenvalues (Floquet multipliers) and its real part provides the average (over a time-period) Lyapunov exponents, $\lambda_{Re}(k)$. In this study, typically four harmonics are considered, which lead to an evolution matrix of the size (16×16) and thus to a set of 16 different eigenvalues for each spatial mode, many of may be degenerate.

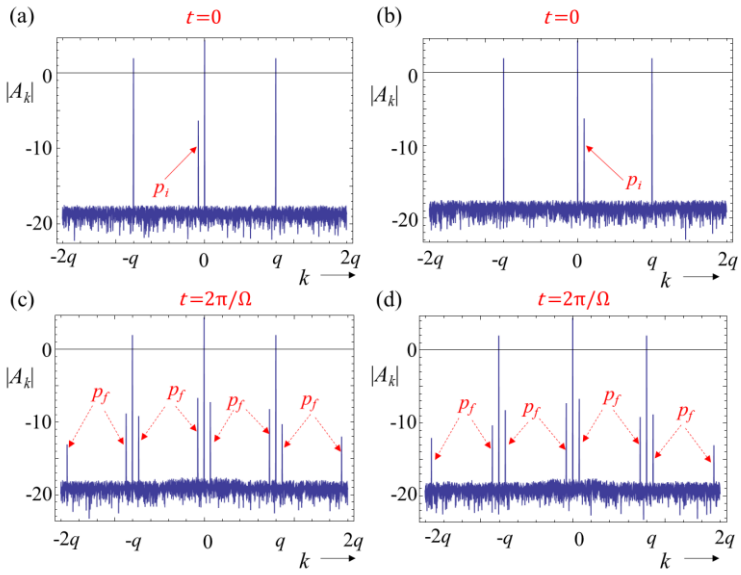

Figure 2.5.3: These plots, in the Fourier space, demonstrate the spatial coupling of the perturbations due to the spatial modulation, after one temporal period. Perturbations introduced at $-k$ (left) and k (right), are marked by the solid arrow in the top figures. After one temporal period, the new excited modes are indicated by the dashed arrows in the bottom figures. The vertical axes is in log scale.

The results of such modified Floquet stability analysis is presented in Fig. 2.5.4, for a particular set of spatial and temporal frequencies. The plot in Fig. 2.5.4(a) shows the result of the modified Floquet analysis for zero modulation depth, $m = 0$, which exactly coincides with the results from the unmodulated CGLE, as expected. Each of the various curves corresponds to one of the 16 eigenvalues of the system, with many of them being degenerate.

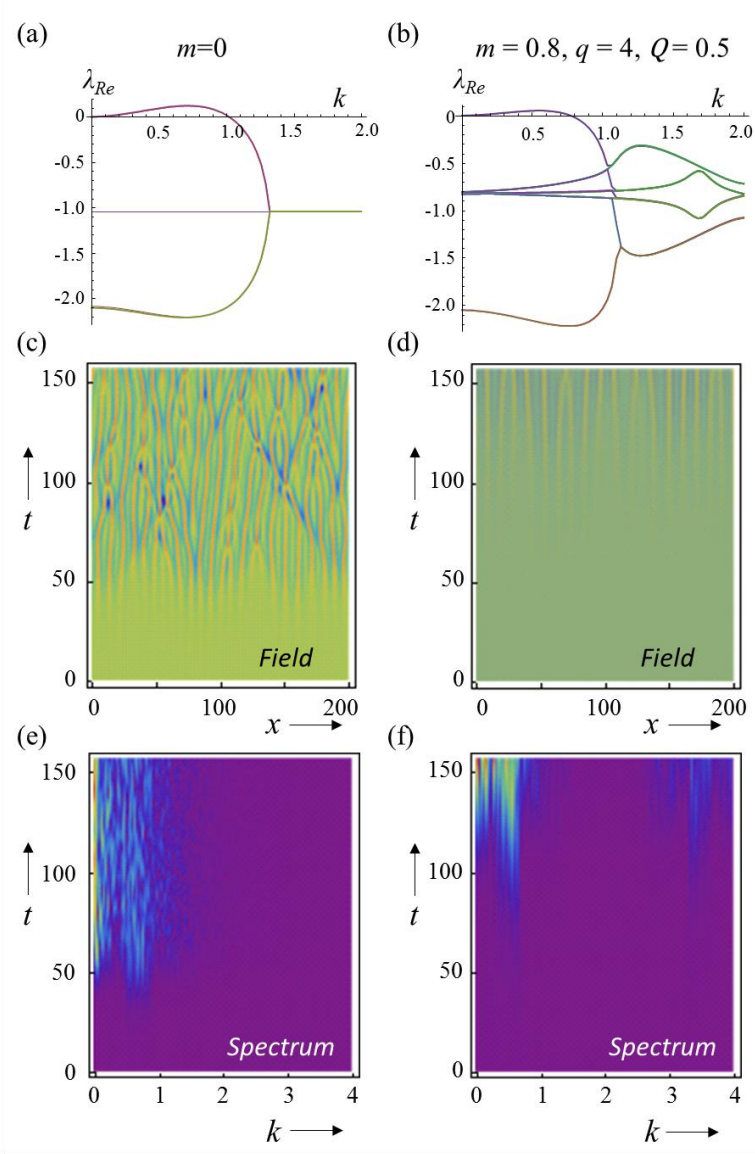

Figure 2.5.4: (a, b) The Lyapunov exponents obtained from the modified Floquet analysis for the unmodulated and modulated CGLE. The presence of nonzero modulation lifts some of the degeneracy in the systems, as seen by the distorted curves in (b). The nonlinear field dynamics from direct integration of the full model (c-d), and their corresponding spectra (e-f). It is evident that the modulation results in partial stability of the system: the field dynamics is quieter (d), and the spectrum narrower (f), as compared to the unmodulated case (c, e). The parameter are: c=0.5, d=0, space=64π, grid=512 points, with periodic boundary conditions.

The presence of a nonzero modulation ($m \neq 0$) lifts the degeneracy from some of the modes, as described in Section 2.4 (also see Fig. 2.4.3), and leads to a modification of the Lyapunov exponents, as shown in Fig. 2.5.4(b). Comparing the two plots it is clear that this particular modulation has two main effects: the spectrum of unstable wavenumbers is reduced and the value of the maximum Lyapunov exponent (λ_{Re}^{max}) is lowered. As a result of a smaller number of unstable modes, the resulting dynamics is comparatively less 'chaotic' than before. While a lowered λ_{Re}^{max} means that the most unstable mode grows comparatively slower, resulting in much longer times for the chaotic dynamics to set in. It is typical in nonlinear systems that the fastest growing mode 'hogs' the available energy the fastest, thereby depleting the other, slower growing modes and eventually dictating the scales of the emerging pattern. Therefore, in most cases, the characteristic wavelength of the pattern formation occurs at wavelength of the maximally unstable Lyapunov exponent. Thus, in the subsequent sections, the value of λ_{Re}^{max} will be the measure used to quantify the instability of the system.

It must be kept in mind that the full nonlinear dynamics cannot be characterized by the modified Floquet linear stability analysis which actually is the linearization of the nonlinear problem around the steady solution. It nevertheless gives us a deep insight into the character of the instability in the fully nonlinear regime of the CGLE, that is, for long propagation times. In any case, the results of the linear stability analysis must be validated by numerical integration of the full nonlinear CGLE, as shown by the plots in Fig. 2.5.4(c-f). The integration is performed using the numerical split-step technique, with periodic boundary conditions. The results bear a direct relation to the linear stability analysis results, which is evident when comparing the widths of the Lyapunov spectra (Fig. 2.5.4(a-b)) with the nonlinear spectra (Fig. 2.5.4(e-f)) during evolution. The spectral evolution demonstrates quantitatively the difference between the two cases of zero and non-zero modulation.

Having confirmed the validity of the modified Floquet analysis, the range of different possible parameters and their implications on the stability of the system is now explored, and the results presented in the following sections.

2.6 Results: Stabilization of MI in Modulated CGLE

In order to comprehensively study the effects of the modulation on the stability of the system, the entire parameter space, comprising of the parameters m, q and Ω, must be explored for any given values of the nonlinearity and diffusion coefficients. As this would have led to a 3-dimensional parameter space, which is already quite a large volume to explore, the parameters q and Ω are coupled into the single parameter Q, as explained in Section 2.4. This brings down the parameter space to 2 dimensions (m, Q), which is much more convenient, while at the same time preserving the interesting phenomena in the limit of finite and long-wavelengths instability. For every point (m_i, Q_j) in the parameter space, the instability of the corresponding modulated CGLE is quantified by the value of the maximum Lyapunov exponent, λ_{Re}^{max}, and a color-coded 'stability map' is plotted, as described next.

2.6.1 Stability Map

One such map is shown in Fig. 2.6.1(a) for the case of the nonlinearity parameter being $c = 0.5$. The value of the maximum Lyapunov exponent is represented by the color-coded map with darker colours for lower values of λ_{Re}^{max}, i.e. for more stable situations. The value of the map at $m = 0$, is identical to the unmodulated CGLE. The central, dark-blue island in the figure is the region of complete stabilization, that is, where all the Lyapunov exponents are negative and the MI is completely suppressed. Around this area are partially-stable regions, with the

demarcated regions representing stabilization by a factor of more than two and four- i.e., the λ_{Re}^{max} in these regions are ½ and ¼th times the unmodulated case. The stabilization area appears in general for $Q < 1$, approaching $Q \approx 1$. This is in accordance with the initial idea that the stabilization occurs close to resonance between the harmonics of plane waves forming the Bloch mode. For much higher values of these parameter, $Q \gg 1$ and $m \gg 1$, the stabilization effect disappears.

The central, completely stabilized island divides the map into three different regions- one where long-wavelength MI remains after partial stabilization (on the left of the island), the regions where short-wavelength instability remains (right side) and where both co-exist (below the island).

In the three cases, the patterns formed are of different characters. As the name implies, long-wavelength instabilities lead to pattern formation with comparatively large characteristic wavelengths (i.e., with small wavenumber). They are formed when smaller wavenumbers are dominant in the Lyapunov spectrum, as is the case in Fig. 2.6.1(b). Long-wavelength instabilities generally lead to a gradual widening of the unstable spectral region, due to effects such as nonlinear four-wave mixing, and eventually lead to turbulence and chaotic patterns.

On the other hand, short-wavelength instabilities lead to pattern formation with comparatively shorter characteristic wavelengths. In this case, the unstable wavenumbers in the Lyapunov spectrum are far from $k = 0$, as is the case in Fig. 2.6.1(c-d). This separation generally helps in keeping the unstable region spectrally confined, and as a result, the patterns formed generally also display regular periodicities.

Finally, it must be noted that around the vertical line corresponding to $Q = 1$, there is the so-called Arnold tongue- a region where the numerically calculated steady-state Bloch modes are highly unstable. This fact is attributed to the strong nonlinear coupling between harmonics near resonance. It is therefore not

possible to perform a perturbation analysis for these parameters and they are excluded from the modified Floquet analysis, as represented by the black region.

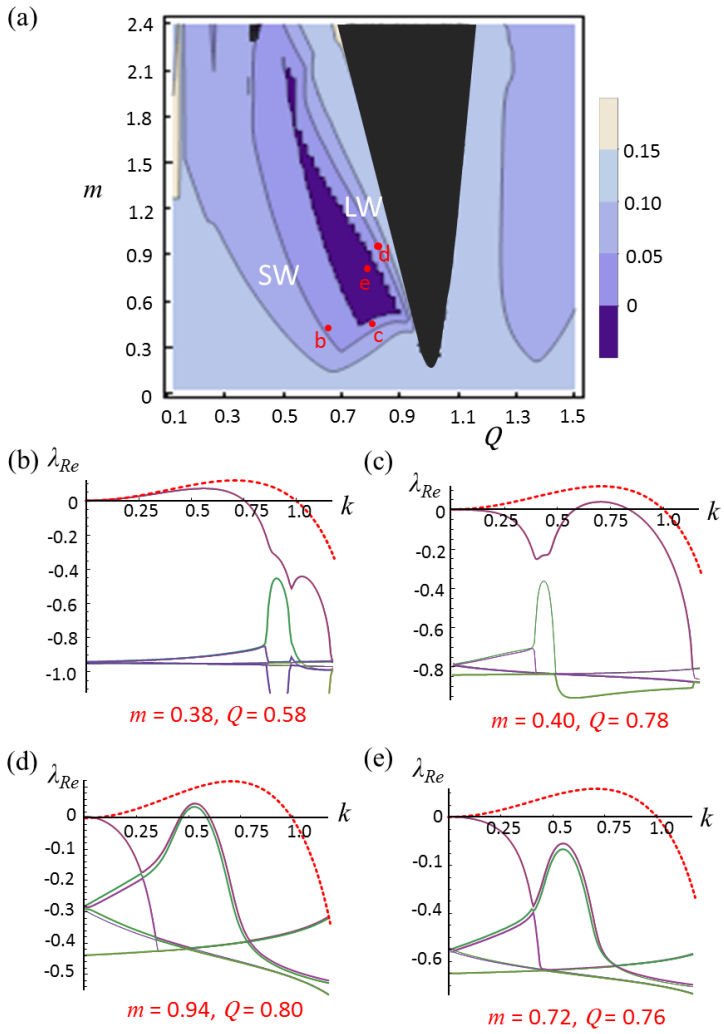

Figure 2.6.1: (a) The color-coded 'stability' map representing λ_{Re}^{max} in the parameter space, (m, Q). The darker regions represent smaller λ_{Re}^{max} and thus, higher stability, with the central island representing complete suppression of MI, i.e.: $\lambda_{Re}^{max} = 0$. Different regions of remaining long-wavelength (LW), and short-wavelength (SW) instabilities are indicated on the map. The black Arnold tongue around $Q = 1$ is where the stationary Bloch solution are unstable and these areas are excluded from the analysis. (b-e) The individual Lyapunov spectra for individual points on the map as compared to the largest Lyapunov exponents of the unmodulated CGLE (red dashed). Here, c=0.5, q=4, space=256π, grid=2048 points.

2.6.2 Effects of Spatial Frequency and Diffusion

In general, the stabilization performance is independent of the choice of the spatial frequency, q. Qualitatively, the results described in the previous section remains the same for arbitrary choice of the spatial modulation frequency while under the limit $|q| \gg |k|, |\Omega| \gg \lambda$, where k and λ are the typical wavenumber and growth exponent of emerging instability. Quantitatively, for small values of q, the stabilization increases for larger q's, that is, the smaller-scale modulations produce better stabilization. However, this trend saturates beyond a certain point and the stability islands remain more or less unchanged upon further reducing the spatial scale of the spatial modulations. The improvement in the stabilization performance for relatively small values of q is demonstrated in Fig. 2.6.2 where different stability maps are plotted for various parameter values. For larger values ($q > 4$) the increase in q cause diminishing increase in the stabilization trend.

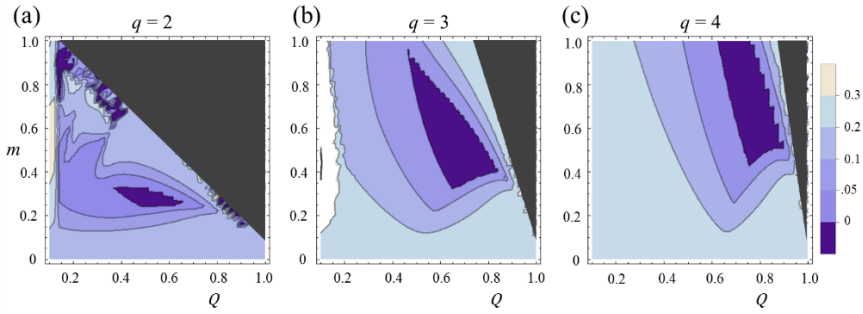

Figure 2.6.2: The stability maps for different values of q, with other parameters being constant. The increase in the stabilization property of the modulation increases with higher q, before eventually saturating. Parameters: *c*=0.5, space=256π, grid=2048 points.

So far these stability maps have been plotted in the absence of diffusion, $d = 0$, with the aim of describing the most symmetric case. However, as mentioned in Section 2.2, in the presence of positive diffusion, $d > 0$, the system tends to be comparatively more stable. While in the presence of negative diffusion, $d < 0$, the stability decreases. This behaviour is demonstrated in Fig. 2.6.3, where different

stability maps, plotted for increasing values of d, show increasing areas of the stabilization island for increasing values of diffusion.

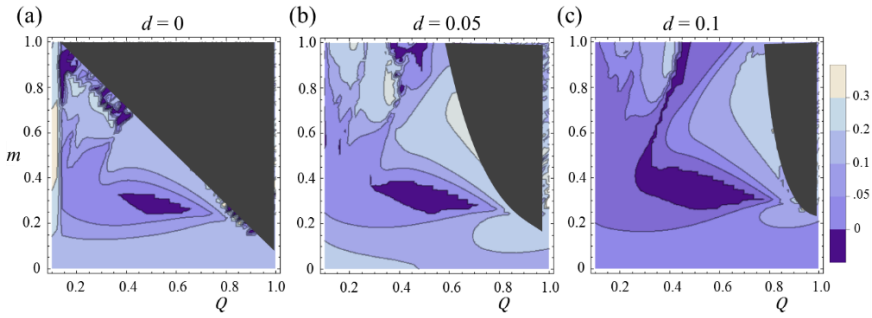

Figure 2.6.3: The properties of the stability maps for different values of the diffusion coefficient. As expected, the stabilization effect increases with increasing diffusion, and the islands of complete stabilization grow larger. Moreover, the presence of diffusion also helps to stabilize the stationary solution, resulting in a reduction of the area of non-stationary solution (black areas). The plots are for $q = 2$, with other parameters the same.

2.6.3 Full Nonlinear Dynamics

The results of the modified Floquet linear stability analysis are confirmed here by numerical integration of the full nonlinear model, Eq.(2.5.1). The steady-state stationary Bloch modes are numerically calculated (in the regions where it exists, i.e.: outside the black tongues of the above figures), and then perturbed by weak, random δ-correlated noise. The perturbed solution is numerically integrated using the split-step technique with periodic boundary conditions. A sufficiently long integration time allows for the identification of the instability of the solution, well beyond the linear regimes.

Let us consider the stability map in Fig. 2.6.1. In all cases, it is found that the instability regions identified by the numerical integration, perfectly coincide with the predictions of the partially and fully stable regions.

The integration results show that within the stable region of the stability map, see Fig 2.6.4(a), all perturbation modes decay, and the steady-state Bloch mode solution is recovered. Outside the stability region, the perturbations grow depending upon the shape of the Lyapunov spectrum in each case, and the modulated regime sets in. The most representative examples of the propagation dynamics of the system are shown in Fig. 2.6.4 for various parameter sets, corresponding to different points on the stability map. The Lyapunov spectra of all these examples have been provided earlier in Fig. 2.6.1, for convenient comparison.

Integration results for the unmodulated CGLE are provided in Fig. 2.6.4(b), where the dynamics of the field is typically chaotic, with a large unstable spectrum, corresponding to the width of the Lyapunov spectrum of the unmodulated situation. The evolution of the modulated CGLE in cases of partial stabilization is typically more 'quiet'. When long-wavelength instability dominates in the partially stabilized cases, the field dynamics gradually turns chaotic, but with a correspondingly narrower spatial spectrum as shown in Fig. 2.6.4(c).

When the weak short-wavelength instability dominates, one may obtain stationary roll patterns, which is characteristic of short-wavelength instabilities. These stationary patterns may or may not be stable, leading, in the latter case, to complex nonlinear phenomena such as wave collapse. Long-time dynamics is generally complicated; even in the case of unmodulated CGLE the long-time regime is not fully understood in spite of extensive analysis of last decades [Coul93, Aran02].

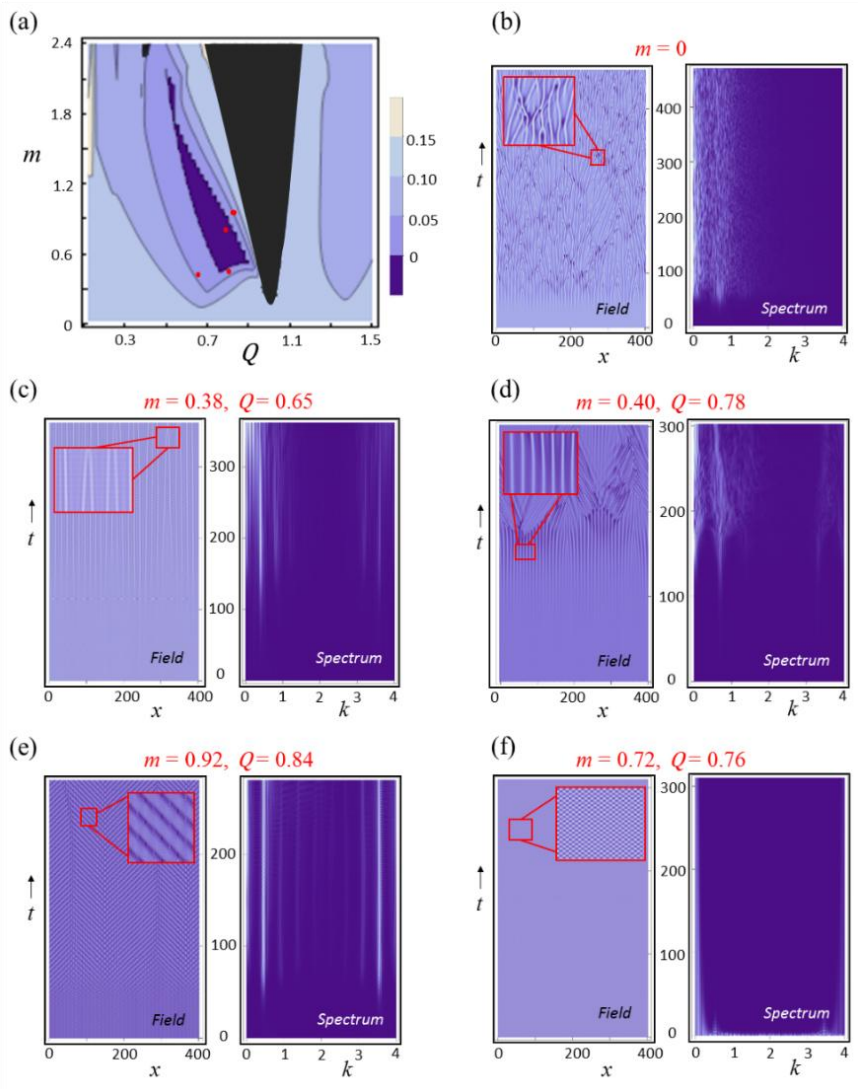

Figure 2.6.4: Integration results of the full nonlinear model. The plots in (b)-(f) represent the space-time dynamics of the field (left) and spectrum (right) for the modulated CGLE, corresponding indicated points on the map (a). The results confirm the predictions of the modified Floquet analysis. The chaotic dynamics in the unstable, unmodulated CGLE (b) and partially stabilized CGLE in (c-e) where the unstable spectrum in each case matches well with the respective Lyapunov spectra (see Fig. 2.6.1) from the modified Floquet analysis. The dynamics of the fully stabilized CGLE is shown in (f) where the steady-state Bloch mode remains stable in propagation. Parameters: c=0.5, q=4, space=256π, grid=2048 points, with periodic boundaries.

Examples of such short-wavelength instabilities are provided; in Fig. 2.6.4(d), an unstable short-wavelength instability first leads to regular roll patterns before eventually breaking into chaotic dynamics, while in Fig. 2.6.4(e) the stationary pattern remains stable. Generally, the stationary modulated patterns are obtained close to the boundaries of the stabilization balloon.

Finally, in Fig. 2.6.4(f), the fully stabilized CGLE is presented, in which case, all perturbation modes decay and the steady-state solution remains stable for arbitrarily long integration times.

2.7 Extension to Two Dimensions (2D)

The stabilization of MI by a modulated spatiotemporal potential can be generalized for two or more spatial dimensions. In this section, we consider the CGLE in two-dimensional (2D) space. The 2D modulated CGLE may be written as:

$$\partial_t A = (i+d)\left(\partial_{xx}^2 + \partial_{yy}^2\right)A + (1-ic)(1-|A|^2)A + 4i\left[m_x Cos(q_x x) + m_y Cos\left(q_y y\right)\right]Cos(\Omega t) \qquad (2.7.1)$$

In this form, the periodic modulation potential has rectangular symmetry in space, with amplitudes m_x and m_y in the x and y coordinates respectively. Similarly, q_x and q_y are the small-scale spatial modulation wavenumbers in those coordinates, and Ω is the fast-scale temporal modulation frequency.

2.7.1 2D Modified Floquet Linear Stability Analysis

The numerical linear stability analysis is performed following the same modified Floquet analysis technique but expanded to 2D space. The concept remains the same: in the Fourier space, a perturbation at any given wavenumber $\left(k_x, k_y\right)$ is

coupled to the wavenumbers $(k_x \pm jq_x, k_y \pm lq_y)$, where j, l=1,2... are the number of harmonics considered in the x and y coordinates respectively.

The linear evolution matrix, in this case, has the size $(16j \times 16l)$. Given that we consider four spatial harmonics in each coordinate, keeping $j = l$, this amounts to the evolution matrix of dimensions (64×64). Diagonalizing the evolution matrix leads to a set of 64 eigenvalues for each mode (k_x, k_y), many of which may be degenerate. Taking the real part of the eigenvalues provides us the Lyapunov exponents for the spatial modes.

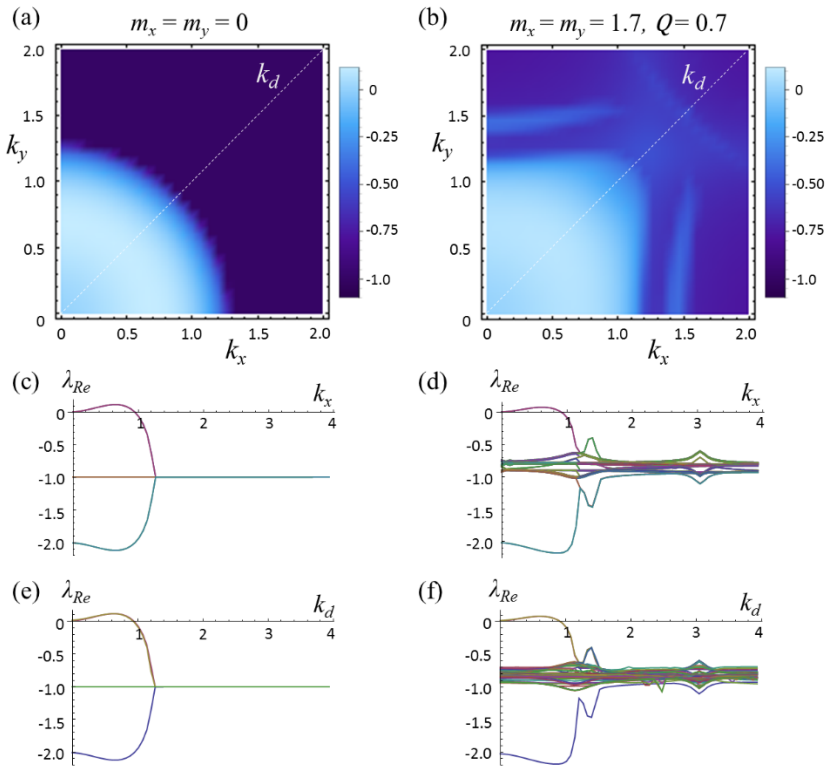

Figure 2.7.1: Representative plots of the 2D modified Floquet linear stability analysis for unmodulated (left) and symmetrically modulated (right) 2D CGLE. (a, b) The color plots represent the maximum Lyapunov exponents in the 2D Fourier plane. The cross-sections of the Lyapunov spectra along the k_x (c-d) and k_d coordinates (e-f). The effect of the spatiotemporal modulation in this case is a weak distortion (reduction) of the Lyapunov growth spectrum of the initial, unmodulated system.

An example of the 2D Floquet analysis is provided in Fig. 2.7.1(a-b), where the maximum Lyapunov exponent is plotted as a 2D color map for the unmodulated and modulated CGLE with the given parameters. The Lyapunov exponents may be analyzed along different cross-sections, which represent the MI in different directions, as shown in Fig. 2.7.1(c-f). A careful examination of the given example reveals that the presence of the modulation has a weakly stabilizing effect on the stability characteristic of the, which can be seen from the slightly weaker Lyapunov spectra in the k_x and k_d cross-sections.

2.7.2 Stabilization of MI in 2D Modulated CGLE

a. Symmetric 2D Modulation

The linear stability analysis is used to identify the different regions of stability. In order to reduce the dimensionality of the parameter space, the most symmetric case of $m_x = m_y = m$ and $q_x = q_y = q$ is used here, and a stability map is plotted in the two dimensional parameter space (m, Q). Although this simplification may seem far from an exhaustive analysis, this stability map gives us quite significant insights into the stabilization characteristics of the 2D modulated CGLE, such as the regions of short-wavelength or long-wavelength remaining instability or regions of full stabilization.

This stability map is plotted in Fig. 2.7.2(a), where we find that the stabilization characteristics are quite similar to the 1D modulated CGLE, as intuitively expected. There are distinct regions where partial stabilization with remaining long-wavelength or short-wavelength instability, and an island of complete stabilization. The suppression is most effective directly along the x and y coordinates, following the profile of the spatial modulation. Analogous to the 1D case, there is also a region where the steady-state solution is unstable, as marked by the black tongue in the map; this area is excluded from the analysis.

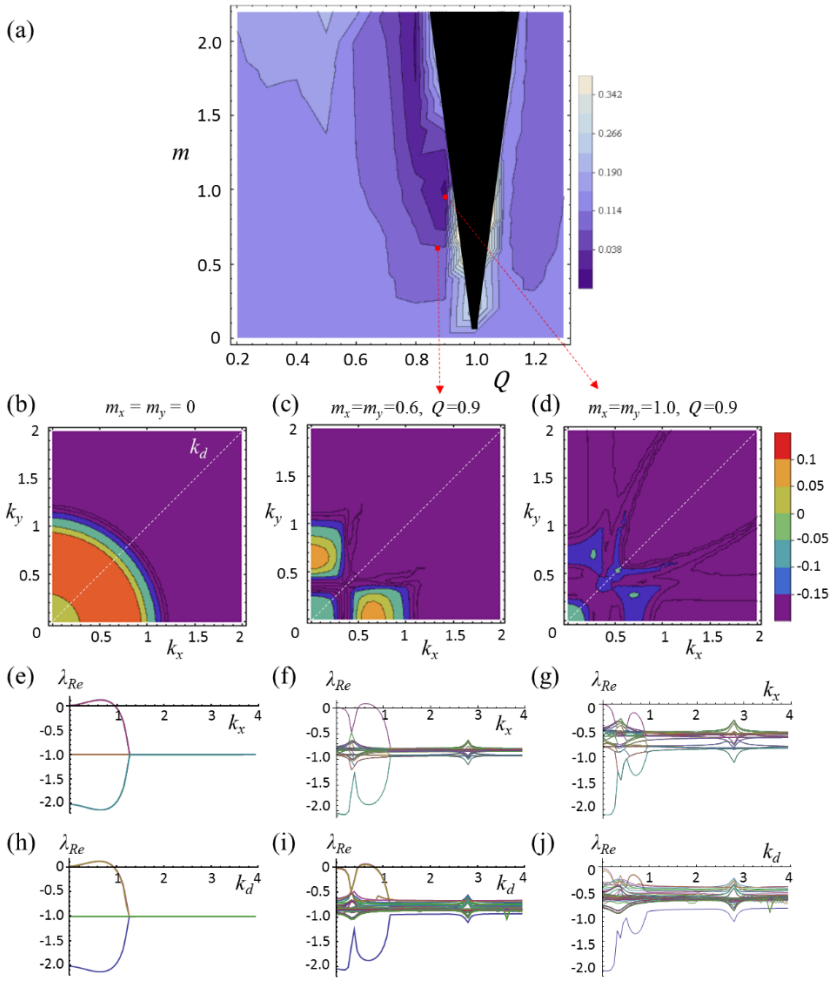

Figure 2.7.2: Results of the linear stability analysis for the case of symmetric modulation, where the modulation parameters are $m_x = m_y = m$ and $q_x = q_y = q$. The stability map, plotted in (a), indicates a clear region of complete suppression of the MI, shown as the dark blue island. The black tongue is the region where the stationary state is unobtainable due to being highly unstable, thus being excluded from the analysis. The surface plots in (b-d) represent $\lambda_{Re}^{max}(k_x, k_y)$ for the different modulations. The plots in (e-g) and (h-j) are the cross-sections of the Lyapunov spectra along the k_x and k_d coordinates respectively. The three cases are representative of the unstabilized MI, partial stabilization with weak remaining SW instability and full stabilization. Parameters: c=0.5, q=8, space=(100x100), grid=(512x512) points, with periodic boundaries.

The results of the 2D modified Floquet analysis under symmetric modulation are validated by direct integration of the full nonlinear model, Eq.(2.7.1). Starting

from the steady-state solution, a complex δ-correlated perturbation is added to the field and integrated. The snapshot of the field and spectral intensity after finite propagation time is recorded, which allows to identify the stable and unstable regimes. The numerical integration results corresponding to the three cases of Fig.2.7.2 are now presented in Fig. 2.7.3.

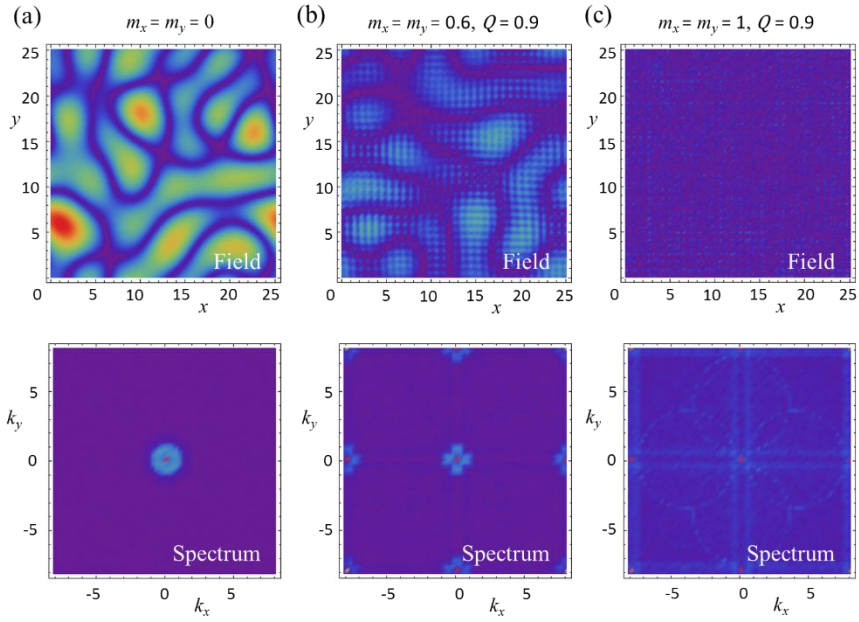

Figure 2.7.3: The results from the integration of the full model confirm the validity of the 2D modified Floquet analysis. The plots represent the field (top) and spectrum (bottom) for the different modulations. (a) The unmodulated CGLE shows significant chaotic dynamics in its field and a broad spectrum after a finite integration time. (b) The partially stabilized CGLE with remaining SW instability has quieter field dynamics and narrower spectrum. (c) In the case of full stabilization, the field is completely stable and the instability spectrum does not develop. Note that the spatial modulations are filtered out in the plots for sake of clear representation. Parameters are the same as in Fig.2.7.2.

For the unmodulated 2D CGLE, in Fig. 2.7.3(a), the long-time snapshot of the field (top) displays typical chaotic dynamics, evident by the large spread of the unstable wavevectors in the spatial spectrum (bottom). For partial stabilization, shown in Fig. 2.7.3(b), the MI develops slower and the field dynamics is therefore much quieter. The range of the unstable wavevectors, in this case, is correspondingly

narrower as seen in the figure. Lastly, in the completely stabilized 2D CGLE, in Fig. 2.7.3(c), the MI has been completely suppressed: the perturbed steady-state Bloch mode solution remains stable for arbitrarily long propagation times, and the spectrum remains confined.

b. Asymmetric 2D Modulation

Apart from the symmetric case, in the general case of an asymmetric 2D modulation, there are many different possibilities of modulation geometries, which could lead to different stabilization effects. For situations of asymmetric partial stabilization, i.e. different degrees of MI suppression in different spatial directions, the result could be the generation of various different types of patterns. The modulation geometry can be of many different types: stripes, rectangles, hexagons and so on… and a comprehensive analysis of all the possible cases an elaborate challenge. This is because the symmetry constraints of the numerical modified Floquet analysis would require it to be redesigned for all cases which do not have a square symmetry; this is a future prospect.

Here, we focus on a stripe-modulation geometry, where the modulation is only in one direction, that is, $m_x \neq 0, m_y = 0$. This analysis is summarised below.

The Lyapunov exponents for the most representative cases of such stripe-modulation profiles are plotted in Fig. 2.7.4 (a-c), for increasing stabilization performances. Also plotted below are the cross-sections of the Lyapunov exponents along the k_x-direction (middle) and along the diagonal direction, k_d,(bottom) in the spectral domains. It is clear that a strip-modulation geometry suppresses the MI only in the direction of the modulation. The numerical integration results of the full model confirm this fact, the results of which are shown alongside in Fig. 2.7.4 (d-f). In the case of the weakest suppression of MI in x-direction, in Fig. 2.7.4 (d), the remaining MI in the x-direction is comparable in magnitude to the MI in the y-direction, resulting in spatiotemporal patterns which

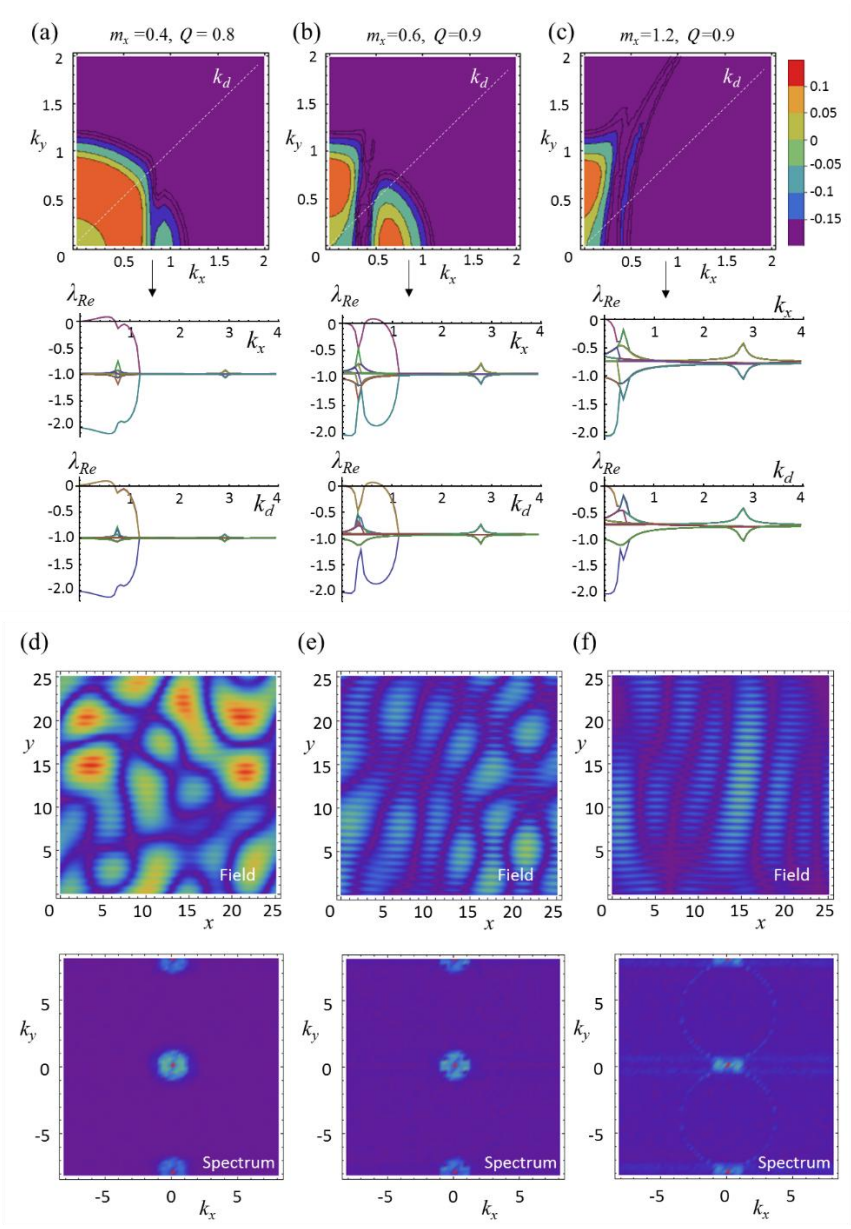

Figure 2.7.4: The results of the stabilization by an asymmetric 2D modulation with a 'stripe' geometry (i.e. $m_x \neq 0, m_y = m$), in three most representative cases. The maximum Lyapunov exponents, λ_{Re}^{max}, remaining after stabilization are plotted in (a-c), along with the cross-sections in the k_x and k_d directions, as indicated. The numerical integration results (c-d), show the snapshots of the field intensity and spectrum for long integration times, confirming the results of the modified Floquet analysis. (The parameters are as in Fig.2.7.2.)

have similar characteristic scales in both coordinates. This is evident from the long-time snapshots of the field intensity (top) and the comparable widths of the unstable wavevectors in the corresponding spectrum (bottom).

For the second case, in Fig. 2.7.4 (e), instability in the x-direction is much smaller than the MI in y-direction, resulting in predominantly vertical patterns, while for the final parameter sets, in Fig. 2.7.4 (f), the MI in the x-direction is completely suppressed, while the MI in the y-direction remains unchanged. This leads to pattern formation only in the vertical direction, as shown in the plots.

2.8 Conclusions

We began this chapter with the proposal that the MI in spatially extended dissipative systems, represented by the CGLE, could be controlled and suppressed by a periodic spatiotemporal modulation of the system's potential. This hypothesis hinged on two different ideas: firstly, the origin of MI was rooted in the presence of unstable bands in the dispersion profile of the system and its character depended solely on the shape of the dispersion profile. And secondly, that the modification of dispersion is possible by a periodic spatiotemporal modulation of the potential of the system. Upon combining these two ideas, the control of MI in a system was made possible by manipulation of its dispersion profile.

The analysis of the MI in the unmodulated and modulated CGLE was performed by a modified Floquet linear stability analysis technique. The modulation of the CGLE indeed led to a modification of the character of MI in the system and eventually to its complete suppression. The stabilization of the CGLE depends on critical parameters such as the modulation amplitude, m, and the so-called resonance parameter, Q. The complete characterization of the parameter space (m, Q) was done by plotting the 'stability map' for the system. Finally, all the results of the stability analysis were corroborated by direct numerical simulations

and the stabilization effect was confirmed.

The analysis was extended to the two-dimensional CGLE, and similar techniques were followed, with the analysis becoming more involved, which was particularly complex for the 2D modified Floquet analysis. The characterization of the MI in 2D CGLE was possible through the 2D Floquet analysis, which led to the stability maps in the simplest cases for symmetric (square) and asymmetric (stripe) modulation profiles. The results bore similar characteristics to the 1D CGLE and complete stabilization in the symmetric case was demonstrated. In the case of asymmetric modulation, various other interesting geometries are possible such as hexagons, octagons and possibly even quasi-periodic structure. This, however, represents demands serious further development of the modified Floquet procedure and remain as a future prospect of this work.

This phenomenon has been shown for a general case, being demonstrated on the universal model of the CGLE. In the presence of diffusion, the stabilization effect persists. In fact, a positive diffusion coefficient enlarges the full stabilization region (as the instability of unmodulated CGLE with diffusion is weaker than that without diffusion). On the contrary, a negative diffusion coefficient (anti-diffusion) reduces the full stabilization region. While the presence of a large anti-diffusion coefficient in the system prevents complete stabilization, partial stabilization is always observed, in all cases.

It is critical that the modulation of the potential must occur necessarily in both spaces and time. Purely spatial modulations, as e.g. in for Bose-Einstein condensates in (stationary) optical lattices [Kevr04], do not lead to the proposed stabilization effect. Hence, the presence of a temporal modulation is crucial, as it allows for near-resonant regimes, i.e. $Q \approx 1$, which lies at the basis of the proposed mechanism.

It is expected that the idea can also be extended to conservative systems, e.g. Bose-Einstein condensates, in order to stabilize the homogenous state of intrinsically unstable attractive condensates. The proposed effect opens a new possibility towards the stabilization of various spatially distributed nonlinear

systems (asymptotically) described by CGLE. Examples in optics are broad aperture lasers and laser-like resonators with Kerr-like focusing nonlinearity, where the MI plays a negative role by destabilizing the emitted radiation. The mechanism is simple, relying only on a resonant spatial and temporal modulation of the potential, and could be implementable in actual experimental setups. As for instance, in the case of Bose-Einstein condensates, it could entail a spatiotemporal modulation of the optical trap amplitude at appropriate frequencies, while in nonlinear optics it would imply a simultaneous transverse and longitudinal modulation of the refractive index.

Chapter 3

Control of Modulation Instability by Genetic Optimization

Contents

3.1 Introduction

In the previous chapter, a new method for the control of Modulation Instability (MI) in spatially-extended systems was presented. The method relies on the displacement of dispersion curves from the modulationally unstable frequency band by introducing an appropriate bandgap in the dispersion spectrum. This is achieved by a small-scale spatiotemporal modulation of the potential of the system, with appropriately 'resonant' spatial and temporal frequencies, which are related by the resonance parameter Q. The technique was demonstrate on the Complex Ginzburg Landau equation (CGLE) in both one and two dimensions, thus forming the basis of a general, universal stabilization mechanism, potentially applicable to a wide range of spatially-extended pattern forming systems. In this way, a completely new approach for the complete suppression of MI in such nonlinear systems was demonstrated, the stabilization of which had always been a challenging task [Kevr04, Segu05].

At the basis of the method is the introduction of a bandgap for the modulationally unstable frequencies ($-2c < k_{unstable} < 0$), which is made possible only when the dispersion 'parabolas' introduced by the spatiotemporal modulation interact close to the instability region, i.e. close to $k = 0$ in the relevant cases of long-wavelength instabilities. However, if in a certain scenario the nonlinearity, c, is so large that the unstable range of wavevectors, $k_{unstable}$, remains wider than the bandgap introduced by the modulation, then this method will begin to saturate. Or considering another hypothetical case, where the unstable frequencies occupy multiple bandgaps distributed arbitrarily across different positions of the dispersion curve: in this complex scenario too, the introduction of a bandgap would be insufficient for the stabilization of the entire system. Thus, in these situations, this stabilization mechanism would be able to only partially suppress the MI, that is, the instabilities may develop slower and cover a smaller spectral range; but the overall system would be unstable nevertheless.

Building on this mechanism of suppression of MI, this chapter provides yet another, much more powerful method for the suppression of MI in utterly complex scenarios. In fact, now one is not only concerned with the suppression of MI but rather with a more general tool for the control and almost arbitrary manipulation of the MI, that is, a reshaping of the Lyapunov spectrum *at-will*. The approach is principally different: rather than attempting to systematically create bandgaps at the 'unstable frequencies' of the dispersion spectra, one may set the desired stability properties of the nonlinear system (the shape of the Lyapunov spectra of modulation modes) and use heuristic optimization algorithms to create a *multi-frequency* spatiotemporal modulation to achieve it. The use of a multi-frequency modulation profile, instead of a simpler sinusoidal modulation profile, enables the generation of multiple bandgaps at different frequencies, depending on the various resonances induced. In other words, it does not count on searching for one, two, or several frequencies of a multiple-frequency stabilizing potential, but directly determine the optimal shape of the temporal modulation using a powerful optimization algorithm. This also opens up the possibility to attain not just the stability of the nonlinear system but also arbitrary shapes of the instability spectrum *on demand.* This method will provide access to unprecedented levels of control over the modulation instability in a system, including the ability to stabilize highly nonlinear systems, selectively reshape certain portions of the instability spectrum or even generate specific patterns in a system *on demand*.

For sake of universal applicability, this method too is developed on the basis of the Complex Ginzburg-Landau Equation (CGLE) while the optimization procedure is based on the, widely popular, Genetic Algorithm (GA).

3.2 Review of Stabilization via Single-Frequency Spatiotemporal Modulation

First, we briefly re-examine the stabilization by a single-frequency spatiotemporal modulation presented in the previous chapter. The term single-frequency spatiotemporal modulation refers to the presence of one frequency *each* in the spatial and temporal domains, and this will be the terminology used throughout the chapter. The stabilization performance of the single-frequency stabilization procedure based on the CGLE with relatively moderate nonlinearity ($c = 0.5$) is summarized in Fig.3.2.1, following directly from the analysis of Chapter 2.

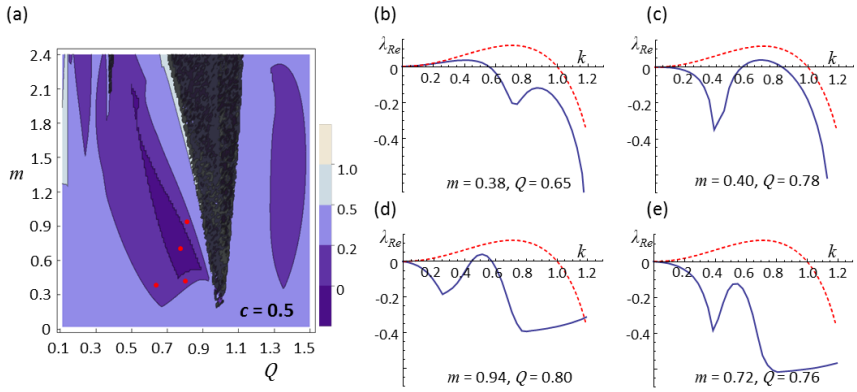

Figure 3.2.1: Summary of stabilization by single-frequency spatiotemporal modulation of the potential, of the CGLE for $c = 0.5$. (a) The color-coded stability map of the largest Lyapunov exponent λ_{Re}^{max} after stabilization reveals an island of complete suppression of MI, as shown by the Lyapunov spectrum in (e), surrounded by regions of partial suppression. Partial suppression may result in a weaker remaining long-wavelength instability (b) or short-wavelength instability (c-d). Parameters: *c*=0.5, *q*=4, space=256π, grid=2048 points, with periodic boundaries.

The stability performance is quantified by means of a color-coded 'stability map' in the parameter space (m, Q), as shown in Fig. 3.2.1(a), representing the maximum Lyapunov exponent, (λ_{Re}^{max}), remaining after stabilization. In such a representation, the region of complete stabilization ($\lambda_{Re} \leq 0$, for every k_x) is

represented by the central, darkest island in the map. The Lyapunov spectra of individual points on the map is plotted alongside, in Fig. 3.2.1(b-e), for some representative cases.

Calculation similar stability maps for different coefficients of nonlinearity, reveals that the stabilization becomes increasingly challenging for higher nonlinearities. That is, the single-frequency stabilization mechanism becomes gradually less effective and it eventually saturates. A detailed analysis of the matter is presented in Fig. 3.2.2, where the stability maps for different nonlinearity coefficients are plotted. It is clear that the islands of complete stabilization diminish as the nonlinearity parameter, c, is increased, and beyond a certain threshold ($c \sim 1.2$), the stabilization island shrinks finally to zero.

It must be kept in mind that although this threshold ($c \sim 1.2$) is not absolute, and the results could perhaps still be further improved by optimizing other modulation parameters, the general tendency is a move towards saturation. For instance, increasing the spatial frequency, q, (i.e., smaller-scale spatial modulations) initially increases the stabilization performance; however eventually this too saturates at sufficiently high values of q. Thus, it suffices to say that in all cases, there comes a point beyond which further improvement by this mechanism saturates.

The saturation tendency can be attributed to the fact that while larger nonlinearities result in an increasingly larger instability band (see Eq. 2.2.3), the increase of the width of the bandgap introduced by the modulation, beyond a certain limit, is not possible by a single spatiotemporal modulation. In this case, as one can intuitively imagine, the need for more than one bandgaps, covering a larger area of the instability spectrum becomes vital. A natural question thus arises- would it be possible to use multiple different modulation geometries simultaneously, so as to create multiple bandgaps, covering a larger area of the unstable dispersion spectrum?

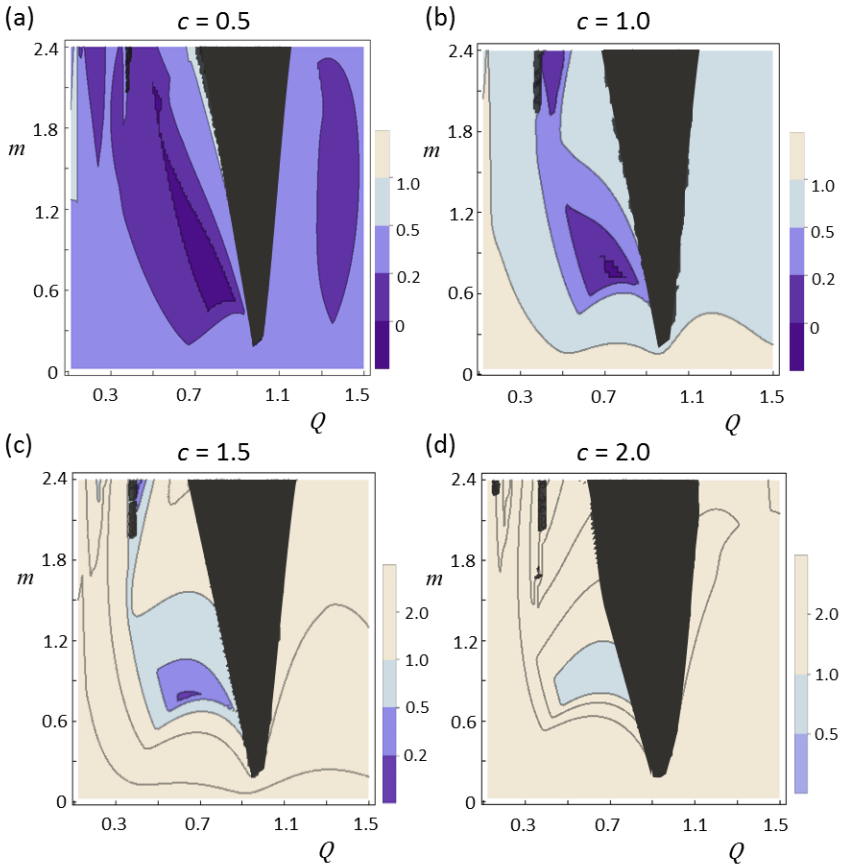

Figure 3.2.2: (a-d) The plots show the saturation of the stabilization mechanism when using the 'single-frequency' spatiotemporal modulation technique for the suppression of MI. The islands of complete stabilization (dark blue) decrease in size for increasing coefficients of nonlinearity, *c*, before eventually vanishing around $c \sim 1.2$. For larger nonlinearities, there is only partial stabilization of the MI. The parameters remain the same as in Fig.3.2.1.

One possibility could be to use a multi-frequency spatiotemporal modulation. That is, a periodic modulation consisting of a single spatial frequency, q, and multiple temporal frequencies Ω_j $(j = 1, 2 \ldots n)$. The modulated CGLE in such a case can be written as:

$$\partial_t A = i\partial_{xx}^2 A + (1 - ic)(1 - |A|^2)A + 4iM(x,t)A \qquad (3.1.1)$$

where,

$$M(x,t) = Cos(qx)[m_1 Cos(\Omega_1 t) + m_2 Cos(\Omega_2 t) + \cdots + m_n Cos(\Omega_n t)] \quad (3.1.2)$$

As a straightforward attempt, we shall begin by exploring, systematically, the effect of introducing additional modulation frequencies, on the stabilization performance of the system. For a certain spatial frequency, q, the temporal frequencies, Ω_j, can be related by a corresponding 'resonance parameter' term: $Q_j = \Omega_j/q^2$. And thus the parameter space can be condensed to $(m_{1,2\ldots j}, Q_{1,2\ldots j})$, where j is the number of frequencies considered.

In the following section, we serially introduce a second and third temporal frequency in the existing single-frequency modulation and analyze its effects on the stabilization performance of the system. These two modulation schemes are denoted as the bi-frequency and tri-frequency modulations respectively.

3.3 Stabilization with Two and Three-Frequency Spatiotemporal Modulation

3.3.1 Bi-Frequency Spatiotemporal Modulation

Here we face the analysis of the stability of the modulated CGLE in the presence of a bi-frequency modulation. Such a modulation implies that, along with a spatial modulation with wavenumber, q, there are *two* temporal modulation frequencies Ω_1 and Ω_2 which make up the spatiotemporal modulation profile: $M_{bi}(x,t) = Cos(qx)[m_1 Cos(\Omega_1 t) + m_2 Cos(\Omega_2 t)]$. The resonances between the spatial and the temporal frequencies in this case, are characterized by the two resonance parameters: $Q_1 = \Omega_1/q^2$ and $Q_2 = \Omega_2/q^2$. The steady-state solution for such a modulated CGLE is a spatiotemporal Bloch mode with a bi-periodicity in the

temporal domain following the temporal bi-periodicity in the modulation profile. A representative plot of such a solution is shown below in Fig.3.3.1 along with its temporal cross-section.

The linear stability analysis of this steady-state is performed using the same modified Floquet procedure, as described earlier in Chapter 2. The modified Floquet analysis provides the spectrum of the Lyapunov exponents averaged over one temporal period, which, however, in this case, must be averaged over the bi-period. This means that the integration needs to be done over a time $t = 2\pi/\Omega_{1,2}$ where $\Omega_{1,2}$ represents the Lowest Common Multiple (LCM) of the two frequencies, $\Omega_{1,2} = LCM(\Omega_1, \Omega_1)$.

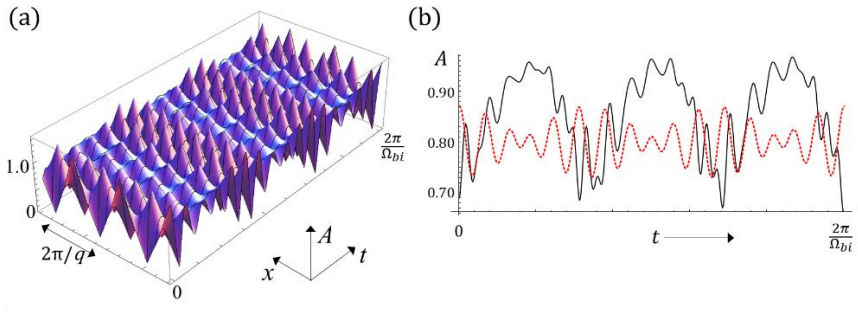

Figure 3.3.1: (a) A representative portion of the stationary Bloch mode solution for such a bi-frequency spatiotemporal modulation. (b) The temporal cross-section of the modulation (dashed red curve) and the steady-state field (solid black curve) profiles reveals the that their temporal periods have the same value, but their exact profiles may differ.

The calculations which follow are for a relatively high nonlinearity ($c = 2$), which corresponds to the case when the system is already beyond the scope of being stabilized by a single-frequency modulation.

To characterize the stability, we begin with the stability map of the single-frequency modulation as plotted in Fig. 3.3.2(a). From this map, it is clear that the region of maximum (partial) stabilization lies in the central (blue) region as denoted. We can identify the modulation parameters corresponding to the point of maximum stabilization, (m_1, Q_1) and, keeping the spatial modulation, q, fixed,

introduce a second temporal frequency Ω_2 with amplitude m_2, leading to a bi-frequency modulation. This opens a new parameter space (m_2, Q_2), which must be explored in order to find the best possible bi-frequency stabilization. Thus, a second stability map is calculated in this parameter space (m_2, Q_2), with parameters from the most stable single frequency modulation case (which is: $m_1 = 0.85$ and $Q_1 = 0.6$). The bi-frequency stability map is plotted in Fig. 3.3.2(b) for the modulated CGLE.

Therefore, to summarize: each point on this map corresponds to a different set of parameters (m_2, Q_2), for the second modulation frequency while the first modulation frequency parameters remain constant $(m_1 = 0.85, Q_2 = 0.6)$.

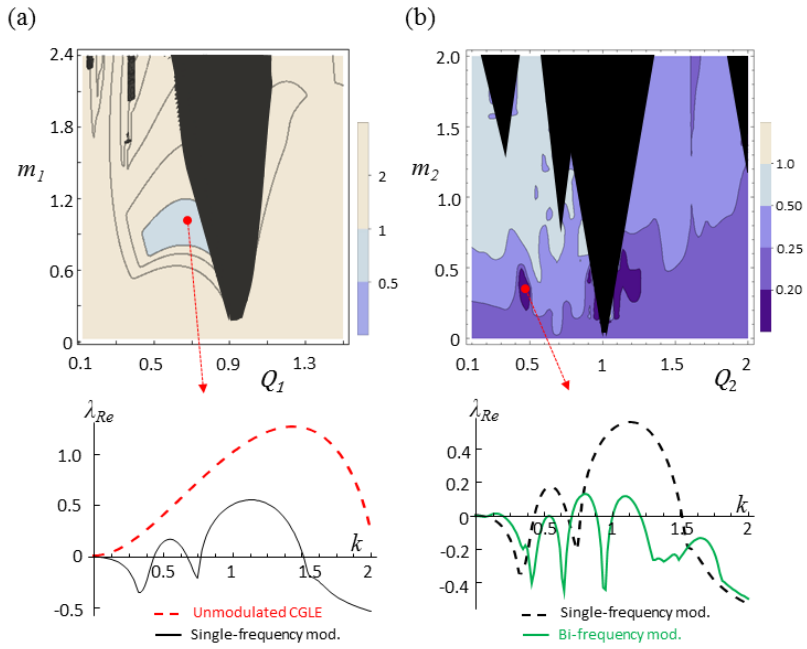

Figure 3.3.2: (a) The stability map of single-frequency modulation for high nonlinearity ($c = 2$) reveals only partial suppression of MI, with the maximumally stabilized Lyapunov spectrum shown in inset (solid black curve), compared with the unstabilized MI (dashed red curve). Fixing these values for (m_1, Q_1), a second temporal frequency is introduced and the resulting new parameter space (m_2, Q_2) explored and the stability map is plotted in (b). The inset compares the Lyapunov spectra of the maximally stabilized bi-frequency modulated CGLE (solid green) with the single-frequency modulation (black, dashed curve). The bi-frequency modulation leads to a substantial improvement in the stabilization, but does not produce complete stabilization. Parameters are as in Fig. 3.2.1.

For both single-frequency and bi-frequency modulations, the stabilization performance of the best set of parameters is shown by the respective Lyapunov spectra in the insets, compared to the Lyapunov spectrum of the unmodulated CGLE (red dashed curve).

It is observed that in the best stabilized case of the bi-frequency modulation, the Lyapunov exponents are comparatively much smaller and spectrally narrower than the single-frequency modulation. However, for some wavenumbers they still remain positive, implying that although the spectrum of the bi-frequency modulation is much more stable than the single-frequency case, complete stabilization is still not achieved.

Nevertheless, the substantially large improvement over the single frequency modulation case gives hope that the idea, in principle, works and it is perhaps only a matter of finding the appropriate combination of frequencies in order to achieve complete stabilization of the system.

3.3.2 Tri-frequency Spatiotemporal Modulation

In search of complete stabilization, this logic is taken forward and a third modulation frequency is introduced, being called the 'tri-frequency' modulation. The parameters of the third frequency are chosen in a similar fashion, that is, by keeping fixed, the parameters of the most stable bi-frequency modulation, obtained from the map in the Fig. 3.2.2(b), which are: $m_1 = 0.85, Q_1 = 0.6$, $m_2 = 0.35$ and $Q_2 = 0.45$. Thus the independent parameter space now becomes (m_3, Q_3) which is explored in another stability map, plotted in Fig. 3.3.3.

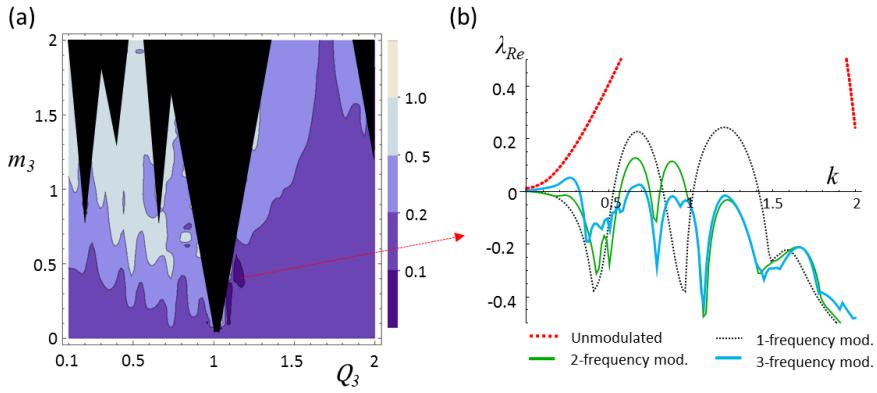

Figure 3.3.3: (a) The stabilization performance of the tri-frequency modulation is summarized in the stability map. There is an increase in the areas of unstable steady-state solutions (multiple black tongues) and decrease in the areas of stabilization (limited to two tiny islands around $Q_3 \sim 1.15$). (b) The maximally stabilized Lyapunov spectra in the cases of the different modulation schemes. While tri-frequency modulation arguably provides slightly better results, the goal of complete stabilization remains elusive.

We recall that the map plots the maximum Lyapunov exponent λ_{Re}^{max} for each point on the map, corresponding to the stabilization performance for different sets of tri-frequency modulation. The darker colours represent lower λ_{Re}^{max} and thus higher stability.

Several interesting features present in the tri-frequency stability map give us an insight into the stabilization performance of this modulation. The first thing to note is that for the most regions of the map, the stability is actually *poorer* than the case with bi-frequency modulation (i.e., with m_3=0). The only regions where this is not so, are two tiny islands around $Q_3 \sim 1.15$. This means that for most cases, the introduction of a third modulation frequency, in this fashion, actually *destabilizes* the system instead of further stabilizing it. Nevertheless, in the two stability islands, the system is comparatively more stable, as shown by the Lyapunov spectra in Fig. 3.3.3(b). Complete stabilization is, however, still not achieved.

Another feature to note in this map is the presence of a large number of areas of unstable steady-state solutions, shown as the black tongues in Fig. 3.3.3(a). This

can be expected, as the presence of multiple interacting frequencies can lead to a large number of non-trivial resonances between them, potentially acting as a destabilizing factor for the steady state solution.

Thus, in summary, we may conclude that by introducing the third modulation frequency, while there may be some small improvement in the stability, it is confined to very small regions of the parameter space, while for most other parts the system has become relatively unstable.

Moreover, it is evident that introducing more and more frequencies dramatically increases the volume of the parameter space, thereby making the task of finding the optimum stabilizing parameters increasingly challenging.

We could expect an improvement in the stabilization performance over single-frequency modulated CGLE by more carefully 'engineering' the frequencies of several modulation harmonics: introducing several $Q's$ which suppress the Lyapunov spectrum at different positions, in k-space, attempting to position suppression areas over all unstable spectral regions (positive λ_{Re} areas). However, it is quite certain that attempting to systematically tailor the bandgaps in this simplistic, 'linear' fashion by sequentially adding more modulation frequencies over previous ones, can be quite problematic and one could expect that it often would *not* lead to the desired stability results. Thus, a new approach to the stabilization by multi-frequency modulation is sought, as explained in the following section.

3.4 'Reverse-Engineering' the Stability Problem

We have seen that the motivation to increase the number of modulation frequencies is justified, as it potentially results in better stabilization performance. However, at the same time, a multi-frequency modulation profile severely increases the dimensionality of the parameter space, making the process of finding the optimum frequency parameters much more complex.

From these two considerations, a new and principally different approach takes shape, which is essentially an inverse stabilization problem. Instead of attempting a systematic stabilization based on the serial introduction of several temporal frequencies, one might instead set the desired optimum shape of the Lyapunov spectrum and then use a heuristic optimization algorithm to find the modulation function which attains this spectrum (see schematic in Fig. 3.4.1).

The modulation function, in this case, will comprise of multiple frequencies, which different amplitudes and phases and all these parameters will be optimized by the algorithm. The generalized modulation function $M(x,t)$ is this case is:

$$M(x,t) = Cos(qx)\sum_{j=1}^{n} m_j Cos\left(\Omega_j t + \varphi_j\right) \tag{3.4.1}$$

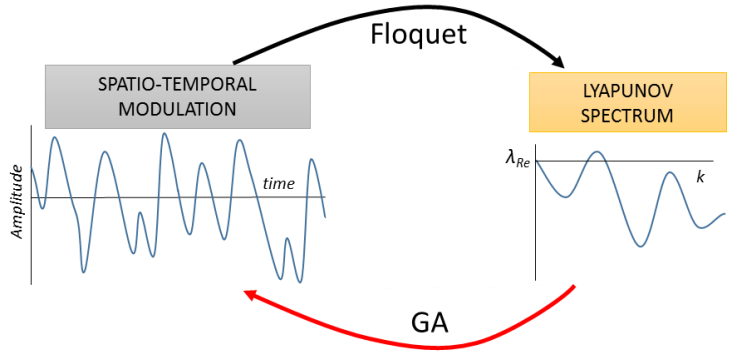

Figure 3.4.1: The 'reverse-stabilization' approach. Normally, one proposes a particular modulation profile and calculates its stabilization capability through a modified Floquet stability analysis. In the reverse approach, a particular stabilization profile (target Lyapunov spectrum) is first specified and then an optimization algorithm is used to design a (multi-frequency spatiotemporal) modulation profile which closely satisfies the specified Lyapunov spectrum upon modified Floquet analysis.

In other words, the aim is to design the bandgap and the Lyapunov spectrum, $\lambda_{Re}(k)$, in a general way; for instance, by setting the property of the Lyapunov spectrum to be completely stable (i.e.: $\lambda_{Re}(k) < 0$, for all k's), one can obtain an optimized modulation profile which results in such stabilization.

The parameter space in these optimization problems is bound to be huge; and this kind of attempt for an *on-demand* stabilization mechanism would not be feasible if not for the availability of modern heuristic optimization algorithms such as the Genetic Algorithm, which is used in this study.

3.4.1 Multi-Frequency Optimization using Genetic Algorithm

In this section, the main objective is the complete suppression of MI, for a highly nonlinear system ($c \geq 2$), using an *optimized* multi-frequency periodic modulation. It may be noted from the beginning, that this is a rather ambitious goal, as in this case the CGLE possesses a broad band of unstable exponents, and all other stabilization methods are unable to stabilize such a strongly nonlinear system. The parameters of the multi-frequency modulation must be selected, or rather optimized, to best achieve the stabilization using the GA. The procedure is described as follows.

In this approach, we start by defining the maximum number of temporal frequencies in the modulation function, which is fixed, by choice, to an arbitrarily large value (in this case to 20, but it can be increased for even more complicated cases). The frequencies are equidistant from each other, that is, $\Omega_j = j \times \Delta\Omega$ where (j=1, 2...). Such an equidistant discretization puts a rather strong constraint on the choice of the possible frequencies, but is a requirement of the modified Floquet stability analysis, for calculating the evolution of perturbations over a fixed time period T (where $T = 2\pi/\Delta\Omega$). The resonance parameters, defined as before, are: $Q_j = \Omega_j/q^2$ and the frequency range is set such that $0.1 < Q_j < 2$, which is sufficiently large to cover all of the interesting region. With these definitions, the size of the entire parameter space, comprising of the amplitudes and phases of the 20 different temporal frequencies $\left(m_{1,2\ldots j}, \varphi_{1,2\ldots j}\right)$ is of dimension 40- a rather large number for an optimization problem!

Next, the Genetic Algorithm (GA) is used for the optimization procedure. The GA is one of the most widely used methods for optimization of high dimensional parameter spaces. It belongs to the larger class of Evolutionary Optimization Algorithms [Back96, Eibe03] which search for the optimized parameters to a problem by minimizing a predefined, so-called, 'fitness function', through processes which tend to mimic the process of natural evolution [Holl92]. The GA begins by creating a 'population' of 'individuals' which are but different combinations of parameters, selected randomly from the available parameter space; in effect, similar to a population of genetically different individuals in any particular species in nature. Each individual is assigned a 'fitness' value determined by the 'fitness function' and the algorithm evolves by minimizing this fitness value. Taking a cue from the biological process of natural selection, 'genetic material' (parameter values) from the 'fittest' individuals is used to produce an offspring (in this case, the generation of new sets of parameter values). In addition, there are random 'mutations' which affect every individual in any given generation. The algorithm, after successive generations, results in a population whose average 'fitness' is sufficiently optimized, and the individual with the best fitness is the final optimized solution.

A rigorous proof of these algorithms still eludes researchers, however, in spite of it, they are a widely used optimization tool due to their high efficiencies. A detailed description of the GA, however, is beyond the scope of this thesis and will not be discussed here. An abundance of literature on this matter can be found easily elsewhere [Holl92, Mich94, Mitc96].

The fitness function, L, can be defined in different ways [Mitc92]. At this point it is defined as the positive area of the Lyapunov spectrum:

$$L = \int [\lambda_{Re}(k)]_{positive} dk \tag{3.4.2}$$

Where, $[\lambda_{Re}(k)]_{positive} = \begin{cases} \lambda_{Re} & if\ \lambda_{Re} > 0 \\ 0 & if\ \lambda_{Re} \leq 0 \end{cases}$

Since the GA searches the parameter space $\left(m_{1,2..j}, \varphi_{1,2..j}\right)$ for combinations of parameter sets which minimize the target function, in this case it means minimizing the positive area of the Lyapunov spectra. Therefore, lower values of L generally increase the stabilization, with $L = L_{min} = 0$ corresponding to complete stabilization. On the other hand, $0 \leq L \leq L_0$, represents partial stabilization, where L_0 is the value of the fitness function in the absence of any modulation.

While in this example of the fitness function, the main aim is to minimize the 'total' instability (i.e. the positive area of the Lyapunov spectrum), its choice may vary for different systems and different requirements, depending on to the final stabilization goal, discussed in detail later in this chapter.

3.5 Results of Genetic Algorithm based Optimization

3.5.1 Complete Stabilization of MI

The results from the GA optimized modulation for described here. It must be noted that the GA is free to give multiple different solutions to the same problem as long as all the solutions reach the global minimum, which is $L = 0$. Moreover, there is no way to capture all the solutions in any kind of a 'stability map' type plot, simply due to the challenge of expressing, sufficiently well, a map of the 40-dimensional parameter space. We therefore are limited to viewing only individual particular solutions at a time.

The results of the GA leads to many stable solutions with complete stabilization $(L = 0)$, and one such solution is summarized in Fig. 3.5.1. Here, the GA

optimization results in a multi-frequency spatio-temporal modulation function, $M(x,t)$, which leads to a completely stabilized steady solution. The optimized modulation parameters are given in Fig. 3.5.1(a) and the modulation profile is shown in Fig. 3.5.1(b) for one time period $T = 2\pi/\Delta\Omega$ and five spatial periods, d_x, where $d_x = 2\pi/q$. Also shown, are the temporal cross-sections of the steady-state field and the modulation itself, in Fig. 3.5.1(c), from which it is clear that the steady state field has the same periodicity as the modulation, but they do not share the same exact profiles.

Finally, the results of the modified Floquet analysis, for this modulation profile, reveals that the Lyapunov spectrum (Fig. 3.5.1(d)) is completely stable, with the value of the fitness parameter $L = 0$.

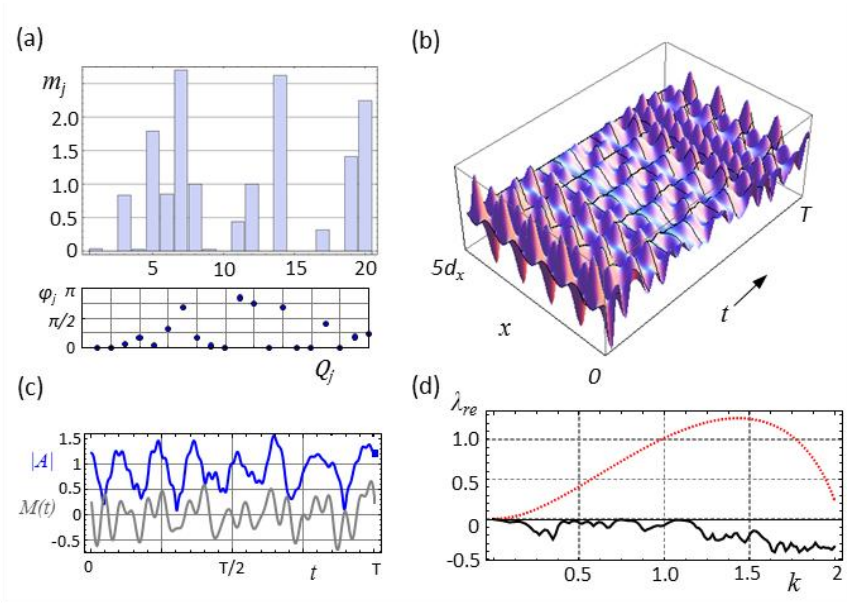

Figure 3.5.1: Results from the GA optimization showing one of the solutions of complete stabilization for *c* =2. (a) The parameters of the multi-frequency GA optimized modulation representing the amplitudes and phases of the 20 different temporal frequencies. (b) The spatiotemporal profile of the modulation for one full temporal period T=2π/ΔΩ, and five spatial periods. (c) The comparison of the temporal cross-sections of the modulation and the field profiles. (d) The Lyapunov spectrum of the GA optimized CGLE showing complete stabilization (solid, black curve) compared with the unmodulated CGLE (dotted red curve).

The results of the stability analysis are confirmed by numerical integration of the modulated CGLE. The results are plotted in Fig. 3.5.2, in comparison with the unmodulated CGLE. In the unmodulated case, in Fig. 3.5.2 (a), we observe that due to the high nonlinearity in the system, the MI quickly sets in making the field (left plot) chaotic in a short amount of time, which is also evident from the spectral profile (right) where a wide range of wavenumbers are unstable.

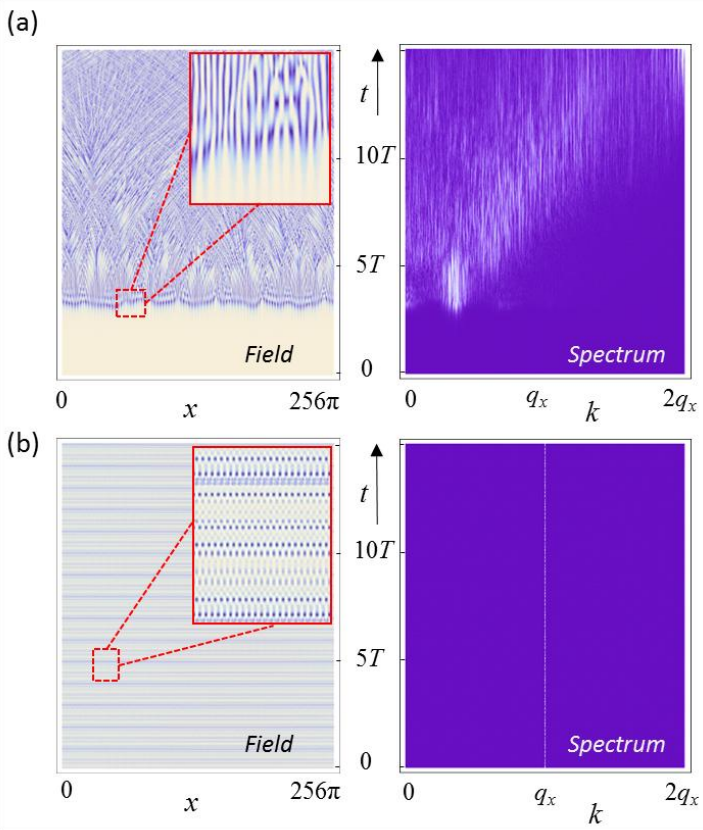

Figure 3.5.2: Integration results showing the field (left) and spectral (right) dynamics for unmodulated CGLE (a), and GA optimized spatiotemporally modulated CGLE (b) with the modulation parameters given in Fig.3.5.1. While in the former case the homogenous steady-state quickly becomes unstable as MI sets in, leading rapidly to chaotic dynamics, in the latter case, the steady state remains stable for arbitrarily long propagation times. The system has high nonlinearity, c=2, which could not stabilize by up to serially introduced tri-frequency modulation. Parameters: q=4, space=256π, grid=2048 points, with periodic boundary conditions.

This is in far contrast from the latter case of the CGLE with GA optimized multi-frequency modulation, shown in Fig. 3.5.2 (b). Here, the complete stabilization of MI is achieved, seen clearly from the plots of the field (left), where only the profile of the nonlinear Bloch mode is visible, and from the spectrum (right), where no unstable wavenumbers are observed.

As a result of the complete suppression of MI, the field remains in the steady-state for indefinitely-long integration times. The validity of the results of the GA optimization is thus verified.

3.5.2 Stabilization Performance Comparison

In the previous, complete stabilization by GA optimized multi-frequency modulation was demonstrated for the case in which complete stabilization was not possible with up to tri-frequency modulation. Therefore, this is a clear evidence of the potential of this powerful new method for stabilization of arbitrarily complex systems. In this section, a quantitative comparison of the stabilization performance through the GA optimization method is presented, with respect to the stabilization performance of single-frequency modulation for different degrees of nonlinearity.

The maximum Lyapunov exponent, λ_{Re}^{max}, remaining after stabilization is plotted, for the different techniques and the results are summarized in Fig. 3.5.3(a). As mentioned earlier, the single-frequency modulation method allows complete stabilization until a certain level of nonlinearity, $(c{\sim}1.2)$ beyond which only partial stabilization is possible; this is denoted by the blue curve in Fig. 3.5.3(a).

The GA optimized multi-frequency stabilization method, on the other hand, is greatly superior, presenting complete stabilization up until substantially higher nonlinearities: $c{\sim}4$.

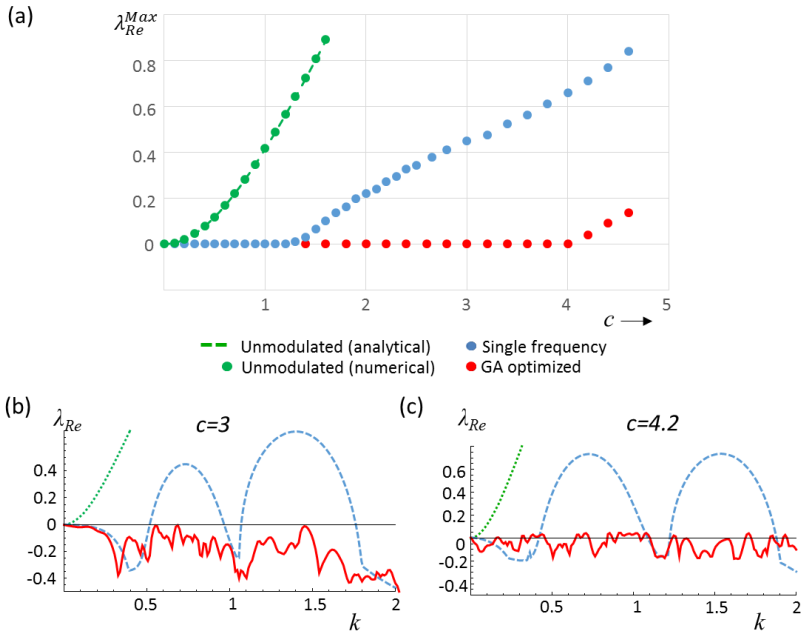

Figure 3.5.3: (a) A comparison of the stabilization performances of single-frequency modulation (blue) and the GA Optimized multi-frequency modulation (red) techniques. It is clear that GA optimization results in a huge improvement of the stabilization performance, allowing the complete suppression of MI in highly nonlinearity systems, as high as $c\sim4$. (b)-(c) Individual plots of the Lyapunov spectra showing the stabilization achieved by the single-frequency (blue) and GA Optimized (red) techniques, compared with the MI (green) in the unmodulated CGLE. Parameters as in Fig.3.5.2.

The stabilization beyond that decreases sharply, due to the presence of a large number of resonant tongues (where the steady-state solution is unstable), possibly invading the complete stabilization island, in the parameter space. Representative Lyapunov spectra, for the two stabilization methods, and for the unmodulated CGLE are also shown, in Fig. 3.5.3(b-c), for different, high nonlinearities, illustrating the effectiveness of the GA optimized method.

3.5.3 Design of Target Spectrum and *On-Demand* Stabilization

Up until now, the proposed procedure has only been used to obtain the complete stabilization of the MI in the system. The method, however, is much more versatile and flexible and can be easily adapted for different stabilization requirements. Some general examples to highlight its adaptability in a '*stabilization on demand*' scheme are now provided.

It is easy to imagine that the stabilization requirements for different systems and different applications may be widely varying. For instance, in some cases the complete stabilization of the system may not be of prime importance, rather it may be sufficient to only suppress either short-wavelength or long- wavelength instabilities. In other systems, stronger suppression around some critically unstable spatial frequency may be the required. One could even imagine a situation in which MI around some critical frequency may need not to be suppressed, but *enhanced*– that is, to be made unstable! All these different situations can essentially be represented by different Lyapunov spectra, which is the defining characteristic of the stability profile. It means that in each case, the appropriate target spectra must be specifically designed. This ability to modify the stabilization property of the system, almost arbitrarily at will, by redesigning the target spectra, is the basis of the so-called *stabilization on demand*. The concept is demonstrated in the examples summarized in Fig. 3.5.4.

The first situation, shown in Fig. 3.5.4(a), represents a scenario in which strong suppression of the short-wavelength instability is required, while the stabilization of the long-wavelength instability is not as important. Such a condition may arise, for instance, in spatially-bounded systems, where the boundaries make large wavelengths already inaccessible to the system, leaving only a short-wavelength instability in the system. The target Lyapunov spectrum (dashed line in the left plots) is thus, designed to be strongly negative around larger k's (short-wavelengths) while less so around smaller $k's$ (long-wavelengths). It is suitably

defined as: $\lambda_{Re}^{target} = -\alpha k$, where α is an arbitrary positive scalar. The results from the optimization procedure, that is, the optimized Lyapunov spectrum is plotted as the solid line. We see that it quite clearly follows the specified target spectrum, being very strongly suppressed at short wavelengths (large $k's$). The accompanying plots (right), denotes the optimized modulation parameters resulting from the GA optimization.

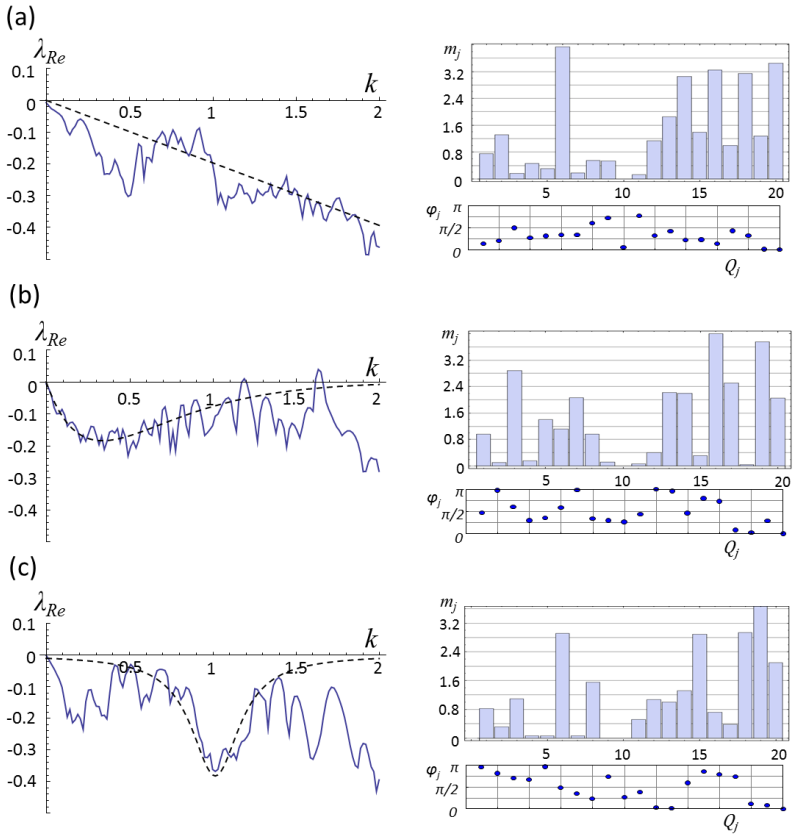

Figure 3.5.4: Examples of the 'on-demand stabilization' scheme where, depending on the stabilization requirements of the system, the target Lyapunov spectra could be designed varyingly. The target Lyapunov spectrum (dashed curves, left) is designed for strong suppression of only short-wavelength (large k's) modes (a), strong suppression of only long-wavelengths (small k's) modes (b), and strong suppression around a critical wavelength, k_{cr}=1, (c). The GA optimization provides suitable solutions whose Lyapunov spectra (solid curves) are plotted alongside. The optimized modulation parameters (amplitudes and phases) are shown on the right panels.

In another example, shown in Fig. 3.5.4(b), the target spectrum (dashed line) is designed for strong suppression at long wavelengths whereas the MI at small wavelengths is not of much relevance. Such a target spectrum can be defined, for example, as: $\lambda_{Re}^{target} = \beta k e^{(-\gamma k)}$, with (β, γ) being positive scalars. The results prove that the GA optimization provides a very good solution: the optimized Lyapunov spectrum (solid line) matches well with the specified target spectrum, especially in the important, long-wavelength region.

In the third example, shown in Figs. 3.5.4(c), the target spectrum is aimed to provide extreme stability around a critical spatial frequency, k_{cr}, by strongly suppressing the instability around this wavenumber, while neglecting other spatial ranges. The target Lyapunov spectrum in this case has been defined as $\lambda_{Re}^{target} = -\eta/[(k-1)2 + \mu]$ with (η, μ) being positive scalars and $k_{cr} = 1$, being the critical frequency. The GA optimization again provides remarkable results as plotted by the solid curve, thereby validating the stabilization *on-demand* concept.

Apart from these three general examples, there exist, certainly, countless different situations, which may arise in different systems where the *stabilization on demand* mechanism can be potentially applied. In all such cases, the efficiency of this method is only limited by the accuracy of the design of the target spectrum and the availability of the computing power.

3.6 Conclusions

We began with a short overview of the stabilization technique based on the (single-frequency) spatiotemporal modulation of the potential, which was proposed in Chapter 2. We have seen that as the systems become increasingly complex and nonlinear, the stabilization of MI becomes greatly challenging and the stabilization performance by the single-frequency modulation technique

tends towards saturation. Eventually, this technique, or any stabilization technique in general, at a high enough complexity of the stabilization problem fails to achieve complete suppression of the MI.

In this chapter, a general new and vastly more powerful stabilization mechanism was proposed, based on a multi-frequency spatiotemporal modulation of the potential. The profile of such a modulation contains multiple temporal frequencies combined with a single spatial frequency.

The stabilization effect emerges from the formation of multiple bandgaps in the dispersion relation, resulting from multiple resonances between the spatiotemporal modulation frequencies, thus covering a wider region(s) of the instability spectrum. The ability to tune the location of the bandgaps, by controlling the modulation parameters, gives us an unprecedented control over the final Lyapunov spectrum of the stabilized system. This provides us with a mechanism for the complete suppression of highly unstable system, and more importantly, a general tool for the arbitrarily tailoring of the stabilization in highly nonlinear unstable systems.

The novelty of this method is in its unique, 'reverse-engineered' approach to the stabilization problem; that is, to first specify the desired stability properties of the system and then search for an optimum multi-frequency spatiotemporal modulation, which satisfies the desired stability properties. The optimization algorithm is based on the Genetic Algorithm.

The concept is demonstrated on the Complex Ginzburg-Landau equation, using the modified Floquet linear stability analysis and through numerical integration of the full model. The successful results demonstrate the potential of this method, which allows for a high degree of control over of the dispersion and thus on the Lyapunov spectrum of the stabilized system.

A quantitative comparison of the stabilization performance of this system over the single-frequency modulation demonstrates a multi-fold improvement in the stabilization performance.

Lastly, the concept of *on-demand* stabilization is proposed. This follows from the ability to define arbitrarily complex target spectrums. Using this approach the instability in the system can be designed for almost arbitrarily complex requirements. Thus any stabilization profile can be produced *on demand*. The performance limits of this technique perhaps only depend on the computation capability available and not due to any fundamental physical limits. In all cases, the proper design of the target spectrum and the fitness function holds the key to the efficiency of the stabilization performance.

The idea is expected to be generic, paving the way for the stabilization of arbitrarily complex nonlinear systems across many branches of physics- from high power lasers and Bose-Einstein condensates of attracting atoms to spatially-extended chemical and biological pattern-forming systems.

Chapter 4

Control of MI in Semiconductor Amplifiers and Lasers

Contents

4.1 Introduction to Semiconductor Amplifiers and Lasers

Optical semiconductor devices such as Broad Area Semiconductor (BAS) lasers and amplifiers and Vertical External Cavity Surface Emitting Lasers (VECSELs) are some of the most widely used coherent light sources in modern technology. This is primarily because they offer some major advantages over other conventional lasers. They have a particular (planar) geometry, such that the pump has effective access to the whole volume of the active amplifying media which allows for high conversion efficiency of the pump, leading to high output intensities for relatively small pump currents. The high degree of efficiency, coupled with low lasing thresholds, and tiny, compact physical dimensions, makes for a very potent combination, attractive for most devices where efficient power and/or space constraints are of vital importance (see Fig. 4.1.1).

A major disadvantage, however, of these devices is the relatively low spatial and temporal quality of the emitted light beam, which becomes worse with increasing pump power [Marc96, Adac93, Ohts12, Tart98]. This fact seriously restricts the maximum power at which the device can be operated before the beam quality becomes unacceptable.

The deterioration of the spatial structure of the beam in BAS amplifiers and VSCELs arises from two distinct features: large transverse widths of the cavity and a high degree of nonlinearity in the optical fields. The large transverse size of the cavity results in the lack of an intrinsic spatial mode selection mechanism in linear stages of amplification, usually resulting in the amplification of higher order transverse modes which significantly diverge in propagation. On the other hand, in the nonlinear stages of amplification, a high degree of nonlinearity leads to the growth of spatiotemporal instabilities through the phenomenon of Modulation Instability (MI) [Prat07], also called as the Bespalov-Talanov instability [Besp66]

after the founders who first explained this phenomenon for light beams in nonlinear liquids.

It is well known that inverted semiconductor materials (where the population inversion of electron-hole pairs or carriers is the source of lasing) typically display self-focusing nonlinearity, due to the dependence of the refractive index on the population inversion– characterized by the so-called linewidth enhancement or Henry factor, α_H [Adac93].

The MI seriously limits the output power of these devices since the larger the intensity, the stronger is the self-focusing effect. As these devices typically operate at comparatively high powers, the instability is quite pronounced and the spatial structure of the beam becomes poor. The output power of these lasers is, therefore, severely restricted, limiting thus, their applications.

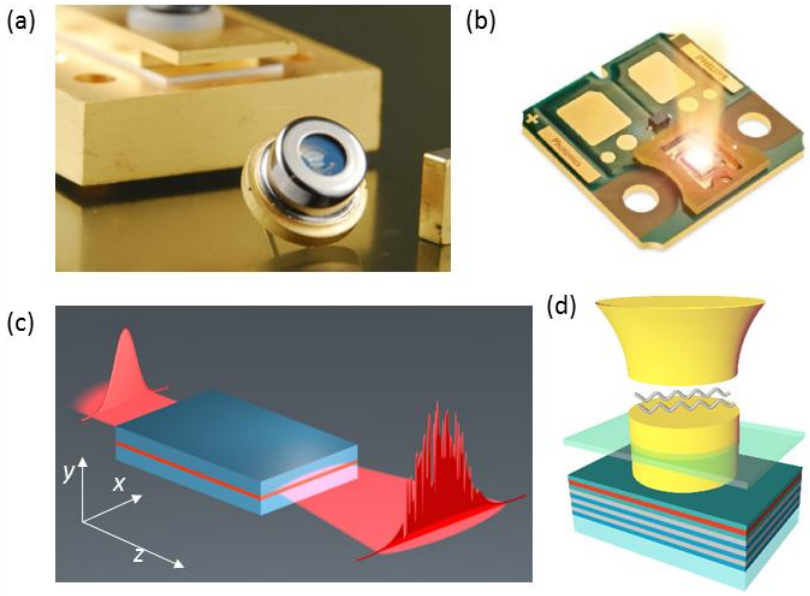

Figure 4.1.1. (a-b) Semiconductor-based optical devices offer compact sources of coherent light, widely used in various modern technological applications (from [Moen16]). MI in broad area semiconductor amplifiers (c), and Vertical Cavity semiconductor lasers (d), leads to poor quality of the optical emission, severely limiting the applicability of these devices at higher optical powers.

Current approaches to solving this issue, that is, the stabilization of output beam's spatial structure, commonly rely on external forcing techniques such as optical injection [Taki09] and optical feedback in various configurations– spatially structured feedback [Mand03, Simm99] and feedback from external cavities [Mart96, Munk97]. All these techniques, however, require various external, often complex, prearrangements which reduce, if not completely destroy, one of the main advantages of these devices: their compactness, and thus again limit their applicability.

A completely different approach to this issue is therefore needed: a method which can suppress the MI at high powers, without relying on external mechanisms and bulky arrangements. An intrinsic control on MI is essential for lasers and amplifiers in order to provide an efficient source of high-quality beam especially at high operating powers, which could open up a whole new realm of possible applications of these semiconductor devices.

In some recent studies, it has been shown that a periodically modulated gain profile can result in an anisotropic net gain of Bloch-like modes in semiconductor media [Herr12, Radz13]. Besides, it is also well-known that a periodic gain profile in the longitudinal direction results in net gain profile in frequency; as it is in the case of the so-called distributed feedback lasers [Koge71, Koge72]. Distributed feedback is considered in one-dimensional (1D) systems, by a 1D modulation of the gain/loss profile on a period of half-wavelength. A two-dimensional (2D) modulation of the gain/loss profile with transverse, $d_{\perp}$, and longitudinal, $d_{||}$, periods, has a similar effect: in an analogous way, it leads to the modification of the angular net gain profile [Herr12, Radz13]. A particular adimensional ratio, Q, relates the two modulation periods. The particular case when $Q \approx 1$ corresponds to a resonance between the Talbot-like longitudinal oscillations of the modulated wave and the longitudinal component of the gain/loss modulation. This leads to a stronger amplification of the on-axis emission than the off-axis one. The references [Herr12, Radz13] study the exponential growth of weak radiation

(linear stage of the amplification), when the depletion of the inversion is not considered, and consequently the, MI does not develop.

The modification of the spatial dispersion profile in BAS amplifiers is at the core of another (linear) physical phenomenon- the angular filtering of the spatial modes of the beam [Herr12, Radz13]. Such spatial filtering leads to partial improvement of the spatial output beam quality but, on its own, does not guarantee high spatial beam. Hence, the problem of MI remains irrespective of the presence of angular filtering mechanism and it is vital to address MI in order to get an improved beam profile in BAS devices.

On the other hand, VECSELs attempt to solve the issues of transverse mode control using an output spherical mirror that ensures operation at the fundamental transverse mode [Trop06]. Being a rather simplistic approach, it brings along with it many new complications, such as the requirement for an external (bulkier) setup and a substantial reduction in the effective volume of the active area of the VECSEL. It is safe to say that this approach is not an effective solution, and thus the problem remains unsolved.

In this chapter, a new solution is proposed which directly addresses this problem. Armed with the findings of Chapters 2 and 3, a mechanism for the suppression of MI in BAS amplifiers and VECESLs is developed which allows for the stabilization of the output beam. By using a periodic modulation of the pump profile, a spatial modulation of the gain profile of the amplifying active medium is created, which, for appropriately tuned periods, leads to the suppression of the MI in these systems.

Moreover, one finds that the suppression of MI can be achieved with realistic modulation parameters. By stabilization, we mean that qualitatively the profile of the MI spectrum (the spectrum of Lyapunov exponents) is substantially narrowed, when modulation is applied, and can even be completely removed in working scenarios. Physically, this means that the MI develops slower, so more intense fields can be produced in a finite-length cavity, with a smaller risk of beam quality deterioration.

These studies are proof that the ideas developed in the previous chapters, on the, rather mathematical, model of the Complex Ginzburg-Landau Equation, and which form the main novelty of the thesis, are indeed suitable for real-world applications in physical systems.

The main analyses in this chapter are structured into three parts, following the introduction. The first part, in Section 4.2, deals with BAS amplifiers where a simple model is developed for the suppression of MI in moderately high nonlinear regimes and successful stabilization is demonstrated.

In Section 4.3, a similar method is then applied to the model of VECSELs, which can be of broadly three types, depending on certain parameters. The results for all three types of VECSELs are discussed.

In Section 4.4, we take a relook into the working of BAS amplifiers and demonstrate another, much more powerful method, for the suppression of MI in highly nonlinear BAS cavities. This method is based on the 'on-demand stabilization' method which was developed and explained in detail in Chapter 3.

Finally, in Section 4.5, a brief conclusion to these studies is provided.

4.2 Broad Area Semiconductor (BAS) Amplifiers

4.2.1 Modelling BAS Amplifiers

The mathematical model of the BAS amplifier is based on the following stationary equation for the evolution of the optical field amplitude, $A(x,z)$, injected at z=0:

$$\partial_z A = \frac{i}{2k_0}\partial_{xx}^2 A + s\left(\frac{p-1}{1+|A|^2}(1-i\alpha_H) - i\alpha_H - \gamma\right)A \qquad (4.2.1)$$

Here, k_0 is the free-space wavenumber of the optical field, $s\gamma$ represents the linear losses in the cavity, and p is proportional to the pump. The parameter s denotes the inverse absorption length in a cold semiconductor media and is introduced here for sake of convenience, that is, for a more direct comparison with experiment. It can be eliminated from the model by scaling the spatial coordinates, which was the case in [Herr12]. The complex amplitude of the electric field, $A(x,z)$, evolves under paraxial approximation, experiencing diffraction and nonlinearities due to the gain and refractive index dependence on the carrier density.

The spatial coordinates are left un-normalized for better comparison with real BAS systems. The Eq. (4.2.1) is derived from the traveling wave model [Ulta03] neglecting gain (chromatic) dispersion, assuming only linear spontaneous recombination, and adiabatically eliminating the carrier density. The linewidth enhancement factor, α_H, for semiconductor lasers ranges between $1.5 < \alpha_H < 8$ [Mull99, Osin87].

The homogeneous solution of Eq. (4.2.1) represents the plane wave propagating in a saturated semiconductor media, with an amplitude $A_0 = \sqrt{-1+(p-1)/\gamma}$. A standard linear stability analysis of this solution can be performed by perturbing A_0 with a weak transverse perturbation, leading to the general form: $A = A_0[1 + a_+ \exp(ik_x x + \lambda z) + a_- \exp(-ik_x x + \lambda z)]$ where $a_\pm \ll 1$. This is

substituted back into Eq. (4.2.1) and then solved for linear order terms of the perturbation, leading to the following expression for the Lyapunov growth exponents, λ_{Re}, of the transverse perturbation modes:

$$\lambda_{Re}(k_x) = \frac{1}{2} Re\left\{-c_1 \pm i\sqrt{\frac{k_x^2}{k_0}\left(\frac{k_x^2}{k_0} - 2\alpha_H c_1\right) - c_1^2}\right\} \tag{4.2.2}$$

where, $c_1 = 2s\gamma(p-1-\gamma)/(p-1)$.

The Eq. (4.2.2) predicts a long wavelength MI of the stationary solution, which can be seen when it is plotted for arbitrary parameters, as represented in Fig.4.2.1. The maximum growth exponent is given by $\lambda_{Re}^{max} = \frac{c_1}{2}(\sqrt{1+\alpha_H^2} - 1)$, which occurs at the modulation wavenumber $k_x = \sqrt{\alpha_H c_1 k_0}$. The instability is closely related with the linewidth factor α_H, as the system becomes increasingly unstable for higher α_H values and for increasing pump values, p, as illustrated by the plots in Fig. 4.2.1.

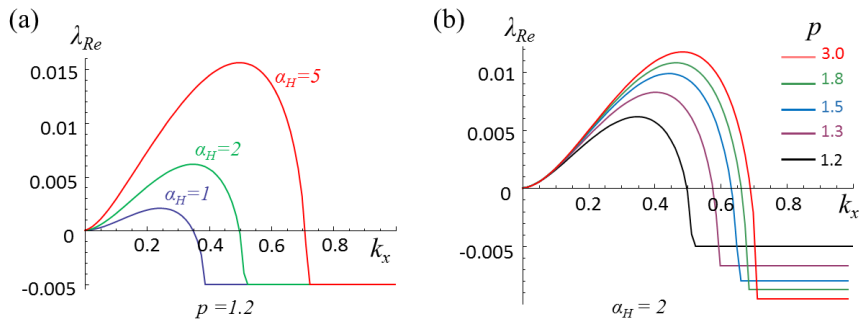

Figure 4.2.1: The results from the linear stability analysis showing the dependence of the Lyapunov growth exponents (λ_{Re}) on: (a) the linewidth enhancement factor, α_H and (b) the pump, p in different scenarios.

A good indicator of the instability is the integral of the positive part of the Lyapunov growth spectra: $L = \int dk_x \lambda(k_x)$, which will be referred to as the

global instability. This parameter L can be used as a quantitative measure of the stabilization performance of the system.

4.2.2 Spatial Modulation of the Pump

The attempt towards stabilization of the MI in BAS is based follows on the lines of a spatiotemporal modulation of the potential. The temporal dispersion as described in the case of the CGLE in Chapter 2 can be equivalently replaced by the spatial dispersion in the case of the BAS amplifier. This can intuitively be understood by visualizing a photon moving in the *z*-coordinate: for the 'flying photon' this direction effectively acts as a temporal coordinate, thereby preserving the essential similarity between the dispersion relations. Thus by reshaping the spatial dispersion through a two-dimensional (2D) spatial modulation, one can expect to suppression the MI in the same fashion.

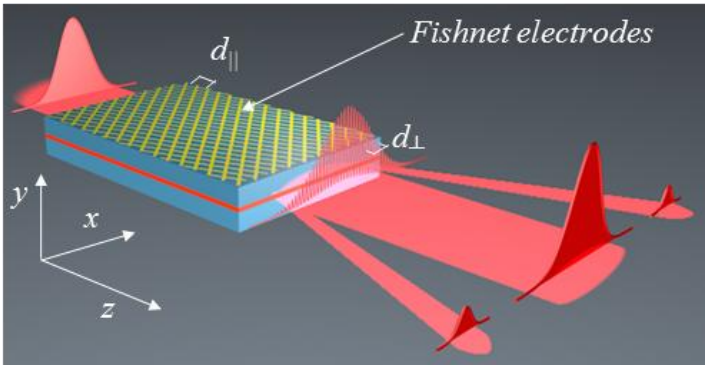

Figure 4.2.2. A periodic spatial modulation scheme for a BAS amplifier. The modulation of the pump is achieved by using a spatially modulated 'fishnet' type electrode structure with appropriate transverse and longitudinal periods. This eventually results in a modulated potential of the system, or more specifically in the gain/loss profile, of the active medium.

However, unlike the previous cases where the modulation was introduced phenomenologically into the equation, in real systems it should be in a physically applicable manner, through the modulation of a system parameter for instance.

In the present case, we consider a spatial modulation profile of the gain/loss of the active semiconductor medium, which can be achieved through a modulation of the pump current, as illustrated in Fig. 4.2.2. Such 2D modulation of the pump may be achieved by different approaches and is discussed later towards the end of Section 4.2.

Mathematically, the 2D pump modulation may be introduced into Eq. (4.2.1), as a function of the following spatial profile:

$$p(x,z) = p_0 + 4mCos(q_x x)Cos(q_z z) \tag{4.2.3}$$

where the modulation geometry is defined by the normalized transverse $q_x = 2\pi/d_x$ and longitudinal $q_z = 2\pi/d_z$ components of the lattice wavevectors. These are combined to define the resonance parameter $Q = 2kq_z/q_x^2 = 2d_x^2/\lambda d_z$. Strictly speaking, it should be noted that $p(x,z)$ is in fact proportional to the pump profile, smoothed by the carrier diffusion by a factor $\left(1 + D(q_x^2 + q_z^2)\right)^{-1}$ where *D* is the carrier diffusion (see e.g. [Radz13, Ulta03]).

The modulations are considered on small spatial scales, in both longitudinal and transverse directions, $|q_x| \gg |k_x|, |q_z| \gg |\lambda|$, where k_x and λ are the typical transverse and longitudinal wavenumbers of the emerging instability. The parameter *m* stands for the modulation amplitude of the potential.

The steady-state solution of Eq. (4.2.1) with modulated pump, Eq. (4.2.3), is a periodic pattern, following the modulation of the gain profile, which is in a sense the nonlinear dissipative Bloch mode. For certain modulation frequencies, however, there can be a phase difference between the modulation profile and the steady state Bloch mode, depending mainly on the resonance parameter *Q*, as shown in Fig. 4.2.3.

In the linear stage of amplification, the field exponentially increases along *z*, therefore one can speak about an evanescent (or exponentially increasing/decreasing) Bloch mode [Herr12]. In the nonlinear case, however, the

field stabilizes due to saturation (of the nonlinearity) and therefore the steady picture is recovered.

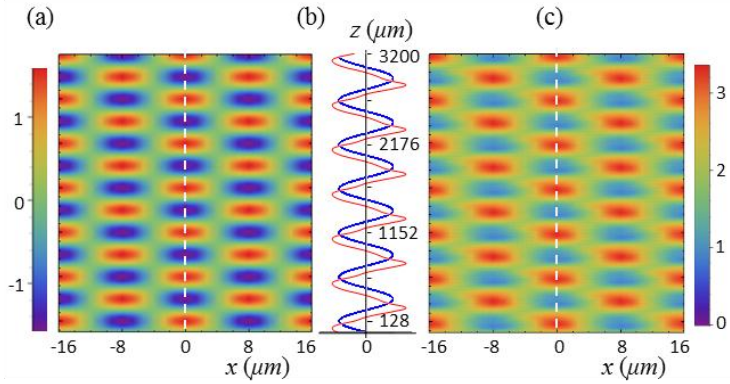

Fig. 4.2.3. (a) A 2D profile of the modulated gain of the semiconductor, and (c) the intensity profile of the steady-state field (the nonlinear Bloch mode). (b) Longitudinal cross-sections (along with the dashed lines) of the modulation profile (blue) and the field intensity (red). We see that the field profile has a phase lag with respect to the gain profile, which is generally expected for a periodically forced system with small negative detuning from resonance.

The calculation of the steady-state is done by expanding the complex field amplitude into harmonics (n, l), of the transverse and longitudinal modulations:

$$A(x,z) = \sum_{n,l} A_{n,l}(z) \exp(inq_x x + ilq_z z) \tag{4.2.4}$$

This is then substituted into Eq. (4.2.1) (with pump modulation) and expanded. The expansion can be truncated to the three most relevant harmonics, which is sufficient to provide realistic results, as will be later shown. Precisely the same truncation has been shown to be useful close to resonance in many relevant linear systems such as photonic crystals [Stal06a], but also in certain nonlinear systems such as repulsive Bose-Einstein condensates [Stal06b, Stal08a] and nonlinear periodic defocusing Kerr media [Stal08b].

4.2.3 Stabilization Results of Modulated BAS Amplifiers

The steady solution (the nonlinear Bloch mode), is a locked state of the harmonics $A_{0,0}, A_{-1,-1}, A_{1,1} \neq 0$, which can be determined by numerical integration of Eq. (4.2.1) using the expansion of Eq. (4.2.4). Such steady solution exists for a broad range of parameters; however, for certain values of the parameters it either ceases to exist or is highly unstable, as shown by the black region in Fig. 4.2.4(a). In such case, instead of a steady solution in form of a nonlinear Bloch mode, the amplitudes of the harmonics develop unstable oscillatory dynamics. These unstable parameter ranges are therefore excluded from the linear stability analysis.

The linear stability analysis is performed numerically following the, previously introduced, modified Floquet procedure, developed for such modulated systems, as described in detail Chapter 2. As noted there, for spatially-homogenous systems, only the harmonics of small complex perturbations at $+k_x$ and $-k_x$ are coupled through the modulation, leading to the evolution of 4 independent perturbations for each perturbation mode $a_{\pm}(k)$, and to the linear evolution matrix of dimensionality (4×4). In contrast, for spatially modulated systems, the number of coupling is greatly enhanced, with $4n$ modes being coupled to each perturbation mode, n being the number of harmonics considered, leading to the linear evolution matrix of dimensionality $(4n \times 4n)$. In this study, it was sufficient to consider 4 harmonics (evolution matrix of dimensionality (16×16)), checking that for larger number of harmonics the results do not alter.

The results of the linear stability analysis in parameter space (m, Q) are summarized in Fig. 4.2.4. In this system, there was no area of complete suppression of the instability, but rather only partial suppression. However, close to the resonance condition, $Q = 1$ there are where the MI is drastically reduced, as shown for instance in Fig. 4.2.4 (d-e). Depending on the parameters, the partial suppression of the MI generally results in a remaining weak instability which could

either be Long-Wavelength (LW) or Short-Wavelength (SW) instability or a combination of both. Some of the most representative cases are plotted in Fig. 4.2.4 (b-e). Thus, unlike, in the case of CGLE, in this model of the BAS amplifier, a weak LW instability remains in the entire parameter space, even for the cases of strongest suppression and complete stabilization seems to be theoretically not possible.

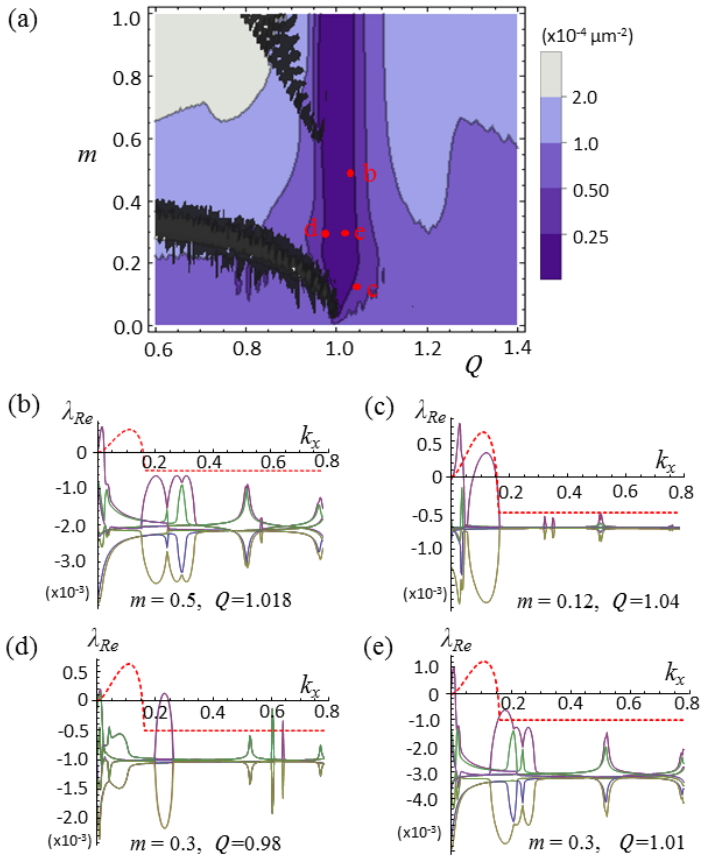

Fig.4.2.4. Results of the by modified Floquet linear stability analysis. (a) The 'stability map' of the global Lyapunov exponent, L, in parameter space (m, Q) with darker regions denoting greater stability and the black tongues denoting unstable steady-state solutions. (b-d) Lyapunov spectra for individual points on the map showing typical cases of: (b) remaining LW instability, (c-d) remaining SW and LW instability and (d) maximum suppression. The red dashed curves represents the unmodulated BAS case. The units of k_x and λ_{Re} are in μm^{-1}. Parameters: p_0 = 1.2, α_H= 2, γ = 0.1, k_0= 2π, s=0.01.

This is, however, not the end of the story, and in reality, full stabilization is still achievable, explained as follows. We recall that the modified Floquet stability analysis is done for an infinite width BAS amplifier, due to constraints put by the numerical algorithm. However, the amplifiers are always of finite width, generally of the order of a few hundred microns. This puts a natural upper limit on the wavelength (lower limit on wavenumber) of the transverse instability that can operate in the region. For a given BAS amplifiers of width w, this lower limit is given by $k_x^{min} = 2\pi/w$. Thus if the spectrum of the remaining LW instability is sufficiently narrow, then the instability becomes irrelevant in a realistic scenario. In other words, if the transverse wavenumber of the first transverse mode of the structure with $k_x \approx 2\pi/w$ is larger than the width of the profiles of instability spectra, then it is no more affected by the remaining LW instability.

In order to demonstrate this, we perform several numerical simulations, integrating Eq. (4.2.1) for a finite-width amplifier (~128 microns wide). The modulation parameters for the pump current is kept the same as in Fig. 4.2.4(d), which has a weak remaining LW instability.

The integration results of the full nonlinear models in both cases, that is, for infinite-width and finite-width amplifiers are presented in Fig. 4.2.5. The dynamics of the unmodulated infinite and finite-width amplifiers are also provided for comparison in Figs. 2.4.5 (a) and (c), respectively. In both the unmodulated amplifiers the field becomes chaotic as MI develops, indicated by the large spread of the corresponding Fourier spectra.

In the more theoretical case of the infinite-width amplifier, as expected, the periodic modulation, only partially stabilizes the dynamics of BAS. In this case, the angular area of growing modes becomes much narrower, as shown in Fig. 2.4.5(b), although the MI still develops for sufficiently long structures.

On the other hand, in the case of a realistic finite-width structure, shown in Fig. 2.4.5(d), the modulation completely stabilizes the system, wherein the field remains stationary for long propagation times and the spectrum does not spread

with increasing time. As shown in the plots, the modulated finite-width BAS amplifier leads to an almost non-diverging beam in angular space.

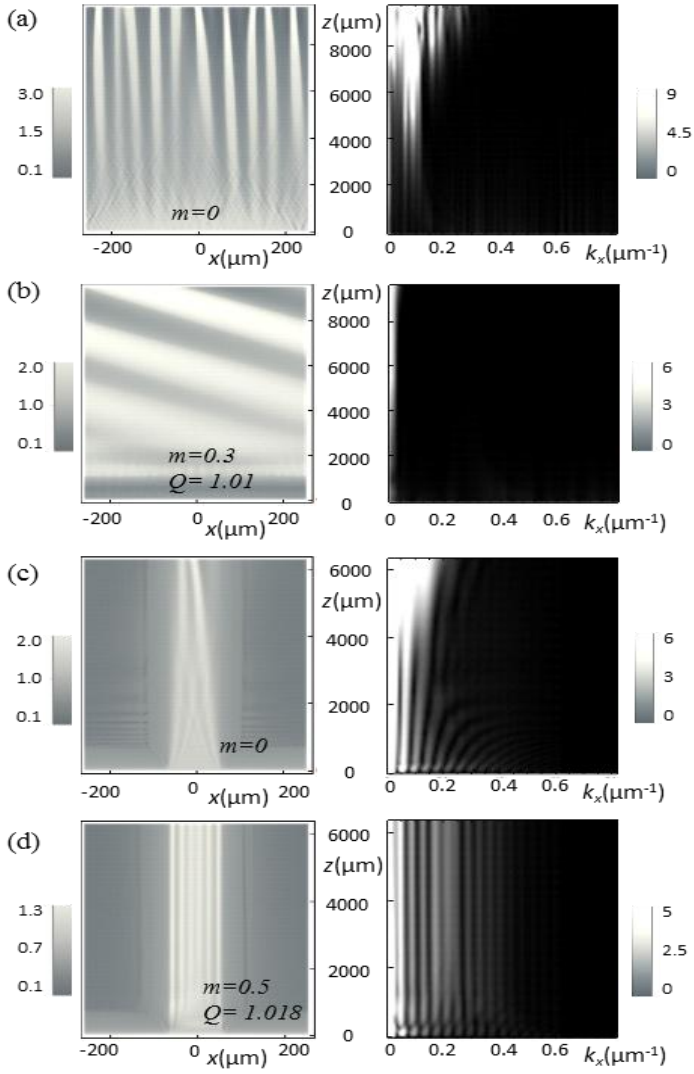

Fig.4.2.5: Numerically calculated field (left) and spectral (right) dynamics along the infinite-width (periodic boundary conditions) (a-b), and finite-width BAS amplifier (c-d), for unmodulated (a,c) and modulated cases. Partial stabilization with remaining LW instability is achieved in (b) while complete stabilization occurs in (d). For sake of clear representation the small-space modulations are filtered out while plotting. Parameters: p_0 = 1.2, α_H= 2, γ= 0.1, k_0= 2π, s=0.01.

4.2.4 Summary

The problem of the stability of the optical field in BAS amplifiers and lasers is currently a key technological challenge and of great relevance for many applications today. The problem of MI, which arises in the highly nonlinear optical fields, has posed a serious limitation on the performance of these devices and so far the efforts to curtail these instabilities have not been very successful. In this study, we proposed a method for the suppression of MI using a spatially modulated gain/loss profile of the active medium. Technically, this kind of spatial (spatiotemporal) modulation can be obtained by spatially modulating the pump current, by using, for instance, a pattern of 'fishnet' electrodes as illustrated earlier in Fig. 4.2.2. There can arguably be many other ways for this which are feasible by current technological means. Some of the possible methods for obtaining the spatial gain/loss modulation are illustrated in Fig. 4.2.6.

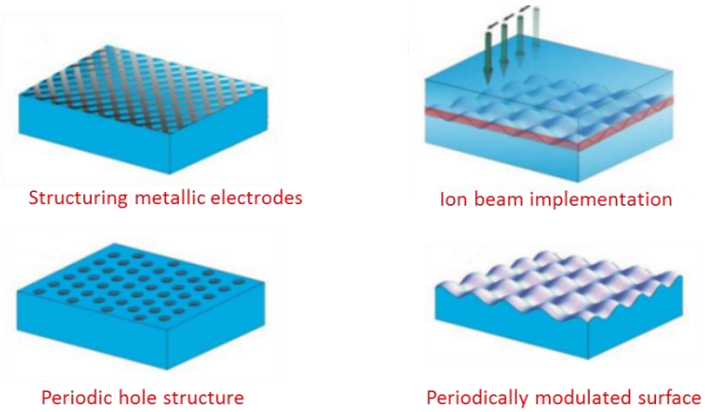

Figure 4.2.6: Schematic representation of potential methods for the implementation of a 2D spatial modulation of the gain/loss and index profile in BAS amplifying mediums.

The stabilization of MI by this method is shown to work satisfactorily well in the theoretical sense, where we have a substantial removal of the instability, but just fall short of complete stabilization. This limitation is, however, merely theoretical

since for real parameters and simulating for finite-width of the amplifier, this remaining instability is removed due to the cut-off effect of the transverse boundaries imposed on the weakly remaining long-wavelength instability. The MI in such BAS amplifiers is, in effect, completely suppressed leading to a stable, non-diverging output beam.

The present study for BAS amplifiers can be straightforwardly extended to BAS lasers, where many roundtrips of the amplifier need to be accounted for. We expect the stabilization mechanism to work equally well, if not better, in the case of BAS lasers, where multiple round-trips of the stable, amplified field, results in further suppression of the unstable modes, leading to a higher quality output beam at much higher powers.

Thus, the proposed mechanism for the control of MI in BAS amplifiers and laser has the potential to be a milestone in the drive towards achieving high-quality output beams in high power optical BAS devices.

4.3 Vertical-External-Cavity Surface-Emitting Lasers (VECSELs)

Like BAS lasers, another relevant class of semiconductor lasers are the Vertical-cavity semiconductor lasers which are equally important key sources of coherent light. The main difference lies in their configuration; unlike BAS lasers which are edge-emitting, VECSELs emit light from their top surfaces (see Fig. 4.3.1) which offers certain advantages over BAS emitters, including convenient fabrication processes. Being very efficient and with low production costs, they find applications in a large number of technical and commercial devices being also a major source of the optical signal in modern telecommunications.

Vertical-cavity semiconductor lasers are commonly distinguished into Vertical-Cavity Surface-Emitting Lasers (VCSELs) which have cavity length of a few micrometers and Vertical-External-Cavity Surface-Emitting Lasers (VECSELs), where an external cavity is used, with resonator lengths typically ranging from millimeters to centimeters. Seeded by intrinsic noise, VCSELs and VECSELs also suffer from dynamical spatiotemporal instabilities, which leads to chaotic oscillations and poor spatial beam quality, as illustrated in Fig. 4.3.1 (b-d). Some common phenomena such as self-focusing, filamentation, and spatial hole burning etc. are all dramatically enhanced with increasing pump power [Vall95, Marc96, Adac93].

While there are no methods which directly aim to suppress the MI in these devices, attempts to address the issue of transverse mode selection are usually made using a spherical output mirror which ensures operation at the fundamental transverse mode [Trop06]. The disadvantage of this technique, however, is that it strongly reduces the effective size of the active semiconductor region, confining it to the center of the device. This brings with it a reduction of the possible output power as well as the introduction of several disjoined elements into the setup, thereby reducing the robustness and compactness of the device. Moreover, long external resonators and external feedback designs in these lasers lead to additional unfavorable temporal effects such as linewidth broadening, coherence collapse and intensity noise enhancement [Law98, Ho93].

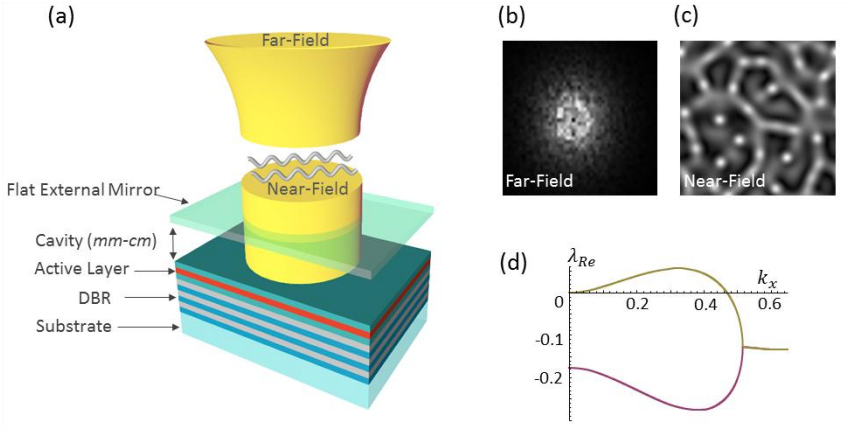

Figure 4.3.1: (a) Schematic representation of VCSELs and VECSELs showing their physical configuration and emission direction. The spatial beam quality of the output beam is poor, as plotted in (b) and (c) representing typical far-field and near-field profiles respectively. This is due to the MI present in the system, as seen from the unstable Lyapunov spectrum (d).

The possibility to use a flat output mirror in VECSELs would allow for the realization of relatively compact and robust devices with higher output powers. However, the MI problem remains to be solved in this case. Therefore, at present, there is a need for finding alternative physical mechanisms to eliminate MI in VCSELs and VECSELs.

In this section, we show that a stabilization of the MI in VECSELs is possible through a periodic spatiotemporal modulation of the potential. The modulation will be introduced into the system, parametrically, through the pump current as in the previous case of BAS amplifiers.

We consider VECSELs operating in three distinct regimes: Class-A laser regime, where a centimeter-long cavity results in a photon lifetime, τ_p, longer than the non-radiative carrier recombination time, τ_N, that is, $\tau_p \gg \tau_N$; Class-B laser regime, with micrometer-long cavities and much shorter photon lifetimes, $\tau_p \ll \tau_N$, and an intermediate laser regime with $\tau_p \approx \tau_p$.

The spatial field structures in all three cases can be described by the same physical model [Spin98], due to the common nature of the active semiconductor media.

Relaxation oscillations do not appear for the relatively long Class-A and the intermediate class lasers, which are characterized by the relative carrier relaxation rate values in the range of $1 < \gamma = \tau_p/\tau_N < 10$.

On the other hand, the few-micrometer-long VCSELs, with $\tau_p \sim ps$ and $\tau_N \sim ns$ photon and carrier lifetimes respectively, can be regarded as Class-B lasers [Uchi12]. As a consequence, contrary to the case of VECSELs, relaxation oscillations are inherent in VCSELs due to the small aspect ratio $\gamma \approx 0.01$.

Semiconductor lasers in all of the above-discussed limits exhibit chaotic oscillations due to MI. A representative plot showing the typical near-field (or the Fourier spectrum) and far-field profiles of these lasers along with the typical shape of the instability spectrum are shown in Fig.4.3.1 (b-c).

4.3.1 Modelling VECSELs

The mathematical model used to describe VECSELs, are a set of coupled equations describing the evolution of the optical field and carrier dynamics. The description of both VECSELs and VCSELs can be done by the well-established model proposed in [Spin98]. The mean field dynamics of the complex field amplitude, E, and the carrier density, N, in the active region are determined by the paraxial equations:

$$\partial_t E = -[1 + i\theta + 2C(i\alpha_H - 1)(N-1)]E + i\nabla_\perp^2 E \quad (4.3.1.a)$$

$$\partial_t N = -\gamma[N - I_p + (N-1)|E|^2] + \gamma d\nabla_\perp^2 N \quad (4.3.1.b)$$

where θ is the cavity detuning parameter, α_H is the linewidth enhancement factor of the semiconductor, and $\gamma = \frac{\tau_p}{\tau_N}$ is the carrier decay rate, normalized to the photon relaxation rate. The time, t, is normalized to the photon life-time, $\tau_p = 2L_c/vT_c$, which depends on the transmissivity factor, T_c, velocity of light, c, and cavity length, L_c. The transverse spatial coordinates (x, y) are normalized to $\sqrt{\lambda_0 L_c/2\pi T_c}$, where λ_0 is the central wavelength of the emitted light. The parameter C represents the interaction between carriers and the field and

depends on the laser differential gain and the photon relaxation rate. The transverse Laplacian operator, $\nabla_{\perp}^{2}$, describes the paraxial diffraction and carrier diffusion in the transverse direction. The pump current, I_p, generates the carriers within the active region which diffuse in the transverse direction according to the diffusion coefficient d. The interaction between carriers and the electromagnetic field corresponds to either absorption or stimulated emission depending on the sign of the $(N-1)$ term in the two coupled equations. The linewidth enhancement factor is a crucial parameter for semiconductor lasers. The laser operates in the amplifying regime for $(N-1)>0$, and lies in the self-focusing regime for $\alpha_H > 0$, which will be the case for the rest of this chapter.

4.3.2 Spatiotemporal Modulation of the Pump

The MI for the VECSEL model in Eq. (4.3.1) is explored through a standard linear stability analysis, in one-dimensional (1D) space. The amplitudes of the homogeneous stationary-state solution, (E_0, N_0), are given by, $E_0 = \left((I_p - N_0)/(N_0 - 1)\right)^{\frac{1}{2}}$ and $N_0 = (1 + 1/2C)$.

We add small amplitude perturbations to the stationary state solutions: $E(x,t) = E_0 + e(t)Cos(k_x x)$ and $N(x,t) = N_0 + n(t)Cos(k_x x)$ where $|e/E_0|$, $|n/N_0| \ll 1$, and substitute these expressions back into Eq. (4.3.1). Neglecting higher order terms of (e, n) we can calculate the eigenvalues, $\lambda_i(k_x)$, of the evolution equations for the small spatial perturbations, the real part of which gives the instability (Lyapunov) spectrum, $\lambda_{Re}(k_x)$, for the system. The typical shape of the Lyapunov spectrum for VECSELs, as shown in Fig. 4.3.1(d), represents finite long wavelength instability, similar to the BAS amplifier.

The bandwidth of unstable growing modes ranges from 0 to the largest unstable wavenumber $k_c = \sqrt{2\alpha_H(\mu-1)/\mu}$, where $\mu = 2C\left(I_p - 1\right)$ is the pump parameter, scaled conveniently so that it the laser threshold is at $\mu = 1$ [Prat07].

We aim to stabilize this MI by a small and fast scale spatiotemporal modulation of the potential, which is introduced through the pump current, $I_p = I_0 + 4mCos(q_x x)Cos(\Omega t)$, with (m, q_x, Ω) being the usual modulation parameters. The condition $4m < I_0$ is maintained, in order to keep I_p positive at all times.

4.3.3 Results: Stabilization of Modulated VECSELs

The solution of Eq. (4.3.1) with modulated pump is the so-called spatiotemporal Bloch mode with spatial and temporal periods of q and Ω respectively, that is, following the modulation profile. The resonance parameter remains $Q = \Omega/q_x^2$. We numerically investigate the stability of the Bloch solutions following the modified Floquet method. The results are presented in the following sections for three characteristic operation regimes.

I. Intermediate Class VECSELs

In the case of millimeter-long optical cavities, the normalized carrier decay rate $\gamma \approx 1$ and VECSELs operate in a relaxation free lasing regime.

In such regimes, by scanning the parameter space, (m, Q), we are able to obtain certain regions (i.e. different parameter sets) where the MI is completely stabilized. Different regions of the parameter space may lead to partial suppression with remaining long-wavelength or short-wavelength instability, while other regions may also show enhancement of the MI. Some of the most representative Lyapunov spectra, showing the different types of kinds of partial and complete stabilization, for various parameter sets are plotted in Fig. 4.3.2.

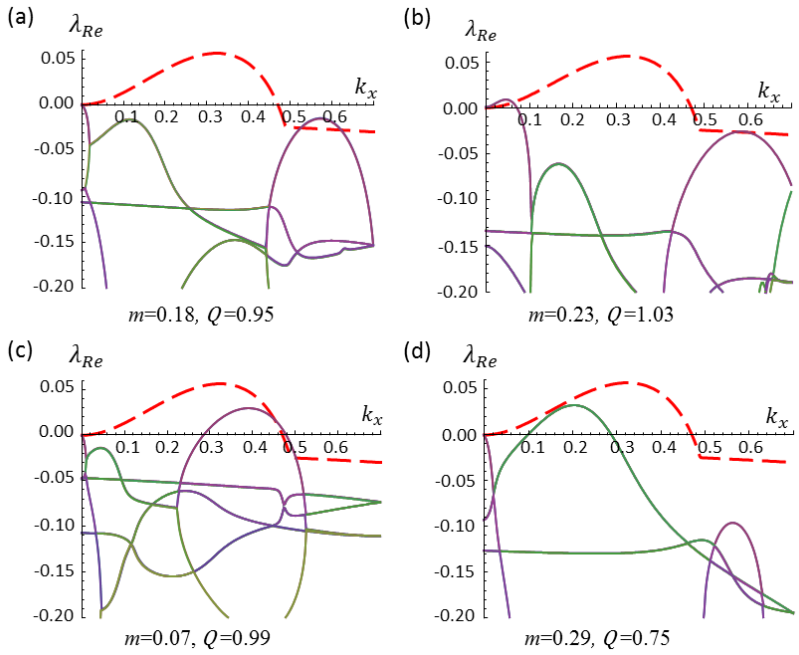

Figure 4.3.2: Representative cases showing partial and complete stabilization of MI in intermediate class VECSELs for various parameter sets. The different plots show complete stabilization (a), and partial stabilizations with weak remaining long-wavelength instability (b) and short-wavelength instability (c-d). The red dashed curve represents the unmodulated VECSEL prior to stabilization. Parameters: α_H=1.5, θ=-1.5, C=0.6, I_0=1.9, d=0.052, γ=1 and q_x=1.4, with periodic boundaries.

A color-coded stability map in the parameter space (m, Q) plots the maximal Lyapunov exponent, λ_{Re}^{max}, of the linear evolution matrix, as shown in Fig. 4.3.3(a). There are, in fact, two distinct islands of complete stabilization, one of which is located close to resonance, $Q \approx 1$, and within reasonable limits of the modulation amplitude $4m < I_0$. The other stable island is located far from resonance, around $Q \approx 0.3$ and for values $4m > I_0$, which could probably be ignored in the case of a real physical model. Like always, we note that there are distinct areas in the map, represented as yellow, where the stationary Bloch-mode solutions are too unstable to isolate. These regions are excluded from the analysis. An accompanying map in Fig. 4.3.3(b) classifies the regions of the

parameter space according to the nature of the remaining instability, which may be either short or long wavelength instability.

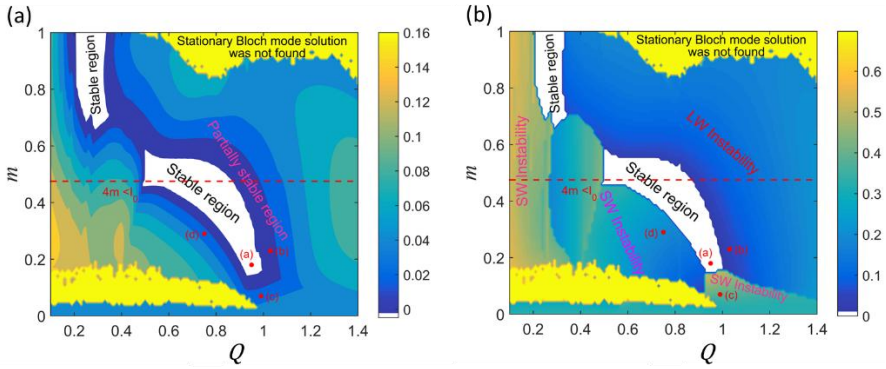

Figure 4.3.3: (a) Stability map of the largest remaining Lyapunov exponent λ_{Re}^{max} after stabilization in the parameter space (m, Q) for intermediate class VECSELs. (b) Map of the corresponding dominant wavenumbers k_x^{max}. The limit for the modulation amplitude of common VECSEL configurations (i.e. $4m < I_0$) is represented by a horizontal red dashed line. The other parameters are as in Fig. 4.3.2.

The modified Floquet stability analysis results are confirmed by numerical integration of the full nonlinear model. These are presented in Fig. 4.3.4, in comparison to the unstable unmodulated VECSEL model. For appropriate pump modulation parameters, the chaotic dynamics is reduced or eliminated, resulting in partial stabilization with remaining weak LW or SW instabilities or complete stabilization, shown in Fig. 4.3.4 (b-d).

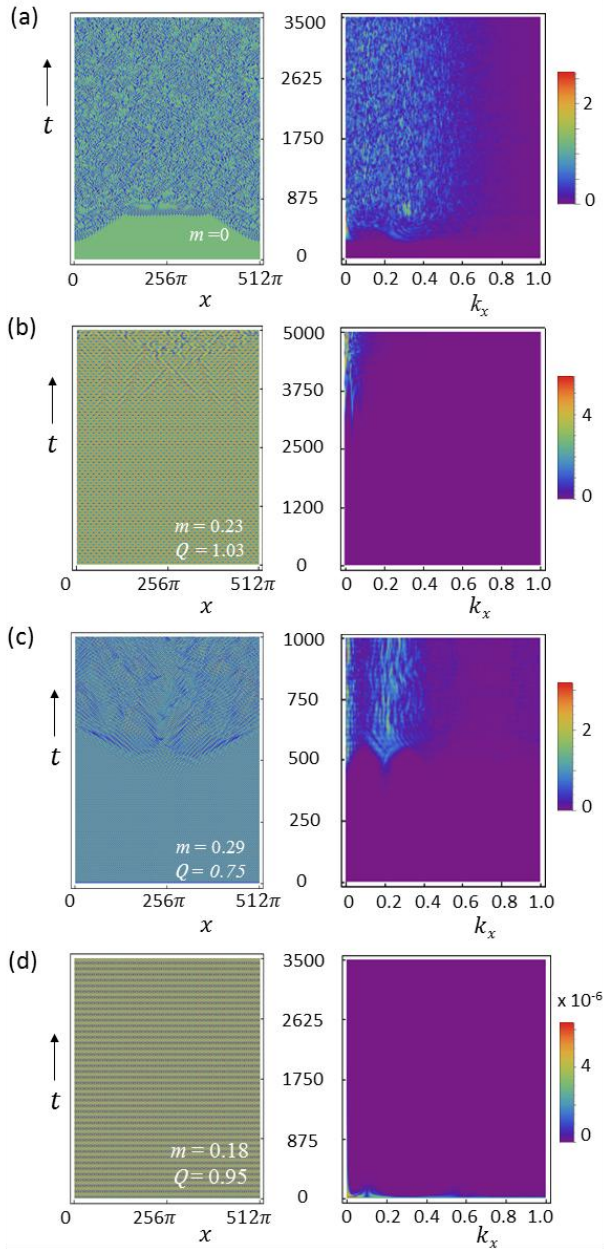

Figure 4.3.4: Numerically calculated field intensity (left) and spatial spectrum (right) dynamics of spatiotemporally modulated VECSELs in the intermediate regime. The plots are for unmodulated (a) and modulated cases (b-d). Full stabilization is realized in (d), while a weak remaining LW MI is seen in (b) and SW MI in (c). The parameters remain the same as in Fig. 4.3.2, with periodic boundary conditions being used.

A more extensive analysis of the results of the integration of the full nonlinear model is presented in comparison with the results of the stability analysis for the entire relevant parameter space, (m, Q), in Fig. 4.3.5. The system's stability under direct integration is determined by following the long-time (typically integration time of ~25000 units) spatiotemporal dynamics of the modulated system after perturbing the steady-state solution with a small, δ-correlated perturbation. The stable and unstable regimes obtained by the numerical integration are superposed onto the stability map obtained from modified Floquet linear stability analysis, represented as solid dots (•) and crosses (x) respectively.

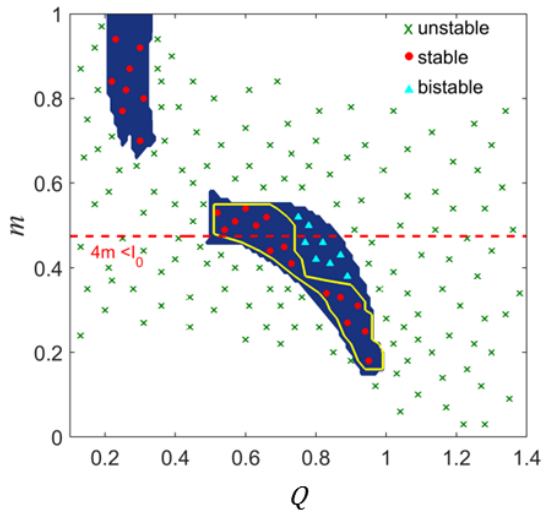

Figure 4.3.5: The results of the numerical integration and the stability analysis are in good agreement with each other as shown in the superposed map. The area outside the yellow contour, but within the central blue region (indicated by triangles) represents a bistable region. The other parameters remain the same as in the previous plots.

We find that the stable points (•) resulting from the numerical integration match well with the stabilized area of the stability map (blue area), confirming the results of the linear stability analysis. There is also a small sub-region within the stabilized region, in Fig.4.3.5, where, depending on the initial conditions, at least two different nonlinear states exist: (a) the stable Bloch-modes as predicted by modified

Floquet analysis (stable regime) or (b) Bloch modes which become turbulent after some time (turbulent regime). Thus, we can say that the parameters in this region lead to bistability. To identify the bistable regimes we perform numerical simulations of Eq.(4.3.1) for a fixed modulation amplitude, m, while step-wise changing (increasing and decreasing) the parameter Q. A comparison of the field dynamics for different directions of sweep of the parameter Q allows us to distinguish a uniquely stable region delimited by the yellow curve and the bistable region located within the blue shaded area but outside the yellow curve and represented by the green triangles. Here, depending on the initial conditions, the calculated solution was attracted either to the stable stationary Bloch-mode solution, or to some chaotic attractor. Note that bistability between different spatiotemporal dynamical regimes is generally typical for intermediate regime of VECSELs, for instance as reported in rocked VCSELs in [Oto14].

II. Class-A VECSELs

Next, we investigate the stability of VECSELs in Class-A limit where the normalized carrier decay rate reaches $\gamma \approx 10$, as a result of centimeter-long optical cavities. This is compatible with the general conclusion that unstable spatio-temporal dynamics are more pronounced for Class-B lasers than for Class-A lasers [Stal03]. We find that in this case, MI is easier to stabilize. The modified Floquet stability analysis is performed and the parameter space is explored by plotting the stability map, in order to determine the complete and partial stabilization regions. The results of this are summarized in Fig. 4.3.6(a), from which it is evident that the completely stabilized region is slightly enhanced as compared to the intermediate class of VECSELs. The spectra of the Lyapunov exponents for the most representative points in the parameter space are shown in in Fig. 4.3.6(b-d).

The model equations for Class-A lasers ($\gamma \approx 10$) can be further simplified by adiabatically eliminating the population inversion. Particularly, for small field

intensities, the model given by Eq.(4.3.1) can be reduced to a single nonlinear field equation:

$$\partial_t E = -\left[1 + i\theta + 2C(i\alpha_H - 1)\left(I_p - 1\right)(1 - |E|^2)\right]E + i\Delta_\perp^2 E \qquad (4.3.2)$$

This is the Complex Ginzburg-Landau equation (CGLE). The complex potential of such CGLE is periodically modulated due to the modulation of the pump current. In this way, stabilization of modulated VECSEL in Class-A limit is directly related to the stabilization of the modulated CGLE of Chapter 2. Different versions of the CGLE have been derived for Class-A and Class-C laser models [Coul89, Oppo91, Stal93], in contrast to Class-B lasers where the models are not reducible to a single equation of the CGLE type [Stal03, Oppo09].

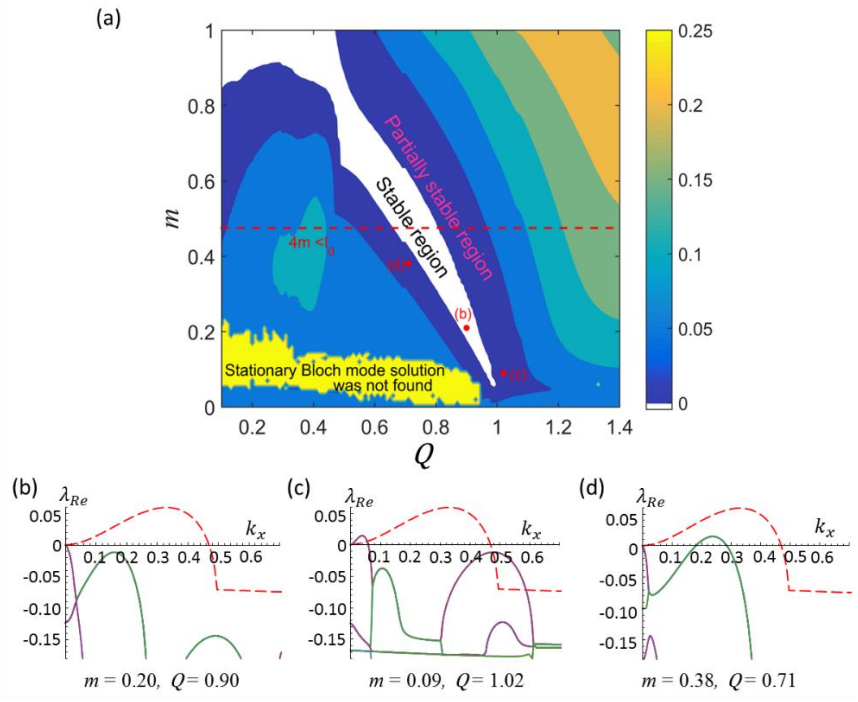

Figure 4.3.6: (a) Stability map for the largest Lyapunov exponent λ_{Re}^{max} in the parameter space (Q, m) for Class-A VECSELs with γ=10 and q_x=1.8. The main Lyapunov exponents (solid lines) in each case are compared to the unmodulated VECSELs (red dashed line). Complete and partial stabilization with remaining weak LW and SW instabilities are shown in the plots in (b), (c) and (d), respectively. Other parameters are the same as in Fig. 4.3.2.

III. Class-B VECSELs

The stabilization of short-cavity Class-B VECSELs is more challenging. The results from the stability analysis show that in this regime full stabilization is possible for VECSELs with cavity lengths only as small as $\sim$100 μm, but not smaller. We consider a normalized carrier decay rate on the order of $\gamma \approx 0.1$, corresponding to the limiting case of a $\sim$100 μm long cavity. The complete suppression of MI can still be achieved for these parameter values in a small region of the parameter space. However, stronger modulation amplitudes are required for such stabilization, as compared to the Class-A and intermediate class VECSELs. This is mainly due to intrinsic relaxation dynamics of the carriers which tends to make the system very unstable.

We see from the stability map, plotted in Fig. 4.3.7, that a complete stabilization region exists, although it is smaller than the Class-A and intermediate class VECSELs. We also note that bistability is obtained in all stabilized regimes for Class-B VECSELs (compare with Fig. 4.3.5).

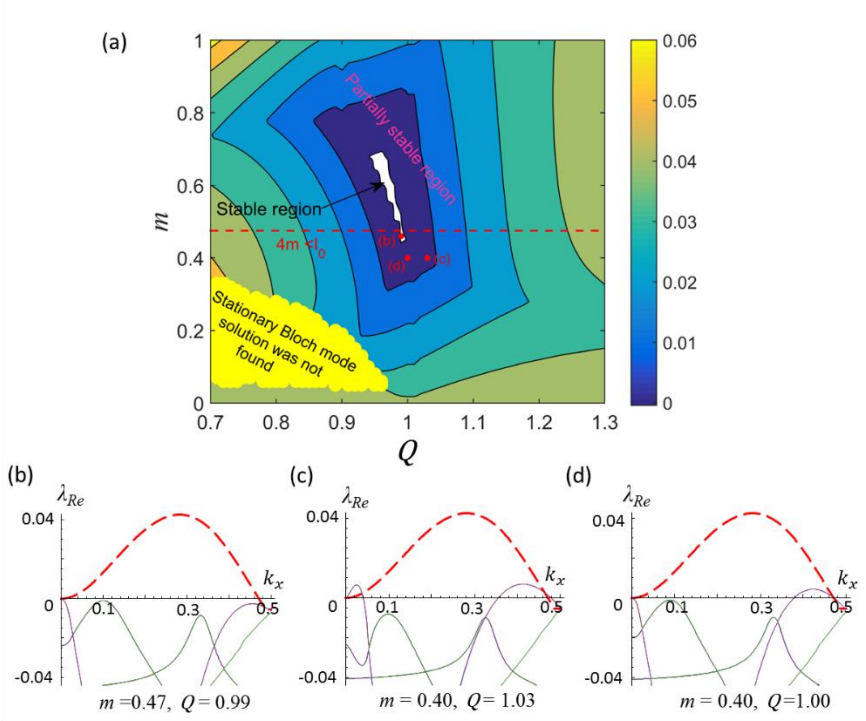

Figure 4.3.7: The stabilization of Class B VECSELs, although a more challenging task, is possible for cavity lengths as small as ~100μm. (a) Stability map in the parameter space for Class-B VECSELs with γ = 0.1 and q_x=1.0. Lyapunov exponents for particular cases showing complete stabilization (b), partial stabilization with remaining weak LW and SW instability in (c) and SW instability alone (d). Other parameters are the same as in Fig. 4.3.2.

4.3.4 Stabilization of MI in Two-Dimensional (2D) VECSELs

Finally, the analysis of the stabilization of VECSELs is extended to two-dimensions (2D) in space (x, y) and time. The modulation of the pump current in this case is of the form: $I_p = I_0 + 4\left[m_x Cos(q_x x) + m_y Cos(q_y y)\right] Cos(\Omega t)$, where, m_x and m_y are the modulation amplitudes along x and y-coordinates respectively while q_x and q_y are the corresponding spatial frequencies of the modulation.

The analysis in this cases is limited to the direct numerical integration method, the typical results of which are shown in Fig. 4.3.8, representing cases of partial

and complete suppressions of the MI. The different plots represent snapshots of the numerically calculated field (left) and spectra (right) of the system after a long transient time (t~400). For comparison, a snapshot of the chaotic field patterns and the unstable spectrum the unmodulated VECSEL is shown in Fig. 3.4.8(a).

In the case of asymmetric modulation, for instance, when the modulation is introduced in only one spatial coordinate, as shown in Fig. 3.4.8(b) where ($m_x \neq 0, m_y = 0$), the suppression of the MI is correspondingly asymmetric, that is, only along the modulated coordinate x.

On the other hand, the symmetric modulation profiles are shown in Fig. 3.4.8(c-d), with square symmetry, for different values of the parameter m. The two representative cases demonstrate the partial and complete stabilization of the MI.

The general conclusion from 2D calculations is that the stabilization mechanism introduced in the 1D model works just as well also in the 2D scenarios. The 2D system, however, offers richer possibilities: one can imagine scenarios where we have different modulation geometries or different modulation frequencies in the two coordinates, perhaps leading to interesting phenomena. These analyses are, however, left for a detailed study of these individual models as it is not the main focus of this thesis.

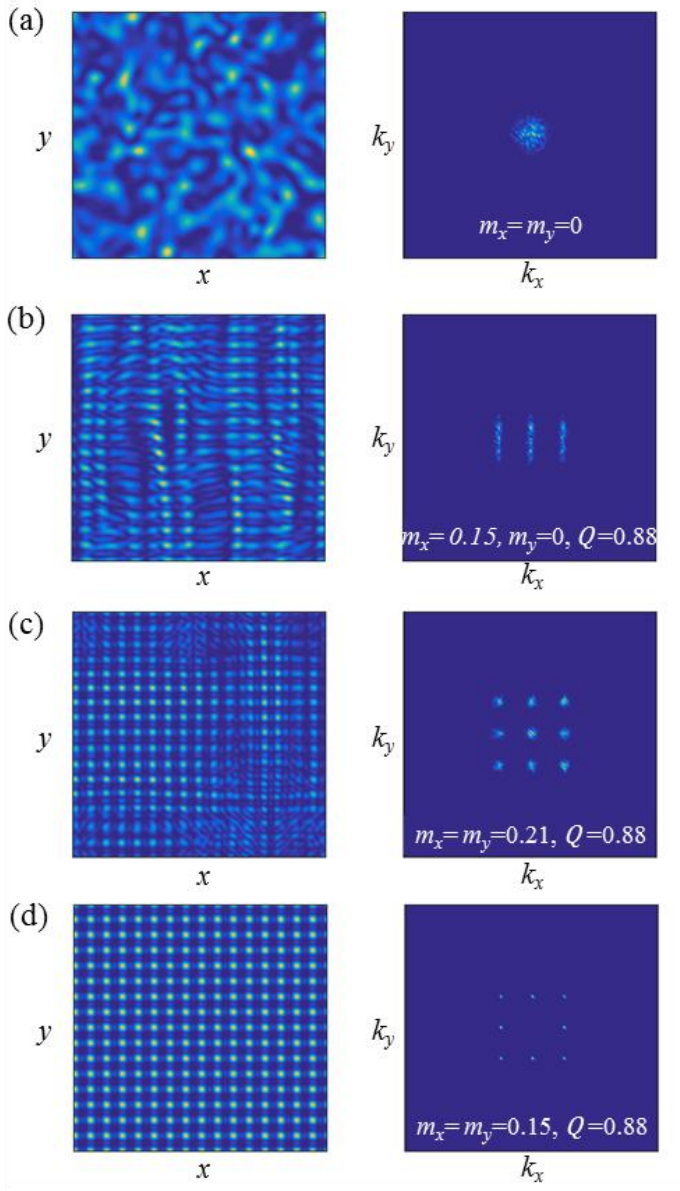

Figure 4.3.8: Analysis of 2D VECSELs. Numerically calculated snapshots of the intensity distribution patterns after a long transient time (t∼400) for the 2D VECSEL model, showing field intensity (left) and spatial spectrum (right). The size of integration window is 100x100. (a) Chaotic intensity distributions for the unmodulated system. (b) Suppression of MI only in the horizontal direction. (c) Partial stabilization in both spatial directions and (d) complete stabilization for a square symmetric modulation. Parameters are as in Fig.4.3.2.

4.3.5 Summary

Summarizing, we have proposed and demonstrated the stabilization of flat-mirror VECSELs by a spatiotemporal modulation of the pump current which can contribute to enhance the stability of such lasers at higher powers and improve the spatial quality of the output beam.

By using a modified Floquet analysis and direct integration methods, we calculate the MI free operating regions, in the parameter space. The analyses are presented for VECSELs operating in different regimes with special attention to the case of intermediate class VECSELs which is expected to have the most important technological impact. We show that Class-A VECSELs can also be efficiently stabilized thus making the proposed stabilization technique well suitable for quantum dot VECSELs, which are characterized by significantly large values of the carrier decay rate [Shan12]. Short cavity, Class-B laser VECSELs (and VCSELs) limit the stabilization since only lasers with length cavities down to around 100 μm can be completely stabilized by the proposed method.

Long cavity VECSELs are not compact light sources and can, therefore, be stabilized by other means, such as by using curved mirrors, as discussed in the introduction. On the contrary, we show that VECSELs of ∼1 mm cavity length, referred to as the intermediate case, can be most efficiently stabilized by the proposed method. This is especially significant since for this class no other regularization mechanisms (e.g. curved mirrors) are applicable. The estimated frequency and period of the modulation required for the stabilization of VECSELs in such intermediate regimes are experimentally achievable and technologically viable, being on the order of 10 GHz and 100 μm, respectively.

4.4 Stabilization of BAS Amplifiers using Genetic Optimization

In Section 4.2 of this chapter, we analyzed the stabilization of the BAS amplifier by a 2D spatial modulation finding that although in real devices the stabilization is achieved, in a strictly theoretical sense, complete stabilization was not possible. This was due to the presence of very weakly remaining long-wavelength MI. We can also recall the work from that Chapter 3 which demonstrated the use of a multi-frequency Genetic Algorithm (GA) optimized multi-frequency modulation to control MI in arbitrarily complex systems.

In this section, we will apply this concept to the BAS amplifier with the aim of fully controlling the MI, even in the theoretical limit of infinite-width amplifiers. We will also present the method of GA optimized multi-frequency modulation of BAS amplifiers for more complicated scenarios, such as for high values of the linewidth enhancement factor α_H.

In order to introduce the modulation into the active medium, we modulate the pump current with a multi-frequency modulation. We consider a 2D pump profile generated by n wavevectors $\vec{q}_j(q_x, q_z)$ with amplitudes m_j and phases ϕ_j:

$$p(x,z) = p_0 + Cos(q_x x)\sum_j^n m_j Cos(q_{z,j} z + \phi_j) \tag{4.4.1}$$

The longitudinal frequencies are distributed in an equidistant manner, such that $q_{z,j} = j \times \Delta q_z$, in order to maintain the Floquet linear stability procedure (for a detailed explanation, see Section 3.4).

We first analyze the case of $\alpha_H = 2$, the same problem as in Section 4.2, by considering the number possible wavevectors limited to $n = 20$, and the corresponding equi-spaced resonance parameters, within the range $0.1 < Q_j < 2$. The target function is defined, in this case, as the integral of the positive Lyapunov exponents $L = \int [\lambda_{re}(k)]_{positive}\, dk$. In this way, as the GA iteratively searches for a minimum value, in each generation, we can expect the 'global

instability' to reduce correspondingly. The parameters of the optimization problem are the amplitudes and phases $(m_{1,2\dots j}, \phi_{1,2\dots j})$ of the modulation function in Eq. (4.4.1), where an upper limit to the modulation amplitudes is specified, $m_j \leq 1$, to keep it within realistic values.

One of the results from the GA optimization is presented in Fig.4.4.1, where complete stabilization is achieved. The multi-frequency modulation profile, as obtained by the algorithm is shown in Fig. 4.4.1(a) for one period, $T_z = 2\pi/\Delta q_z$, in the z-coordinate, along with the values for the parameters $(m_{1,2\dots j}, \phi_{1,2\dots j})$ in Fig. 4.4.1(b-c). The stabilized Lyapunov spectrum of the system is presented along with the unmodulated system for comparison.

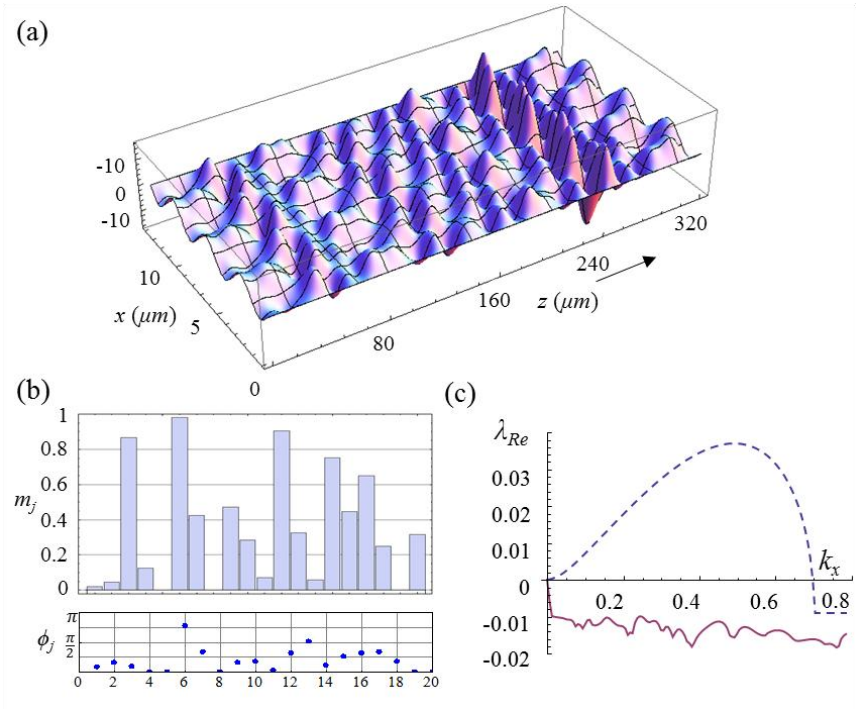

Figure 4.4.1: Results from GA optimized stabilization of BAS amplifier for large linewidth enhancement factor and pump values $(\alpha = 5, p_0 = 2)$. (a) The profile of the spatiotemporal modulation for one period. (b) Values of the calculated modulation parameters and (c) the stable Lyapunov spectrum (solid) compared to the unmodulated BAS amplifier (dashed).

The results of the stability analysis are confirmed by straightforward integration of the modulated system in Fig.4.4.2, where the longitudinal periodicity is visible. The evolution along the propagation axis is compared with the unmodulated case. It is evident from the figures that the complete stabilization of MI is achieved in the GA optimized modulation, where the steady-state Bloch-mode remains stable for indefinitely long propagation times. This is in sharp contrast to the highly unstable case of the unmodulated BAS amplifier MI leads to turbulent regimes and highly chaotic field dynamics.

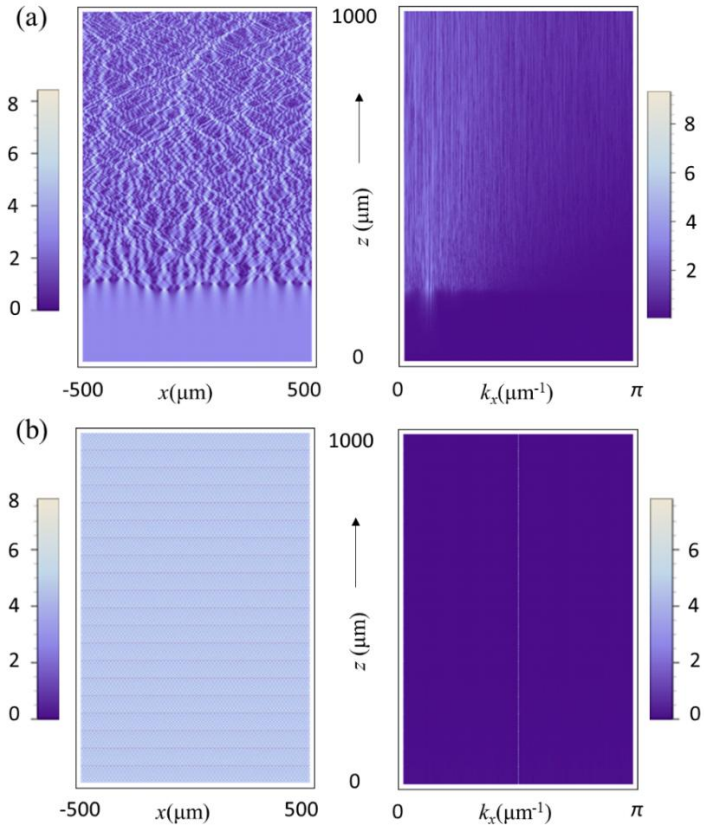

Figure 4.4.2: Complete stabilization of the BAS laser with an optimized multi-frequency 2D spatial modulation. The parameters are for a linewidth enhancement factor, αH=2, an average pumping of p_0=1.2, γ=0.1 and s=0.1. The direct integrations are calculated for a free space wavenumber$\lambda_0 = 1\mu m$, for the transverse width of 64μm active area and an integrated length of 3mm.

The successful stabilization of the MI in a BAS amplifier with such a high value of the α_H parameter demonstrates the huge potential of the genetically optimized multi-frequency method. One of the main advantages of this method is the possible stabilization of transverse modes with small wavenumbers that transports a lot of energy and previously always remained unstable.

Increasing the number of modulation frequencies, however, brings with it certain challenges too, such as an increase in the number of regions of unstable stationary Bloch solutions, similar to what was encountered in the single-frequency modulations (for example, the black tongues in Fig. 4.2.4). This further adds to the decrease in the areas of complete stabilization, which was already smaller for higher instabilities. As a result, the areas of complete stabilization in the parameter space shrinks substantially as the stabilization problem becomes more complex, leading to an eventual saturation of the stabilization performance of the multi-frequency GA optimized method. A full quantitative study of the saturation limits of this method is still a work in progress.

4.5 Conclusions

The modern technological revolution is based on many key pillars, and perhaps one of the most transformative are has been the field of photonics. This has been mainly possible with the availability of cheap and robust photonic devices among which semiconductor amplifiers and laser occupy a central place. There are numerous benefits that these coherent light sources offer over other conventional types of lasers but, however, there is one key drawback- the inherent lack of good optical quality of the emission; which puts a serious limit on their potential applications. In this chapter, it has been demonstrated that by means of a new method for the control of MI in BAS amplifiers and VECSELs we can obtain an improved optical beam quality from these devices at high operating powers, and this limit can be substantially overcome.

The method works based on a spatiotemporal (or 2D spatial) modulation of the gain/loss profile of the active semiconductor medium. This spatiotemporal modulation causes a modification of the temporal dispersion (spatial dispersion in BAS device) relation, by introducing bandgaps in the unstable regions of the dispersion profile, most effective close to the resonance condition $Q \approx 1$.

The characterization of the instability is done through a modified Floquet linear stability analysis, a numerical technique, which was developed for this study and which provides a very accurate analysis of the stabilization performance. Using this technique, the parameter space of the independent modulation parameters is explored through a 'stability map' which quantifies the stabilization performance for all sets of parameters.

In the context of Vertical Cavity Semiconductor lasers, complete stabilization was possible in some cases such as the Intermediate class of VECSELs in 1D and 2D, the Class-A VECSELs, and to some extent the Class-B VECSELs. In the context of BAS amplifiers, while partial stabilization was achieved by this method, in a theoretical sense, with weak remaining long-wavelength instability, in real physical systems with finite-widths, this remaining instability does manifest. All

these results were confirmed by direct numerical integration of the full nonlinear models.

A further improvement of the stabilization by spatiotemporal modulation method, which follows from the work of Chapter 3, was demonstrated in the case of BAS amplifiers. This method uses multiple modulation frequencies in the longitudinal direction, leading to the creation of multiple bandgaps in the dispersion profile of the system. This is required for complicated or highly unstable systems when the instability band is too large to be covered by a single modulation induced bandgap. The effectiveness of this method was demonstrated for BAS amplifiers with much larger linewidth enhancement factors, up to α_H=*5*, and the results confirmed by direct integration.

Thus, in this chapter, the first realization of a powerful new technique for the stabilization of different types of semiconductor amplifiers and lasers is demonstrated. Future works in this direction would be the application of this stabilization technique to BAS lasers, and the experimental demonstrations of the working of these stable semiconductor amplifiers and lasers.

Chapter 5

General Conclusions and Future Perspectives

The promise of the stabilization of MI in spatially-extended systems has been an alluring but challenging one. In spite of the efforts of the last few decades there still does not exist a general mechanism for the control and suppression of this instability, yet some steps have been advanced towards the comprehension of the problem. In this thesis, a fundamental mechanism for the same was proposed, based on a newfound understanding of this old phenomenon.

In Chapter 2, the initial idea is exposed, and a method is described to exploit the deep physical insight of the link between the modulation instability in a system and the profile of its dispersion curve. It is found that the presence of unstable bands in the dispersion profile is the root cause of the modulation instability, with the character of the instability directly depending on the shape of the dispersion curves within certain unstable bands. The modification of these unstable dispersion bands automatically leads to a modification of the instability, thus providing an intrinsic powerful method for its manipulation and ultimately suppression. Specifically, the introduction of appropriately located bandgaps in the dispersion profile would allow for the suppression of the continuum of unstable modes in that frequency band, thereby eliminating MI.

An appropriate manipulation of the dispersion- one which leads to the suppression of the MI- is indeed possible through a properly designed

spatiotemporal modulation of the potential of the system, at small spatial and fast temporal scales. The mechanism of MI suppression relies on a 'resonant' interaction between the spatial and temporal frequencies of the modulation, which only occurs when the, aptly named, 'resonance parameter', Q, is close to or equal to unity, $Q \approx 1$.

For such modulation geometries, the bandgaps introduced by the periodic modulations are located close to the origin, i.e. in the Fourier space close to, which results in a suppression of the long-wavelength type instabilities, which are very difficult, if not impossible to suppress otherwise. The results comprising this chapter have been published in [J4].

This initial idea is then further explored and generalized, leading to a much more powerful mechanism in a '*stabilization on demand*' scheme. In Chapter 2, the suppression of MI was obtained by a periodic spatiotemporal potential: i.e. through sinusoidal modulation profiles in the spatial and transverse coordinates. In Chapter 3, this concept has been adapted for arbitrary modulation profiles, which is represented through multiple sinusoidal modulations in the temporal coordinate, leading to the concept of stabilization by a multi-frequency spatiotemporal modulation. The presence of multiple frequencies creates multiple resonances which lead to the creation of multiple different bandgaps in the dispersion profile. These can be tuned so that they cover a much broader area of the unstable spectrum or create bandgaps around different spatial wavevectors, depending on the stabilization requirements. To achieve the desired stabilization profile, i.e. a desired shape of the Lyapunov spectrum, an appropriate modulation is created using a 'reverse optimization process', in which a target Lyapunov spectrum is first specified and then an optimization algorithm is tasked to find the corresponding multi-frequency modulation profile which best fulfills the stabilization requirement. Due to the huge volumes of the parameter space, this optimization problem is very complex and challenging task, and can only be approached using the modern heuristic search algorithms, such as the Genetic Algorithm (GA).

This reverse approach to the stabilization problem, that is, the understanding of the dispersion dependent instability, when used in conjunction with the powerful, GA-based optimization method, yields a very powerful tool for not just the suppression of modulation instability, but its manipulation in an arbitrarily desired manner. In other words, one has the ability to create *stabilization on demand*, in systems described by the complex Ginzburg-Landau model. This can be used, for instance, to suppress pattern forming modulation instabilities at short wavelengths, long wavelength or strictly over a finite band of wavelengths. Lastly, it may also be used for the *generation* of patterns at desired wavelengths, by specifying appropriately designed unstable Lyapunov spectra, and this could lead to potentially new applications in the future. The results of this Chapter have been published in [J2].

The mechanism of stabilization of MI by these methods are potentially applicable to a large class of spatially-extended systems- those which are described by the complex Ginzburg-Landau equation. The universality of the CGLE for the description of the phenomenon of MI was the main motive behind its use as the central equation in the study. This applicability is demonstrated in Chapter 4, for the case of Broad Area Semiconductor (BAS) amplifiers and Vertical Cavity Surface Emitting Lasers (VCSELs).

There is no doubt that semiconductor light sources have revolutionized the field of photonics and find innumerable application in modern technology. Being both, a very efficient source of coherent light, and having very tiny physical dimensions, they offer unparalleled advantages. However, at the same time, these devices suffer seriously from modulation instability, leading to very poor spatial quality of the output beam, which deteriorates with increasing operating powers.

A novel method for the suppression of these instabilities is provided in this chapter, which relies on our proposed stabilization methods.

In the case of the BAS amplifier, using a two-dimensional spatial modulation of the pump current (which is in essence similar to a spatiotemporal modulation in this system) the MI can be partially (for infinitely broad amplifiers) and

completely (for finite width amplifiers) suppressed for realistic parameters. The suppression of MI leads to a large improvement in the output beam quality, which shows little to no divergence in propagation as compared with the unmodulated amplifiers. The results of this study have been published in [J5].

In VECSELs, the range of parameters is quite broad and depending on the cavity length, γ, these lasers can be divided roughly into three categories: Class- A, Class-B and intermediate VECSELs regimes. The stabilization procedure remains the same, and although the suppression of MI is achieved all three cases, the success of the results vary. In Class-A VECSELs the MI is efficiently suppressed, making the proposed stabilization technique well suitable for quantum dot VECSELs. While in the case of short cavity, Class-B VECSELs (and VCSELs) the stabilization is limited for cavity lengths down to around 100 μm, below which the stabilization effects is reduced.

Of most special interest, however, is the intermediate regime VECSELs with cavity lengths of $\sim$1 mm, which are very effectively stabilized by this method, and for which no other stabilization mechanisms (e.g. using external curved mirrors) are applicable. These class of VCSELs is expected to have the widest impact in technological areas. The results of this part of the study have been published in [J3].

Finally, the BAS amplifier is revisited and in the context of stabilization by a GA optimized multi-frequency 2D spatial modulation. This method is the most powerful as it allows for the complete suppression of MI even for very high nonlinear regimes. The results are verified through numerical integration of the full nonlinear model and corroborate the results of the Floquet stability analysis. A more detailed study on the stabilization of MI by this method, in the context of BAS amplifiers, is in progress, although expected to be completed soon and submitted for publication.

Apart from this ongoing work, there are a few potential ideas and lines of research which have come to light during the development of this thesis. Following the successful demonstration of stabilization in the 2D CGLE, the scope

for further investigation remains open. The dynamics of 2D CGLE provides a rich playground for many interesting phenomena which are not necessarily present in the 1D analysis. The development of the 2D modified Floquet analysis is an important first step in that direction, although much remains to be explored. For instance, the effect of various other asymmetric modulations geometrics such as hexagonal, octagonal, quasi-periodic etc. on the MI of the system is a challenge. At the same time, it is also a great opportunity, as these case have never been researched before.

The successful suppression of MI in BAS amplifiers also leads naturally towards the next phase, which is the stabilization of BAS lasers. The expectation is that the stabilization of lasers will also prove successful. Simultaneously, the possibility of experimental demonstration of this stabilization phenomenon is also high, and there are already steps being taken in this direction with new collaborations with experimental groups and semiconductor laser companies.

Bibliography

[Abas01] Abas, S. J. (2001). Islamic geometrical patterns for the teaching of mathematics of symmetry. Symmetry: Culture and Science, 12(1-2), 53-65.

[Ablo11] Ablowitz, M. J. (2011). Nonlinear dispersive waves: asymptotic analysis and solitons (Vol. 47). Cambridge University Press.

[Adac93] Adachihara, H., Hess, O., Abraham, E., Ru, P., & Moloney, J. V. (1993). Spatiotemporal chaos in broad-area semiconductor lasers. JOSA B, 10(4), 658-665.

[Agra07] Agrawal, G. P. (2007). Nonlinear Fiber Optics. Academic press.

[Akhm05] Akhmediev, N., & Ankiewicz, A. (2005). Dissipative solitons in the complex Ginzburg-Landau and Swift-Hohenberg equations. Dissipative solitons, 17-34.

[Anti81] Antipov, S. V., Nezlin, M. V., Trubnikov, A. S., & Kurchatov, I. V. (1981). Experimental studies of Langmuir solitons. Physica D: Nonlinear Phenomena, 3(1-2), 311-328.

[Aran02] Aranson, I. S., & Kramer, L. (2002). The world of the complex Ginzburg-Landau equation. Reviews of Modern Physics, 74(1), 99.

[Back96] Back, T. (1996). Evolutionary algorithms in theory and practice: evolution strategies, evolutionary programming, genetic algorithms. Oxford university press.

[Baiz02] Baizakov, B. B., Konotop, V. V., & Salerno, M. (2002). Regular spatial structures in arrays of Bose–Einstein condensates induced by modulational instability. Journal of Physics B: Atomic, Molecular and Optical Physics, 35(24), 5105.

[Ball99] Ball, P., & Borley, N. R. (1999). The self-made tapestry: pattern formation in nature (Vol. 198). Oxford: Oxford University Press.

[Bart90] Bartuccelli, M., Constantin, P., Doering, C. R., Gibbon, J. D., & Gisselfält, M. (1990). On the possibility of soft and hard turbulence in the complex Ginzburg-Landau equation. Physica D: Nonlinear Phenomena, 44(3), 421-444.

[Bena01] Bénard, H. (1901). Les tourbillons cellulaires dans une nappe liquide propageant de la chaleur par convection: En régime permanent. Gauthier-Villars.

[Benj67a] Benjamin, T. B., & Feir, J. E. (1967). The disintegration of wave trains on deep water Part 1. Theory. Journal of Fluid Mechanics, 27(03), 417-430.

[Benj67b] T.B. Benjamin, (1967). Instability of periodic wavetrains in nonlinear dispersive systems, Proc. Roy. Soc. A. 299, 59–75.

[Berg98] Bergé, L. (1998). Wave collapse in physics: principles and applications to light and plasma waves. Physics Reports, 303(5), 259-370.

[Besp66] Bespalov, V. I., & Talanov, V. I. (1966). Filamentary structure of light beams in nonlinear liquids. ZhETF Pisma Redaktsiiu, 3, 471.

[Biel94] Bielawski, S., Derozier, D., & Glorieux, P. (1994). Controlling unstable periodic orbits by a delayed continuous feedback. Physical Review E, 49(2), R971.

[Bocc00] Boccaletti, S., Grebogi, C., Lai, Y. C., Mancini, H., & Maza, D. (2000). The control of chaos: theory and applications. Physics Reports, 329(3), 103-197.

[Brit86] Britton, N. F. (1986). Reaction-diffusion equations and their applications to biology. Academic Press.

[Burk06] Burke, J., & Knobloch, E. (2006). Localized states in the generalized Swift-Hohenberg equation. Physical Review E, 73(5), 056211.

[Buss71] Busse, F. H., & Whitehead, J. A. (1971). Instabilities of convection rolls in a high Prandtl number fluid. Journal of Fluid Mechanics, 47(02), 305-320.

[Camp73] Campillo, A. J., Shapiro, S. L., & Suydam, B. R. (1973). Periodic breakup of optical beams due to self-focusing. Applied Physics Letters, 23(11), 628-630.

[Cant04] Cantrell, R. S., & Cosner, C. (2004). Spatial ecology via reaction-diffusion equations. John Wiley & Sons.

[Carr04] Carr, L. D., & Brand, J. (2004). Spontaneous soliton formation and modulational instability in Bose-Einstein condensates. Physical Review Letters, 92(4), 040401.

[Caru13] Carusotto, I., & Ciuti, C. (2013). Quantum fluids of light. Reviews of Modern Physics, 85(1), 299.

[Chab11] Chabchoub, A., Hoffmann, N. P., & Akhmediev, N. (2011). Rogue wave observation in a water wave tank. Physical Review Letters, 106(20), 204502.

[Cont04] Conti, C., & Trillo, S. (2004). Nonspreading wave packets in three dimensions formed by an ultracold Bose gas in an optical lattice. Physical Review Letters, 92(12), 120404.

[Coul89] Coullet, P., Gil, L., & Rocca, F. (1989). Optical vortices. Optics Communications, 73(5), 403-408.

[Coul93] Coullet, P., Frisch, T., & Plaza, F. (1993). Sources and sinks of wave patterns. Physica D: Nonlinear Phenomena, 62(1-4), 75-79.

[Cros93] Cross, M. C., & Hohenberg, P. C. (1993). Pattern formation outside of equilibrium. Reviews of Modern Physics, 65(3), 851.

[Dell05] Della Villa, A., Enoch, S., Tayeb, G., Pierro, V., Galdi, V., & Capolino, F. (2005). Band gap formation and multiple scattering in photonic quasicrystals with a Penrose-type lattice. Physical Review Letters, 94(18), 183903.

[Demi05] Demircan, A., & Bandelow, U. (2005). Supercontinuum generation by the modulation instability. Optics Communications, 244(1), 181-185.

[Doua90] Douady, S. (1990). Experimental study of the Faraday instability. Journal of Fluid Mechanics, 221, 383-409.

[Dyke82] Van Dyke, M., & Van Dyke, M. (1982). An album of fluid motion (Vol. 176). Stanford: Parabolic Press.

[Eckh65] Eckhaus, W. (1965) Studies in Non-linear Stability Theory, Springer-Verlag, Berlin

[Egor07] Egorov, O., Lederer, F., & Staliunas, K. (2007). Subdiffractive discrete cavity solitons. Optics Letters, 32(15), 2106-2108.

[Eibe03] Eiben, A. E., & Smith, J. E. (2003). Introduction to evolutionary computing (Vol. 53). Heidelberg: Springer.

[Eier03] Eiermann, B., Treutlein, P., Anker, T., Albiez, M., Taglieber, M., Marzlin, K. P., & Oberthaler, M. K. (2003). Dispersion management for atomic matter waves. Physical Review Letters, 91(6), 060402.

[Epst06] Epstein, I. R. (2006). Predicting complex biology with simple chemistry. Proceedings of the National Academy of Sciences, 103(43), 15727-15728.

[Fang00] Fang, H., Malendevich, R., Schiek, R., & Stegeman, G. I. (2000). Spatial modulational instability in one-dimensional lithium niobate slab waveguides. Optics Letters, 25(24), 1786-1788.

[Fara31] Faraday, M. (1831). On a peculiar class of acoustical figures; and on certain forms assumed by groups of particles upon vibrating elastic surfaces. Philosophical transactions of the Royal Society of London, 121, 299-340.

[Gail16] Gailevicius, D., Koliadenko, V., Purlys, V., Peckus, M., Taranenko, V., & Staliunas, K. (2016). Photonic Crystal Microchip Laser. Scientific Reports, 6, 34173.

[Garf92] Garfinkel, A. (1992). Controlling cardiac chaos. Science, 257.

[Gibs16] Gibson, C. J., Yao, A. M., & Oppo, G. L. (2016). Optical rogue waves in vortex turbulence. Physical Review Letters, 116(4), 043903.

[Gold84] Goldman, M. V. (1984). Strong turbulence of plasma waves. Reviews of Modern Physics, 56(4), 709.

[Gome15] Gomes, S. N., Pradas, M., Kalliadasis, S., Papageorgiou, D. T., & Pavliotis, G. A. (2015). Controlling spatiotemporal chaos in active dissipative-dispersive nonlinear systems. Physical Review E, 92(2), 022912.

[Gora03] Credit: Illustration: Royal Swedish Academy of Sciences, (observed on 8 August 2003 by Göran Scharmer and Kai Langhans)

[Haar81] Ter Haar, D., & Tsytovich, V. N. (1981). Modulation instabilities in astrophysics. Physics Reports, 73(3), 175-236.

[Hake75] Haken, H. (1975). Generalized Ginzburg-Landau equations for phase transition-like phenomena in lasers, nonlinear optics, hydrodynamics and chemical reactions. Zeitschrift für Physik B Condensed Matter, 21(1), 105-114.

[He12] He, P. B., Gu, G. N., & Pan, A. L. (2012). Modulational instability and gap solitons in periodic ferromagnetic films. The European Physical Journal B-Condensed Matter and Complex Systems, 85(4), 1-5.

[Herr12] Herrero, R., Botey, M., Radziunas, M., & Staliunas, K. (2012). Beam shaping in spatially modulated broad-area semiconductor amplifiers. Optics Letters, 37(24), 5253-5255.

[Hilb94] Hilborn, R. C., & Sprott, J. C. (1994). Chaos and nonlinear dynamics: an introduction for scientists and engineers. American Journal of Physics, 62(9), 861-862.

[Ho93] Ho, K. P., Walker, J. D., & Kahn, J. M. (1993). External optical feedback effects on intensity noise of vertical-cavity surface-emitting lasers. IEEE Photonics Technology Letters, 5(8), 892-895.

[Holl92] Holland, J. H. (1992). Adaptation in natural and artificial systems: an introductory analysis with applications to biology, control, and artificial intelligence. MIT press.

[Holl92] Holland, J. H. (1992). Genetic algorithms. Scientific American, 267(1), 66-72.

[Ikez76] Ikezi, H., Chang, R. P., & Stern, R. A. (1976). Nonlinear evolution of the electron-beam-plasma instability. Physical Review Letters, 36(17), 1047.

[Ipse97] Ipsen, M., Hynne, F., & Sørensen, P. G. (1997). Amplitude equations and chemical reaction–diffusion systems. International Journal of Bifurcation and Chaos, 7(07), 1539-1554.

[Jaco97] Ben-Jacob, E. (1997). From snowflake formation to growth of bacterial colonies II: Cooperative formation of complex colonial patterns. Contemporary Physics, 38(3), 205-241.

[Joan11] Joannopoulos, J. D., Johnson, S. G., Winn, J. N., & Meade, R. D. (2011). Photonic crystals: molding the flow of light. Princeton University Press.

[Kapl00] Kaplan, C. S. (2000). Computer generated islamic star patterns. Bridges, 105-112.

[Kapl04] Kaplan, C. S., & Salesin, D. H. (2004). Islamic star patterns in absolute geometry. ACM Transactions on Graphics (TOG), 23(2), 97-119.

[Kapr12] Kapral, R., & Showalter, K. (Eds.). (2012). Chemical waves and patterns (Vol. 10). Springer Science & Business Media.

[Kart11] Kartashov, Y. V., Malomed, B. A., & Torner, L. (2011). Solitons in nonlinear lattices. Reviews of Modern Physics, 83(1), 247.

[Keel08] Keeling, J., & Berloff, N. G. (2008). Spontaneous rotating vortex lattices in a pumped decaying condensate. Physical Review Letters, 100(25), 250401.

[Kevr02] Kevrekidis, P. G., Bishop, A. R., & Rasmussen, K. Ø. (2001). Hysteresis and metastability in the quenched turbulent dynamics of the complex Ginzburg-Landau equation. Physical Review E, 65(1), 016122.

[Kevr04] Kevrekidis, P. G., & Frantzeskakis, D. J. (2004). Pattern forming dynamical instabilities of Bose-Einstein condensates. Modern Physics Letters B, 18(05n06), 173-202.

[Kevr04] Kevrekidis, P. G., Theocharis, G., Frantzeskakis, D. J., & Trombettoni, A. (2004). Avoiding infrared catastrophes in trapped Bose-Einstein condensates. Physical Review A, 70(2), 023602.

[Khar03] Kharif, C., & Pelinovsky, E. (2003). Physical mechanisms of the rogue wave phenomenon. European Journal of Mechanics-B/Fluids, 22(6), 603-634.

[Kip00] Kip, D., Soljacic, M., Segev, M., Eugenieva, E., & Christodoulides, D. N. (2000). Modulation instability and pattern formation in spatially incoherent light beams. Science, 290(5491), 495-498.

[Klau08] Klausmeier, C. A. (2008). Floquet theory: a useful tool for understanding nonequilibrium dynamics. Theoretical Ecology, 1(3), 153-161.

[Koge71] Kogelnik, H., & Shank, C. V. (1971). Stimulated emission in a periodic structure. Applied Physics Letters, 18(4), 152-154.

[Koge72] Kogelnik, H., & Shank, C. V. (1972). Coupled-wave theory of distributed feedback lasers. Journal of Applied Physics, 43(5), 2327-2335.

[Kond10] Kondo, S., & Miura, T. (2010). Reaction-diffusion model as a framework for understanding biological pattern formation. Science, 329(5999), 1616-1620.

[Kond14] Kondepudi, D., & Prigogine, I. (2014). Modern thermodynamics: from heat engines to dissipative structures. John Wiley & Sons.

[Kono02] Konotop, V. V., & Salerno, M. (2002). Modulational instability in Bose-Einstein condensates in optical lattices. Physical Review A, 65(2), 021602.

[Kosc74] Koschmieder, E. L. (1974). Bénard convection. Adv. Chem. Phys, 26(177-212), 605.

[Kozy07] Kozyreff, G., & Tlidi, M. (2007). Nonvariational real Swift-Hohenberg equation for biological, chemical, and optical systems. Chaos: An Interdisciplinary Journal of Nonlinear Science, 17(3), 037103.

[Kram85] Kramer, L., & Zimmermann, W. (1985). On the Eckhaus instability for spatially periodic patterns. Physica D: Nonlinear Phenomena, 16(2), 221-232.

[Kram95] Kramer, L., & Pesch, W. (1995). Convection instabilities in nematic liquid crystals. Annual Review of Fluid Mechanics, 27(1), 515-539.

[Krol01] Krolikowski, W., Bang, O., Rasmussen, J. J., & Wyller, J. (2001). Modulational instability in nonlocal nonlinear Kerr media. Physical Review E, 64(1), 016612.

[Kuma12] Kumar, N., Botey, M., Herrero, R., Loiko, Y., & Staliunas, K. (2012). High-directional wave propagation in periodic loss modulated materials. Photonics and Nanostructures-Fundamentals and Applications, 10(4), 644-650.

[Kuma17] Kumar, M., Porsezian, K., Tchofo-Dinda, P., Grelu, P., Mithun, T., & Uthayakumar, T. (2017). Spatial modulation instability of coupled surface plasmon polaritons in a dielectric–metal–dielectric structure. JOSA B, 34(1), 198-206.

[Kuma17] Kumar, S., Perego, A. M., & Staliunas, K. (2017). Linear and Nonlinear Bullets of the Bogoliubov–de Gennes Excitations. Physical Review Letters, 118(4), 044103.

[Kura76] Kuramoto, Y., & Tsuzuki, T. (1976). Persistent propagation of concentration waves in dissipative media far from thermal equilibrium. Progress of Theoretical Physics, 55(2), 356-369.

[Lake77] Lake, B. M., Yuen, H. C., Rungaldier, H., & Ferguson, W. E. (1977). Nonlinear deep-water waves: theory and experiment. Part 2. Evolution of a continuous wave train. Journal of Fluid Mechanics, 83(01), 49-74.

[Law98] Law, J. Y., & Agrawal, G. P. (1998). Feedback-induced chaos and intensity-noise enhancement in vertical-cavity surface-emitting lasers. JOSA B, 15(2), 562-569.

[Lega94] Lega, J., Moloney, J. V., & Newell, A. C. (1994). Swift-Hohenberg equation for lasers. Physical Review Letters, 73(22), 2978.

[Li05] Li, L., Li, Z., Malomed, B. A., Mihalache, D., & Liu, W. M. (2005). Exact soliton solutions and nonlinear modulation instability in spinor Bose-Einstein condensates. Physical Review A, 72(3), 033611

[Lian13] Lian, X., Wang, H., & Wang, W. (2013). Delay-driven pattern formation in a reaction–diffusion predator–prey model incorporating a prey refuge. Journal of Statistical Mechanics: Theory and Experiment, 2013(04), P04006.

[Lin09] Lin, Y. Y., Lee, R. K., & Kivshar, Y. S. (2009). Transverse instability of transverse-magnetic solitons and nonlinear surface plasmons. Optics Letters, 34(19), 2982-2984.

[Long96] Longhi, S. (1996). Hydrodynamic equation model for degenerate optical parametric oscillators. Journal of Modern Optics, 43(6), 1089-1094.

[Lu07] Lu, P. J., & Steinhardt, P. J. (2007). Decagonal and quasi-crystalline tilings in medieval Islamic architecture. Science, 315(5815), 1106-1110.

[Maig14] Maigyte, L. (2014). Shaping of light beams with photonic crystals: spatial filtering, beam collimation and focusing. (https://upcommons.upc.edu/handle/2117/95427)

[Maig15] Maigyte, L., & Staliunas, K. (2015). Spatial filtering with photonic crystals. Applied Physics Reviews, 2(1), 011102.

[Male01] Malendevich, R., Jankovic, L., Stegeman, G., & Aitchison, J. S. (2001). Spatial modulation instability in a Kerr slab waveguide. Optics Letters, 26(23), 1879-1881.

[Mama96] Mamaev, A. V., Saffman, M., Anderson, D. Z., & Zozulya, A. A. (1996). Propagation of light beams in anisotropic nonlinear media: from symmetry breaking to spatial turbulence. Physical Review A, 54(1), 870.

[Mand03] Mandre, S. K., Fischer, I., & Elssser, W. (2003). Control of the spatiotemporal emission of a broad-area semiconductor laser by spatially filtered feedback. Optics Letters, 28(13), 1135-1137.

[Mann95] Manneville, P. (1990). Dissipative Structures and Weak Turbulence Academic. New York, 55.

[Marc96] Marciante, J. R., & Agrawal, G. P. (1996). Nonlinear mechanisms of filamentation in broad-area semiconductor lasers. IEEE Journal of Quantum Electronics, 32(4), 590-596.

[Mart96] Martin-Regalado, J., Van Tartwijk, G. H. M., Balle, S., & San Miguel, M. (1996). Mode control and pattern stabilization in broad-area lasers by optical feedback. Physical Review A, 54(6), 5386.

[Mcle95] McLeod, R., Wagner, K., & Blair, S. (1995). (3+ 1)-dimensional optical soliton dragging logic. Physical Review A, 52(4), 3254.

[Mich94] Michalewicz, Z. (1994). GAs: What are they?. In Genetic algorithms+ data structures= evolution programs (pp. 13-30). Springer Berlin Heidelberg.

[Mile90] Miles, J., & Henderson, D. (1990). Parametrically forced surface waves. Annual Review of Fluid Mechanics, 22(1), 143-165.

[Mitc92] Mitchell, M., Forrest, S., & Holland, J. H. (1992, December). The royal road for genetic algorithms: Fitness landscapes and GA performance. In Proceedings of the first European conference on artificial life (pp. 245-254).

[Mitc96] Mitchell, M. (1998). An introduction to genetic algorithms. MIT press.

[Miur04] Miura, T., & Maini, P. K. (2004). Periodic pattern formation in reaction–diffusion systems: An introduction for numerical simulation. Anatomical Science International, 79(3), 112-123.

[Moen16] Moench, H., Carpaij, M., Gerlach, P., Gronenbron, S., Gudde, R., Hellmig, J., & van der Lee, A. (2016, March). VCSEL-based sensors for distance and velocity. In SPIE OPTO (pp. 97660A-97660A). International Society for Optics and Photonics.

[Moha05] Mohamadou, A., Jiotsa, A. K., & Kofané, T. C. (2005). Pattern selection and modulational instability in the one-dimensional modified complex Ginzburg–Landau equation. Chaos, Solitons & Fractals, 24(4), 957-966.

[Mull99] Mullane, M., & McInerney, J. G. (1999). Minimization of the linewidth enhancement factor in compressively strained semiconductor lasers. IEEE Photonics Technology Letters, 11(7), 776-778.

[Munk97] Münkel, M., Kaiser, F., & Hess, O. (1997). Stabilization of spatiotemporally chaotic semiconductor laser arrays by means of delayed optical feedback. Physical Review E, 56(4), 3868.

[Newe93] Newell, A. C., Passot, T., & Lega, J. (1993). Order parameter equations for patterns. Annual Review of Fluid Mechanics, 25(1), 399-453.

[Nico77] Nicolis, G., & Prigogine, I. (1977). Self-organization in nonequilibrium systems (Vol. 191977). Wiley, New York.

[Ohts12] Ohtsubo, J. (2012). Semiconductor lasers: stability, instability and chaos (Vol. 111). Springer.

[Oppo09] Oppo, G. L., Yao, A. M., Prati, F., & De Valcárcel, G. J. (2009). Long-term spatiotemporal dynamics of solid-state lasers and vertical-cavity surface-emitting lasers. Physical Review A, 79(3), 033824.

[Oppo91] Oppo, G. L., D'Alessandro, G., & Firth, W. J. (1991). Spatiotemporal instabilities of lasers in models reduced via center manifold techniques. Physical Review A, 44(7), 4712.

[Osbo10] Osborne, A. (2010). Nonlinear ocean waves and the inverse scattering transform (Vol. 97). Academic Press.

[Osin87] Osinski, M., & Buus, J. (1987). Linewidth broadening factor in semiconductor lasers--An overview. IEEE Journal of Quantum Electronics, 23(1), 9-29.

[Ostr03] Ostrovskaya, E. A., & Kivshar, Y. S. (2003). Matter-wave gap solitons in atomic band-gap structures. Physical Review Letters, 90(16), 160407.

[Ostr72] Ostrovskii, L. A., & Soustov, L. V. (1972). "Selfmodulation" of electromagnetic waves in nonlinear transmission lines. Radiophysics and Quantum Electronics, 15(2), 182-187.

[Oto14] Fernandez-Oto, C., de Valcárcel, G. J., Tlidi, M., Panajotov, K., & Staliunas, K. (2014). Phase-bistable patterns and cavity solitons induced by spatially periodic injection into vertical-cavity surface-emitting lasers. Physical Review A, 89(5), 055802.

[Ott90] Ott, E., Grebogi, C., & Yorke, J. A. (1990). Controlling chaos. Physical Review Letters, 64(11), 1196.

[Pass94] Passot, T., & Newell, A. C. (1994). Towards a universal theory for natural patterns. Physica D: Nonlinear Phenomena, 74(3-4), 301-352.

[Pecc03] Peccianti, M., Conti, C., & Assanto, G. (2003). Optical modulational instability in a nonlocal medium. Physical Review E, 68(2), 025602.

[Pena03] Pena, B., Pérez-García, C., Sanz-Anchelergues, A., Míguez, D. G., & Muñuzuri, A. P. (2003). Transverse instabilities in chemical Turing patterns of stripes. Physical Review E, 68(5), 056206.

[Pere16] Perego, A. M., Tarasov, N., Churkin, D. V., Turitsyn, S. K., & Staliunas, K. (2016). Pattern generation by dissipative parametric instability. Physical Review Letters, 116(2), 028701.

[Pere83] Peregrine, D. H. (1983). Water waves, nonlinear Schrödinger equations and their solutions. The Journal of the Australian Mathematical Society. Series B. Applied Mathematics, 25(01), 16-43.

[Petr09] Credit&License: Mick Petroff, http://creativecommons.org/licenses/by-sa/3.0

[Pita03] Pitaevskii, L., & Stringari, S. (2016). Bose-Einstein condensation and superfluidity (Vol. 164). Oxford University Press.

[Prat07] Prati, F., & Columbo, L. (2007). Long-wavelength instability in broad-area semiconductor lasers. Physical Review A, 75(5), 053811.

[Prig84] Prigogine, I., Stengers, I., & Prigogine, I. (1984). Order out of chaos: Man's new dialogue with nature (Vol. 13). New York: Bantam books.

[Pyra92] Pyragas, K. (1992). Continuous control of chaos by self-controlling feedback. Physics Letters A, 170(6), 421-428.

[Pyra93] Pyragas, K., & Tamaševičius, A. (1993). Experimental control of chaos by delayed self-controlling feedback. Physics Letters A, 180(1-2), 99-102.

[Ques16] Martínez-Quesada, M., & de Valcárcel, G. J. (2016). Pattern formation in a complex Swift-Hohenberg equation with phase bistability. arXiv preprint arXiv:1607.02113.

[Radz13] Radziunas, M., Botey, M., Herrero, R., & Staliunas, K. (2013). Intrinsic beam shaping mechanism in spatially modulated broad area semiconductor amplifiers. Applied Physics Letters, 103(13), 132101.

[Saar92] van Saarloos, W., & Hohenberg, P. C. (1992). Fronts, pulses, sources and sinks in generalized complex Ginzburg-Landau equations. Physica D: Nonlinear Phenomena, 56(4), 303-367.

[Sala03] Salasnich, L., Parola, A., & Reatto, L. (2003). Modulational instability and complex dynamics of confined matter-wave solitons. Physical Review Letters, 91(8), 080405.

[Saye15] Sayed, F., Vladimirov, S. V., Tyshetskiy, Y., & Ishihara, O. (2015). Modulational and filamentational instabilities of a monochromatic Langmuir pump wave in quantum plasmas. Physics of Plasmas, 22(5), 052115.

[Segu05] Segur, H., Henderson, D., Carter, J., Hammack, J., Li, C. M., Pheiff, D., & Socha, K. (2005). Stabilizing the Benjamin–Feir instability. Journal of Fluid Mechanics, 539, 229-271.

[Shan12] Shan, G., Zhao, X., Hu, M., Shek, C. H., & Huang, W. (2012). Vertical-external-cavity surface-emitting lasers and quantum dot lasers. Frontiers of Optoelectronics, 1-14.

[Shra92] Shraiman, B. I., Pumir, A., Van Saarloos, W., Hohenberg, P. C., Chaté, H., & Holen, M. (1992). Spatiotemporal chaos in the one-dimensional complex Ginzburg-Landau equation. Physica D: Nonlinear Phenomena, 57(3), 241-248.

[Simm99] Simmendinger, C., Preißr, D., & Hess, O. (1999). Stabilization of chaotic spatiotemporal filamentation in large broad area lasers by spatially structured optical feedback. Optics Express, 5(3), 48-54.

[Smer02] Smerzi, A., Trombettoni, A., Kevrekidis, P. G., & Bishop, A. R. (2002). Dynamical superfluid-insulator transition in a chain of weakly coupled Bose-Einstein condensates. Physical Review Letters, 89(17), 170402.

[Soll07] Solli, D. R., Ropers, C., Koonath, P., & Jalali, B. (2007). Optical rogue waves. Nature, 450(7172), 1054-1057.

[Spin98] Spinelli, L., Tissoni, G., Brambilla, M., Prati, F., & Lugiato, L. A. (1998). Spatial solitons in semiconductor microcavities. Physical Review A, 58(3), 2542.

[Stal00] Staliunas, K. (2000). Why Patterns Appear Spontaneously in Dissipative Systems?. arXiv preprint nlin/0002015.

[Stal02] Staliunas, K., Longhi, S., & de Valcárcel, G. J. (2002). Faraday patterns in Bose-Einstein condensates. Physical Review Letters, 89(21), 210406.

[Stal03] Staliunas, K., & Sanchez-Morcillo, V. J. (2003). Transverse patterns in nonlinear optical resonators (Vol. 183). Springer Science & Business Media.

[Stal06a] Staliunas, K., & Herrero, R. (2006). Nondiffractive propagation of light in photonic crystals. Physical Review E, 73(1), 016601.

[Stal06b] Staliunas, K., Herrero, R., & de Valcárcel, G. J. (2006). Subdiffractive band-edge solitons in Bose-Einstein condensates in periodic potentials. Physical Review E, 73(6), 065603.

[Stal06c] Staliunas, K., Herrero, R., & de Valcárcel, G. J. (2006). Subdiffractive band-edge solitons in Bose-Einstein condensates in periodic potentials. Physical Review E, 73(6), 065603.

[Stal07] Staliunas, K., Peckus, M., & Sirutkaitis, V. (2007). Sub-and superdiffractive resonators with intracavity photonic crystals. Physical Review A,76(5), 051803.

[Stal08a] Staliunas, K., & Longhi, S. (2008). Subdiffractive solitons of Bose-Einstein condensates in time-dependent optical lattices. Physical Review A, 78(3), 033606.

[Stal08b] Staliunas, K., Egorov, O., Kivshar, Y. S., & Lederer, F. (2008). Bloch cavity solitons in nonlinear resonators with intracavity photonic crystals. Physical Review Letters, 101(15), 153903.

[Stal09a] Staliunas, K., Herrero, R., & Vilaseca, R. (2009). Subdiffraction and spatial filtering due to periodic spatial modulation of the gain-loss profile. Physical Review A, 80(1), 013821.

[Stal09b] Staliunas, K., & Sánchez-Morcillo, V. J. (2009). Spatial filtering of light by chirped photonic crystals. Physical Review A, 79(5), 053807.

[Stal11] Staliunas, K. (2011). Removal of excitations of Bose-Einstein condensates by space-and time-modulated potentials. Physical Review A, 84(1), 013626.

[Stal93] Staliunas, K. (1993). Laser Ginzburg-Landau equation and laser hydrodynamics. Physical Review A, 48(2), 1573.

[Stal97] Staliūnas, K., Šlekys, G., & Weiss, C. O. (1997). Nonlinear pattern formation in active optical systems: shocks, domains of tilted waves, and cross-roll patterns. Physical Review Letters, 79(14), 2658.

[Stal98] Staliunas, K., & Sanchez-Morcillo, V. J. (1998). Spatial-localized structures in degenerate optical parametric oscillators. Physical Review A, 57(2), 1454.

[Stee98] Steel, M. J., & Zhang, W. (1998). Bloch function description of a Bose-Einstein condensate in a finite optical lattice. arXiv preprint cond-mat/9810284.

[Stro14] Strogatz, S. H. (2014). Nonlinear dynamics and chaos: with applications to physics, biology, chemistry, and engineering. Westview press.

[Stub92] Stubbe, P., Kohl, H., & Rietveld, M. T. (1992). Langmuir turbulence and ionospheric modification. Journal of Geophysical Research: Space Physics, 97(A5), 6285-6297.

[Swif77] Swift, J., & Hohenberg, P. C. (1977). Hydrodynamic fluctuations at the convective instability. Physical Review A, 15(1), 319.

[Tada12] Tadapatri, P., Krishnamurthy, K. S., & Weissflog, W. (2012). Patterned flexoelectric instability in a bent-core nematic liquid crystal. Soft Matter, 8(4), 1202-1214.

[Taki09] Takimoto, S., Tachikawa, T., Shogenji, R., & Ohtsubo, J. (2009). Control of spatio-temporal dynamics of broad-area semiconductor lasers by strong optical injection. IEEE Photonics Technology Letters, 21(15), 1051-1053.

[Tara98] Taranenko, V. B., Staliunas, K., & Weiss, C. O. (1998). Pattern formation and localized structures in degenerate optical parametric mixing. Physical Review Letters, 81(11), 2236.

[Tart98] Van Tartwijk, G. H., & Agrawal, G. P. (1998). Laser instabilities: a modern perspective. Progress in Quantum Electronics, 22(2), 43-122.

[Tayl23] Taylor, G. I. (1923). Stability of a viscous liquid contained between two rotating cylinders. Philosophical Transactions of the Royal Society of London. Series A, Containing Papers of a Mathematical or Physical Character, 223, 289-343.

[Thor78] Thornhill, S. G., & Ter Haar, D. (1978). Langmuir turbulence and modulational instability. Physics Reports, 43(2), 43-99.

[Tikh96] Tikhonenko, V., Christou, J., & Luther-Davies, B. (1996). Three dimensional bright spatial soliton collision and fusion in a saturable nonlinear medium. Physical Review Letters, 76(15), 2698.

[Tlid08] Tlidi, M., Lefever, R., & Vladimirov, A. (2008). On vegetation clustering, localized bare soil spots and fairy circles. In Dissipative Solitons: From Optics to Biology and Medicine (pp. 1-22). Springer Berlin Heidelberg.

[Tlid12] Tlidi, M., Averlant, E., Vladimirov, A., & Panajotov, K. (2012). Delay feedback induces a spontaneous motion of two-dimensional cavity solitons in driven semiconductor microcavities. Physical Review A, 86(3), 033822.

[Tlid14] Tlidi, M., Staliunas, K., Panajotov, K., Vladimirov, A. G., & Clerc, M. G. (2014). Localized structures in dissipative media: from optics to plant ecology. Philosophical transactions of Royal Society A, 372(2027).

[Tlid94] Tlidi, M., Mandel, P., & Lefever, R. (1994). Localized structures and localized patterns in optical bistability. Physical Review Letters, 73(5), 640.

[Trit88] Tritton, D. J. (1988). Physical fluid mechanics. Clarendon, Oxford.

[Trom01] Trombettoni, A., & Smerzi, A. (2001). Discrete solitons and breathers with dilute Bose-Einstein condensates. Physical Review Letters, 86(11), 2353.

[Trop06] Tropper, A. C., & Hoogland, S. (2006). Extended cavity surface-emitting semiconductor lasers. Progress in Quantum Electronics, 30(1), 1-43.

[Turi52] Turing, A. M. (1990). The chemical basis of morphogenesis. Bulletin of Mathematical Biology, 52(1-2), 153-197.

[Uchi12] Uchida, A. (2012). Optical Communication with Chaotic Lasers: Applications of Nonlinear Dynamics and Synchronization. John Wiley & Sons.

[Ulta03] Ultanir, E. A., Michaelis, D., Lederer, F., & Stegeman, G. I. (2003). Stable spatial solitons in semiconductor optical amplifiers. Optics Letters, 28(4), 251-253.

[Vall95] Valle, A., Sarma, J., & Shore, K. A. (1995). Spatial holeburning effects on the dynamics of vertical cavity surface-emitting laser diodes. IEEE Journal of Quantum Electronics, 31(8), 1423-1431

[Vlad06] Vladimirov, A. G., Skryabin, D. V., Kozyreff, G., Mandel, P., & Tlidi, M. (2006). Bragg localized structures in a passive cavity with transverse modulation of the refractive index and the pump. Optics Express, 14(1), 1-6.

[Wach16] Wächtler, F., & Santos, L. (2016). Quantum filaments in dipolar Bose-Einstein condensates. Physical Review A, 93(6), 061603.

[Walg12] Walgraef, D. (2012). Spatio-temporal pattern formation: with examples from physics, chemistry, and materials science. Springer Science & Business Media.

[Whit02] Whitesides, G. M., & Grzybowski, B. (2002). Self-assembly at all scales. Science, 295(5564), 2418-2421.

[Winf72] Winfree, A. T. (1972). Spiral waves of chemical activity. Science, 175 (4022), 634-636.

[Wong75] Wong, A. Y., & Quon, B. H. (1975). Spatial collapse of beam-driven plasma waves. Physical Review Letters, 34(24), 1499.

[Xia10] Xia, H., Shats, M., & Punzmann, H. (2010). Modulation instability and capillary wave turbulence. Europhysics Letters, 91(1), 14002.

[Yalb87] Yablonovitch, E. (1987). Inhibited spontaneous emission in solid-state physics and electronics. Physical Review Letters, 58(20), 2059.

[Yuen82] Yuen, H. C., & Lake, B. M. (1982). Nonlinear dynamics of deep-water gravity waves. Advances in Applied Mechanics, 22, 67-229.

[Zakh09] Zakharov, V. E., & Ostrovsky, L. A. (2009). Modulation instability: the beginning. Physica D: Nonlinear Phenomena, 238(5), 540-548.

[Zakh68] Zakharov, V. E. (1968). Stability of periodic waves of finite amplitude on the surface of a deep fluid. Journal of Applied Mechanics and Technical Physics, 9(2), 190-194.

[Zakh72] Zakharov, V. E. (1972). Collapse of Langmuir waves. Sov. Phys. JETP, 35(5), 908-914.

[Zhou12] Zhou, Y. L., Zou, Z. L., & Yan, K. (2012). Experimental study on modulational instability and evolution of crescent waves. Water Science and Engineering, 5(4), 419-427.

[Zved83] Zvezdin, A. K., & Popkov, A. F. (1983). Contribution to the nonlinear theory of magnetostatic spin waves. Sov. Phys. JETP, 2, 350.

List of Journal Publications

[J1] **Kumar, S**., Perego, A. M., & Staliunas, K. (2017). Linear and Nonlinear Bullets of the Bogoliubov–de Gennes Excitations. **Physical Review Letters**, 118(4), 044103.

[J2] **Kumar, S**., Herrero, R., Botey, M., & Staliunas, K. (2016). Suppression of pattern-forming instabilities by genetic optimization. **Physical Review E**, 94(1), 010202.

[J3] Ahmed, W. W., **Kumar, S**., Herrero, R., Botey, M., Radziunas, M., & Staliunas, K. (2015). Stabilization of flat-mirror vertical-external-cavity surface-emitting lasers by spatiotemporal modulation of the pump profile. **Physical Review A**, 92(4), 043829.

[J4] **Kumar, S**., Herrero, R., Botey, M., & Staliunas, K. (2015). Taming of modulation instability by spatio-temporal modulation of the potential. **Scientific Reports**, 5, 13268.

[J5] **Kumar, S**., Herrero, R., Botey, M., & Staliunas, K. (2014). Suppression of modulation instability in broad area semiconductor amplifiers. **Optics Letters**, 39(19), 5598-5601.

Other Publications and Participations

Book Chapters

1. Kumar, S., Ahmed, W. W., Herrero, R., Botey, M., Radziunas, M., & Staliunas, K. (2016). Stabilization of Broad Area Semiconductor Amplifiers by Spatially Modulated Potentials. In Nonlinear Dynamics: Materials, Theory and Experiments (pp. 139-151). Springer International Publishing.

Conferences with Proceedings

1. Kumar, S., Botey, M., Herrero, R., & Staliunas, K. (2016, July). Stabilization of semiconductor amplifiers with large linewidth enhancement factors. In Transparent Optical Networks (ICTON), 2016 18th International Conference on (pp. 1-4). IEEE. (10th -14th July 2016) (Invited Talk)
2. Ahmed, W. W., Kumar, S., Herrero, R., Botey, M., Radziunas, M., & Staliunas, K. (2016, April). Suppression of modulation instability in pump modulated flat-mirror VECSELs. In SPIE Photonics Europe (pp. 989406-989406). International Society for Optics and Photonics. (3rd -07th Apr 2016) (Oral Presentation)
3. Kumar, S., Herrero, R., Botey, M., & Staliunas, K. (2015, August). Control and manipulation of modulation instability. In Spatiotemporal Complexity in Nonlinear Optics (SCNO), 2015 (pp. 1-3). IEEE. (Lake Como, Italy, 31st Aug– 4th Sept 2015) (Poster Presentation)
4. Kumar, S., Herrero, R., Botey, M., & Staliunas, K. (2015, June). Beam quality improvement by suppression of Modulation Instability in broad area semiconductor laser amplifier. In The European Conference on Lasers and Electro-Optics (p. CB_P_4). Optical Society of America. (Munich, Germany, 21-25 June, 2015) (Poster)
5. Herrero, R., Kumar, S., Radziunas, M., Botey, M., & Staliunas, K. (2014, July). Improving beam quality in broad area semiconductor amplifiers. In Transparent Optical Networks (ICTON), 2014 16th International Conference on (pp. 1-3). IEEE. (Budapest, Hungary, 05-09 July 2015) (Invited Talk)

6. Herrero, R., Kumar, S., Radziunas, M., Botey, M., & Staliunas, K. (2014, July). Improving beam quality in broad area semiconductor amplifiers. In Transparent Optical Networks (ICTON), 2014 16th International Conference on (pp. 1-3). IEEE. (Graz, Austria 6th-10th July, 2014) (Invited Talk)

Conferences with Abstracts

1. Nanometa, (Tirol, Austria, 4-7 Jan 2017) Poster Presentation. Title: Improving beam quality in Broad Area Semiconductor amplifiers by spatiotemporal modulation. http://www.nanometa.org/programme
2. Recent Trends in Modern Optics, (Porto, Portugal, 21-23 June 2016) Invited Talk. Title: Suppression and Manipulation of Modulation Instability https://sites.google.com/site/rtmoporto/home
3. XXXIV Dynamics Days Europe, (Bayreuth, Germany, 8-12 Sept. 2014) , Oral Presentation Title: Control and manipulation of modulation instability. http://dynamicsdays2014.uni-bayreuth.de/en/schedule/index.php

Schools and Workshop Participations

1. Europhotonics Spring School 5th Edition, (Porquerolles Island, France, 29 March- 1 April, 2016) with Poster Presentation. Title: Stabilization of semiconductor amplifiers with large linewidth enhancement factors. http://www.europhotonics.org/wordpress/spring-school
2. Benasque School on Quantum Optics and Nonlinear Optics, (Benasque, Spain, 5-10 Oct 2014) http://benasque.org/2014optica/
3. Europhotonics Spring School 3rd Edition, (Porquerolles Island, France, 31 March-3 April, 2014) with Poster Presentation. Title: Control of Modulation Instability. http://www.europhotonics.org/wordpress/spring-school